Mechanism of Ribosome Rescue by Alternative Release Factor B

Dissertation

for the award of the degree

"Doctor of Philosophy" (Ph.D.)

in the International Max Planck Research School (IMPRS) for Molecular Biology

of the Georg-August University School of Science (GAUSS)

Georg-August-Universität Göttingen

submitted by

Kai-Hsin Chan

From Taipei, Taiwan

Göttingen 2020

Members of the Thesis Committee

Prof. Dr. Marina Rodnina
Department of Physical Biochemistry
Max Planck Institute for Biophysical Chemistry, Göttingen, Germany

Prof. Dr. Kai Tittmann
Department of Molecular Enzymology
Schwann-Schleiden-Forschungszentrum
Georg-August-Universität Göttingen, Göttingen, Germany

Prof. Dr. Markus Bohnsack
Department of Molecular Biology
University Medical Centre, Göttingen, Germany

Members of the Examination Board

Prof. Dr. Marina Rodnina (1st Referee)
Department of Physical Biochemistry
Max Planck Institute for Biophysical Chemistry, Göttingen, Germany

Prof. Dr. Kai Tittmann (2nd Referee)
Department of Molecular Enzymology
Schwann-Schleiden-Forschungszentrum
Georg-August-Universität Göttingen, Göttingen, Germany

Prof. Dr. Markus Bohnsack (3rd Referee)
Department of Molecular Biology
University Medical Centre, Göttingen, Germany

Further members of the Examination Board

Prof. Dr. Holger Stark
Department of Structural Dynamics
Max Planck Institute for Biophysical Chemistry, Göttingen, Germany

Dr. Ricarda Richter-Dennerlein
Department of Cellular Biochemistry
University Medical Center, Göttingen, Germany

Dr. Sarah Adio
Department of Molecular Structural Biology
Institute for Microbiology and Genetics
Georg-August-Universität Göttingen, Göttingen, Germany

Date of the oral examination: June 23rd, 2020

Affidavit

I hereby declare that the presented dissertation entitled "Mechanism of Ribosome Rescue by Alternative Release Factor B" has been written independently and with no other sources and aids than quoted.

Göttingen, April 30th, 2020

Kai-Hsin Chan

Related publications

Chan, K., Petrychenko V., Mueller C., Maracci C., Holtkamp W., Wilson D., Fischer N., & Rodnina M.V. (2020) Mechanism of Ribosome Rescue by Alternative Ribosome-Rescue Factor B (in revision).

TABLE OF CONTENTS

1 ABSTRACT

Rescue of ribosomes stalled on non-stop mRNAs is essential in bacteria and in the mitochondria of all eukaryotes. The lack of a stop codon causes ribosomes to stall at the 3' end of mRNA with an empty A site, and specialized rescue mechanisms are required to release the truncated translation product and allow ribosome recycling. Of the known bacterial ribosome rescue systems, only ArfB has intrinsic peptidyl-tRNA hydrolysis activity, and is conserved in all eukaryotic mitochondria. The precise mechanism of ArfB-mediated ribosome rescue is not well understood.

In this study, we use rapid kinetics in conjunction with FRET- and anisotropy-based methods to construct a detailed kinetic model for ArfB-mediated ribosome rescue. We find that ArfB binds to the ribosome rapidly regardless of mRNA length, and that the association rate for the majority of ArfB molecules in the ensemble is close to diffusion controlled. This is likely due to the flexibility of its unstructured C-terminal tail, which allows ArfB to associate with the ribosome in different orientations. A slow engagement step follows, which allows ArfB to discriminate between stalled ribosomes with and without mRNA extending past the P site. The engaged state of ArfB involves specific interactions that strongly increase the affinity of ArfB for the ribosome, and is the active state in which ArfB performs peptidyl-tRNA hydrolysis. ArfB dissociates slowly from the post-hydrolysis ribosome, which leads to a low turnover rate that can be increased somewhat by the presence of ribosome recycling factors.

Cryo-electron microscopy structures of ArfB bound to two different substrates, one with 3' mRNA extensions and one without, provide structural snapshots of ArfB-ribosome complexes along the rescue pathway. By superimposing the NMR structure of ArfB, in which the C-terminal tail is unstructured, on the pre-hydrolysis stalled ribosome, we model possible initial binding complexes that support the kinetic data on multiple binding rates. The 2.6 Å structure of ArfB in the active state show an extensive network of specific interactions between ArfB and the ribosome, all of which involve residues that were previously found to be functionally important in a mutational study. These structures provide explanations for the high affinity and slow dissociation of ArfB. Our study demonstrates the role of intrinsic disorder in protein-ribosome interactions and provides a basis for the understanding of ArfB-like proteins in mitochondria.

2 INTRODUCTION

2.1 Bacterial protein synthesis

Proteins are the main effectors of the biochemical reactions that underlie life, which include but are not restricted to signal transduction, catalysis, and movement. Protein synthesis represents the final step in the flow of genetic information that starts from DNA: nucleotide triplets, called codons, encode twenty commonly occurring amino acids, which are the building blocks of proteins. Sequences of amino acids in turn confer both three-dimensional structure and function to proteins. In the process of expressing a protein, the information stored in DNA is first transcribed into messenger RNA (mRNA), and finally converted into protein in a process termed translation. Efficient and accurate translation is essential to the growth and replication of the cell, and regulation of translation allows the cell to execute different genetic programs as well as rapidly respond to external stimuli.

During translation, transfer RNAs (tRNA) carrying amino acids interact with mRNA via the anticodon, which base-pairs with the complementary codon on the mRNA. The growing peptide is thus transferred from one tRNA to the next by aminolysis and re-forming of the ester bond. In this way, tRNAs serve as the bridge between nucleotides and amino acids. The platform for this conversion of information is the ribosome, a large ribonucleoprotein complex that catalyzes peptide bond formation between amino acids. The ribosome facilitates translation through a dynamic and complex sequence of events, and along with a number of auxiliary translation factors, ensures the processivity and fidelity of translation.

2.1.1 Ribosome structure

The bacterial ribosome is a dynamic macromolecule consisting of two subunits: the 30S small subunit, which contains the 16S ribosomal RNA (rRNA) and 21 ribosomal proteins, and the 50S large subunit, which is composed of 5S rRNA, 23S rRNA, and 34 ribosomal proteins (reviewed in (Melnikov et al., 2012; Schmeing and Ramakrishnan, 2009)).

The 30S subunit is home to the decoding center and the mRNA entry channel. Codon-anticodon interactions take place in the decoding center, and the mRNA entry channel is the path of the mRNA through the ribosome during translation. The 50S subunit hosts the peptidyl-transferase center and the peptide exit tunnel. The peptidyl-transferase center is the

site of both peptide-bond formation and peptidyl-tRNA hydrolysis, and the peptide exit tunnel is occupied by the nascent peptide (**Figure 2.1**).

Upon subunit joining, the interface between the subunits define the A, P, and E tRNA binding sites. The A site accommodates the incoming aminoacyl-tRNA, while the deacylated tRNA leaves the ribosome via the E site. The P site holds the peptidyl-tRNA, where the newly synthesized peptide is attached to the tRNA.

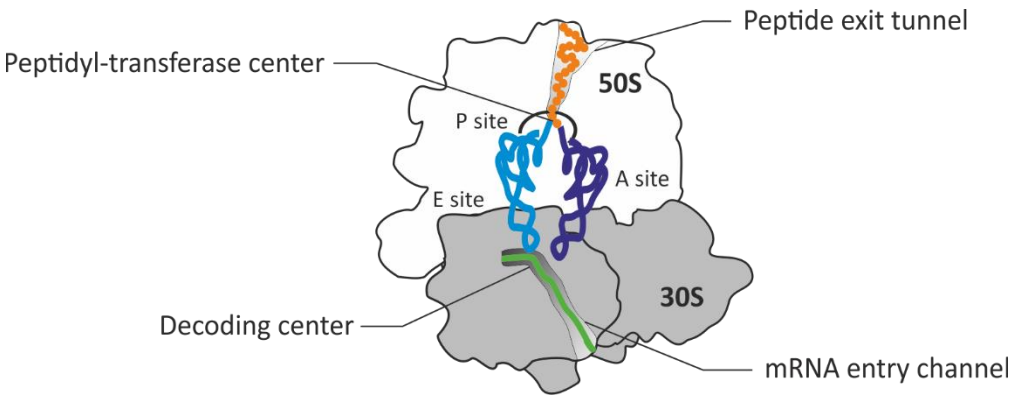

Figure 2.1. Schematic of the 70S bacterial ribosome. The A-site tRNA is shown in purple. The P-site tRNA is shown in blue with the nascent peptide in orange. The mRNA is shown in green.

The central importance of translation is reflected in the conservation of ribosome structure throughout different kingdoms of life. The functional core of the ribosome, in particular the decoding center and the peptidyl-transferase center, is made of structured RNA and does not vary much amongst different species (Melnikov et al., 2012). This allows us to infer the function of factors involved in translation based on homology.

2.1.2 Initiation

The first stage of translation is initiation. In this step, the ribosome recruits an mRNA and identifies the start codon (usually AUG in all kingdoms of life) that marks the beginning of a coding sequence. The most well-studied mode of initiation involves mRNAs that have a Shine-Dalgarno sequence 8-10 nucleotides upstream of the start codon, and requires the initiation factors IF1, IF2, and IF3 (reviewed in (Milon and Rodnina, 2012)).

In the first step of Shine-Dalgarno-led initiation, IF1, IF2, IF3, and the initiator tRNA fMet-tRNA^{fMet} are recruited to the small subunit, forming the 30S pre-initiation complex (PIC, **Figure 2.2a**). The sequence of initiation factor binding can vary, but kinetics data suggests that IF1 is

the last to bind, with fMet-tRNA^{fMet} completing 30S PIC assembly by docking to IF2 (Milon et al., 2010; Milon et al., 2012).

The 30S PIC becomes a stable 30S initiation complex after mRNA recruitment, when the Shine-Dalgarno sequence interacts with the anti-Shine-Dalgarno sequence in the 16S rRNA of the 30S subunit by complementary base-pairing (**Figure 2.2b**). Recognition of the start codon by the fMet-tRNA^{fMet} anticodon triggers a conformational change in the 30S PIC and destabilizes IF3 binding (Milon et al., 2012). Finally, the large subunit docks on the 30S subunit. fMet-tRNA^{fMet} accommodates in the ribosomal P site after GTP hydrolysis by IF2, and dissociation of IF1 and IF2 allows intersubunit bridges to form, resulting in the mature 70S initiation complex (IC) (Goyal et al., 2015; Milon et al., 2008).

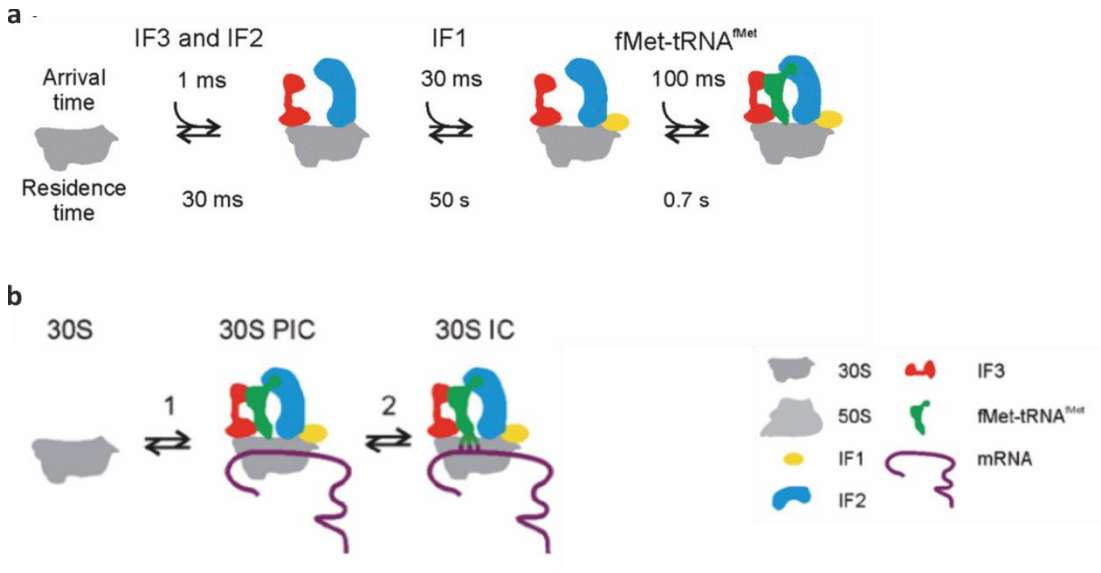

Figure 2.2. Formation of the **(a)** 30S pre-initiation complex and the **(b)** 30S initiation complex (adapted from (Milon and Rodnina, 2012)).

It is important to note that in bacteria, translation initiation is a co-transcriptional process; in other words, initiation occurs on mRNA that is still being transcribed (Rodnina, 2018). This is in stark contrast to eukaryotic initiation, where the transcript undergoes maturation that involves processing of the 3' end and circularization before being translated (Wells et al., 1998). Proteins that bind to the 5' 7-methylguanosine cap and to the 3' poly(A) tail are involved in activating eukaryotic mRNAs for translation (reviewed in (Jackson et al., 2010)). In prokaryotes, however, the main determinant for translational efficiency lies in the ribosome binding site on the 5' end of mRNA (Milon and Rodnina, 2012). According to the kinetic partitioning model, different features of the ribosome binding site affect the kinetics of initiation at different steps

of the pathway (**Figure 2.3**). These features include the structure of the ribosome binding site, which affects the unfolding and association of the mRNA to the 30S PIC. The identity of the start codon, on the other hand, affects the strength of the codon-anticodon interaction in the 30S IC (Milon and Rodnina, 2012). The sequence context around the ribosome binding site affects the conformation of the 30S IC, which in turn modulates the rate of large subunit association and 70S IC formation. Unlike in eukaryotes, the 3' end of bacterial mRNAs is not monitored prior to initiation (Milon et al., 2008; Milon and Rodnina, 2012).

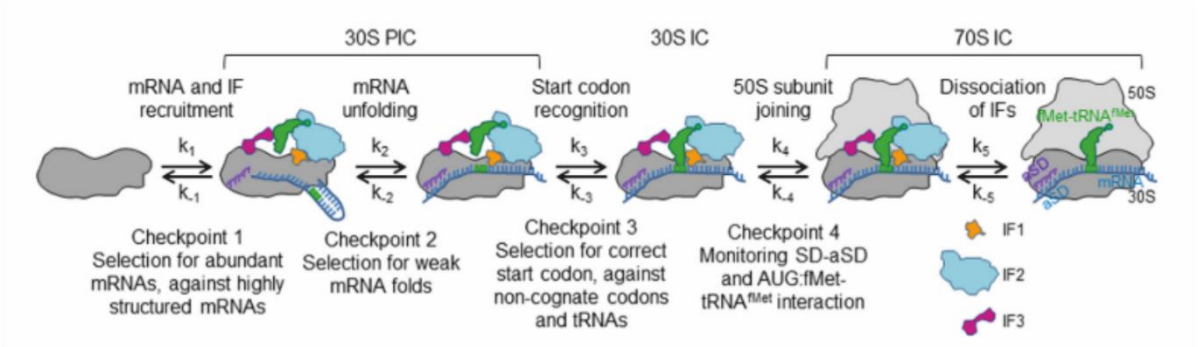

Figure 2.3. mRNA selection by kinetic partitioning (Rodnina, 2016).

2.1.3 Elongation

Elongation, the repeated process of adding one amino acid at a time to the growing peptide chain, follows the initiation phase. Each amino acid is added in a cycle of decoding, peptide bond formation, and translocation. During decoding, elongation factor EF-Tu delivers aminoacyl-tRNA to the ribosome in a ternary complex with GTP, and the aminoacyl-tRNA with an anticodon complementary to the mRNA codon exposed in the ribosomal A site is selected (**Figure 2.4**) (Rodnina et al., 2017).

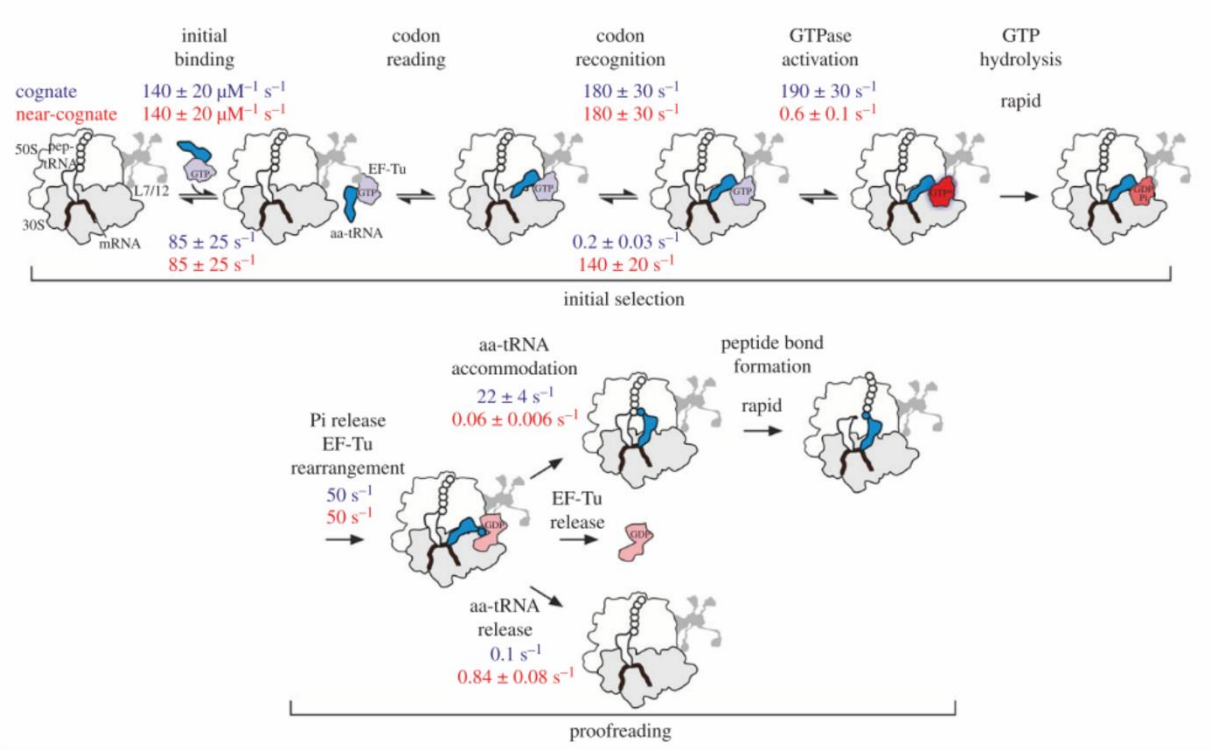

Figure 2.4. Kinetic mechanism of decoding peptide bond formation (Rodnina et al., 2017). EF-Tu is shown in blue, GTP in purple, GDP•Pi in red, and GDP-bound EF-Tu in pink.

Correct codon-anticodon interactions in the A site trigger a conformational change in the 16S rRNA in the codon recognition step. Key residues in the decoding center are involved in this conformational change, namely A1492, A1493, and G530. A1492 and A1493 adopt a "flipped-out" orientation, closing around the codon-anticodon complex, which also interacts with G530 (Fischer et al., 2016; Loveland et al., 2017). Concurrently, the small subunit moves the ternary complex so that GTP hydrolysis by EF-Tu is activated (Fischer et al., 2016; Rodnina et al., 2017). The subsequent structural rearrangement of GDP-bound EF-Tu promotes the release of the aminoacyl-tRNA into the A site. At the codon recognition step and at the GTPase activation step, kinetic partitioning allows the ribosome to discriminate between cognate and non-cognate aminoacyl-tRNAs (Rodnina et al., 2005). The accommodation of aminoacyl-tRNA into the A site further increases translation fidelity, because non-cognate aminoacyl-tRNAs accommodate at a slower rate (reviewed in (Rodnina et al., 2017)).

Peptide bond formation occurs once the incoming aminoacyl-tRNA is accommodated in the A site. Formation of the peptide bond between two amino acids is catalyzed by the peptidyl-transferase center, the active site of the ribosome which is almost entirely constituted of rRNA (Ban et al., 2000). The reaction is a nucleophilic attack of the amino group of the A site

aminoacyl-tRNA on the carbonyl carbon of the ester bond in the P site peptidyl-tRNA (**Figure 2.5**) (Rodnina, 2013). The ribosome ensures the correct positioning of rRNA and tRNA, and assists the reaction by ordering water molecules and by electrostatic shielding (Rodnina, 2013; Sharma et al., 2005; Wallin and Aqvist, 2010).

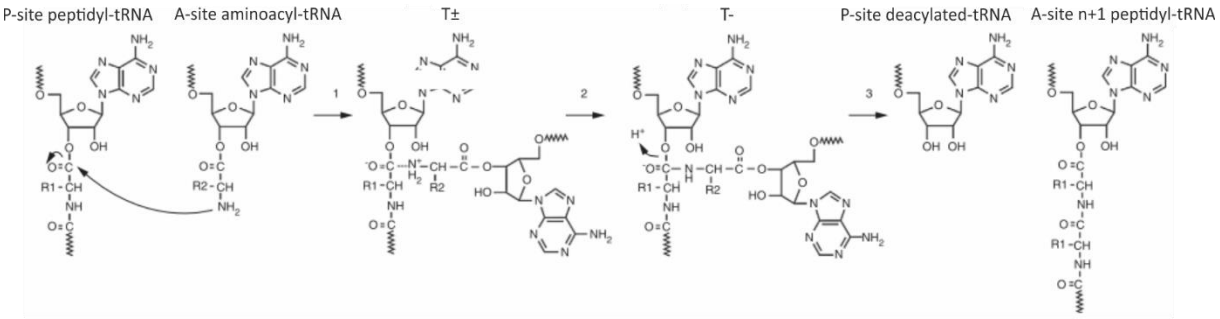

Figure 2.5. Peptide bond formation reaction scheme (Rodnina, 2013).

Once a new peptide bond is formed, the nascent peptide is transferred to the A-site tRNA. For another round of elongation to occur, the P-site tRNA must shift into the E site, and the A site tRNA must move into the P site, allowing ternary complexes carrying subsequent aminoacyl-tRNAs to enter the A site (reviewed in (Dunkle and Cate, 2010; Rodnina et al., 2017; Rodnina and Wintermeyer, 2011)). The mRNA must also move by one codon so that the next codon is exposed in the A site. This is the process of translocation, which is promoted by the GTPase EF-G in concert with spontaneous movements of the ribosomal subunits in relation to each other (**Figure 2.6**) (Belardinelli et al., 2016). EF-G serves to destabilize interactions between the small subunit and the tRNA-mRNA complex, which allow the movement of the tRNA and mRNA by three nucleotides; it also provides the directionality of translocation so that the ribosome moves in the 5’ to 3’ direction with respect to the mRNA. Through interactions between EF-G and the P site tRNA, and by accelerating movements of the ribosome, EF-G ensures that the ribosome remains in the same reading frame throughout translocation (Peng et al., 2019).

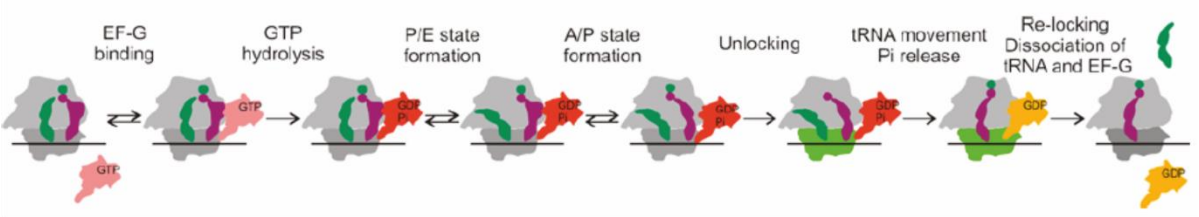

Figure 2.6. Kinetic scheme of translocation. GTP-bound EF-G is shown in pink, GDP•Pi-bound EF-G is shown in red, and GDP-bound EF-G is shown in yellow. The 30S subunit goes from a locked (gray) state to an unlocked (green) state (Rodnina et al., 2011).

2.1.4 Termination

When the ribosome reaches the end of an open reading frame, the fully translated nascent peptide must be released from the P-site tRNA and allowed to dissociate from the ribosome. Under normal conditions, a stop codon is presented in the A site which can be recognized by canonical release factors RF1 and RF2. RF1 recognizes UAA and UAG, while RF2 recognizes UAA and UGA (reviewed in (Korostelev, 2011)). Following recognition of the stop codon, release factors catalyze hydrolysis of the peptidyl-tRNA bond in the peptidy-transferase center. RF3 then assists the dissociation of release factors from the ribosome (**Figure 2.7**) (reviewed in (Dunkle and Cate, 2010; Korostelev, 2011).

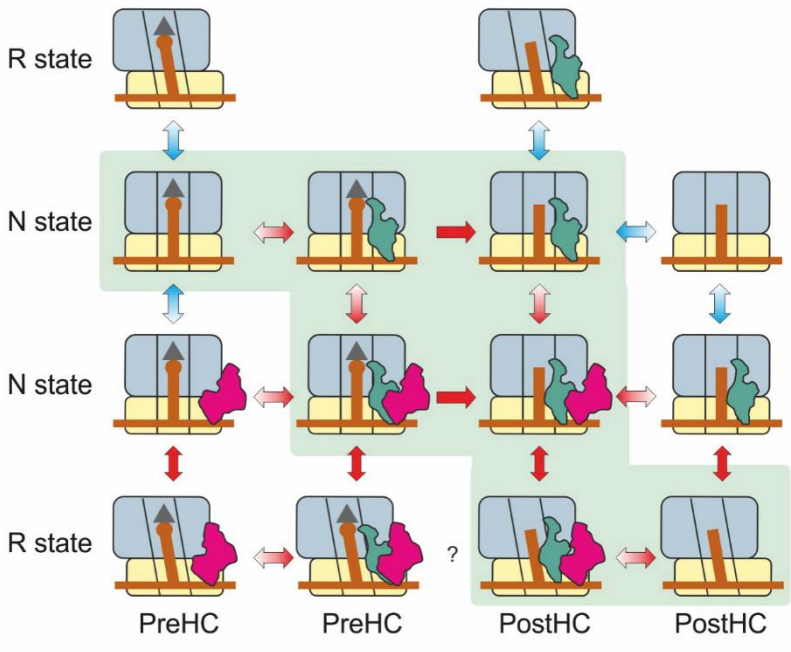

Figure 2.7. Dynamic model of bacterial translation termination. RF1 is shown in green and RF3 is shown in fuchsia. Red arrows represent rapid reactions, blue arrows represent slow conversion, and single-headed arrows represent irreversible peptide hydrolysis. The rotational states of the ribosomes are indicated (adapted from (Adio et al., 2018)).

Stop codon recognition during termination is performed by domains 2, 3 and 4 of the release factors, which contain the PxT motif of RF1, and the SPF motif of RF2 (**Figure 2.8**). Structural studies have revealed interactions between the release factors and each individual nucleotide of the stop codon: helix α5 recognizes the first invariant uracil, while residues in the PxT motif and the SPF motif recognize the second nucleotide. The third and final residue of the stop codon is read by conserved residues in the recognition loop that contains the PxT/SPF motifs (Korostelev et al., 2010; Laurberg et al., 2008).

Upon stop codon recognition, the release factors undergo a conformational rearrangement, with the switch loop interacting with the universally conserved decoding center residues A1492, A1493, and G530 in 16S rRNA, as well as A1913 in 23S rRNA (Jin et al., 2010; Korostelev et al., 2008; Laurberg et al., 2008; Weixlbaumer et al., 2008). These interactions stabilize the release factor in a catalytically active conformation, positioning the conserved GGQ motif of domain 3 in the peptidyl-transferase center. In this way, the catalytic activity of release factors is contingent on stop codon recognition, preventing premature termination of translation.

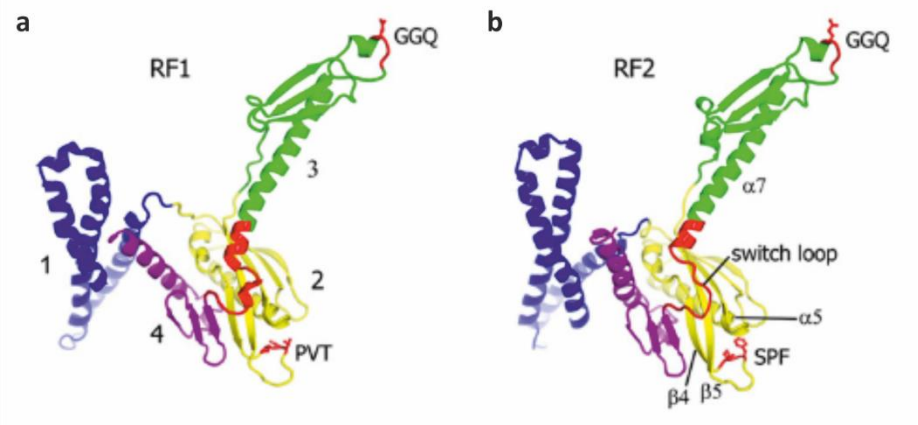

Figure 2.8. Crystal structures of **(a)** RF1 and **(b)** RF2. Individual domains are numbered (adapted from (Korostelev, 2011)).

Peptidyl-tRNA hydrolysis is the second reaction catalyzed by the peptidyl-transferase center, the first being peptide bond formation. Hydrolysis takes place as a nucleophilic attack by a water molecule or a hydroxide ion (Kuhlenkoetter et al., 2011). As a result, the reaction is highly dependent on the pH of the solution (Indrisiunaite et al., 2015; Kuhlenkoetter et al., 2011). The GGQ motif of release factors is directly involved in peptidyl-tRNA hydrolysis; it reaches into the peptidyl-transferase center and contacts nucleotides of the 23S rRNA and the P-site tRNA. In crystal structures of the termination complex, U2506 and U2585 of the 23S

rRNA are in positions analogous to when the 50S A site binding pocket is occupied by aminoacyl-tRNA (Jin et al., 2010; Korostelev et al., 2008; Laurberg et al., 2008; Weixlbaumer et al., 2008). The exact role of the GGQ motif in catalysis is not yet clear, however evidence suggests that the backbone NH group of the glutamine residue stabilizes the tetrahedral transition state intermediate and the leaving group (**Figure 2.9**) (Laurberg et al., 2008). The two glycine residues appear to facilitate the optimal positioning of the glutamine residue. Interestingly, the GGQ motif of both RF1 and RF2 have been shown to be methylated by HemK *in vivo* (Mora et al., 2007; Nakahigashi et al., 2002). The role of the methylation appears to contribute to the binding affinity of the release factor, and increases the rate of hydrolysis up to 10 fold so that all amino acids are hydrolyzed at a uniform rate (Pierson et al., 2016). It is worth noting that while release factors are not conserved, the GGQ motif is universally conserved (Dunkle and Cate, 2010). It can therefore be inferred that the catalytic mechanism of release factor-induced peptidyl-tRNA hydrolysis in the peptidyl-transferase center is similar between prokaryotes and eukaryotes.

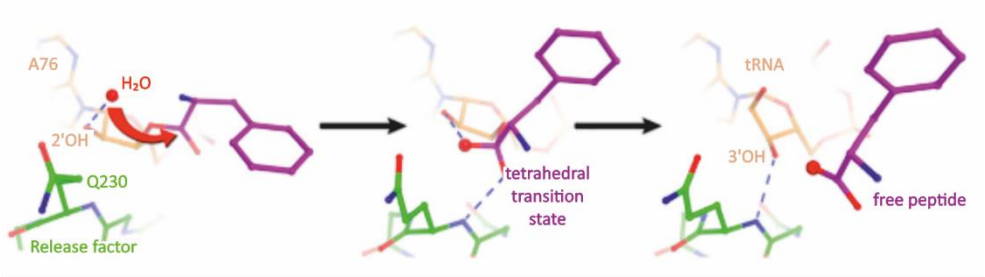

Figure 2.9. Stabilization of the tetrahedral transition state intermediate (purple) and the leaving group (orange) by the GGQ motif (green) (Korostelev, 2011).

After the nascent peptide is released, release factors need to dissociate from the ribosome. RF2 can dissociate from the post-termination ribosome spontaneously, whereas RF1 cannot (Peske et al., 2014; Zaher and Green, 2011). Dissociation of both factors is facilitated by the translational GTPase RF3 (Zavialov et al., 2001). RF3 can bind to the release factor-bound ribosome, and binding is stabilized upon peptide release, promoting dissociation of the release factor. GTP hydrolysis then promotes RF3 dissociation. Recent studies have shown that the ribosome undergoes a complex landscape of dynamics during termination, with each release factor influencing the conformation of the ribosome differently (Adio et al., 2018).

2.1.5 Recycling

The final step in translation is the recycling of the ribosomal subunits, which frees them to undergo initiation and perform further rounds of translation. In bacteria, this is mediated by translation factors RRF, EF-G, and IF3. Key events that occur during recycling include the dissociation of tRNA and mRNA, and the splitting of the ribosome into individual subunits (reviewed in (Rodnina, 2018)).

It has been shown that effective EF-G binding occurs when RRF is bound to the post-termination ribosome (Borg et al., 2016), and that IF3 promotes tRNA dissociation and prevents the individual subunits from re-associating before 70S IC formation (Rodnina, 2018). However the exact sequence of recycling events is still a matter of debate, in particular with regards to the timing of mRNA dissociation. In one model, EF-G hydrolyzes GTP, and the Pi (inorganic phosphate) release splits the ribosome with the tRNA and mRNA still attached to the small subunit (**Figure 2.10**). IF3 then displaces the tRNA and the mRNA dissociates spontaneously (Borg et al., 2016; Fu et al., 2016; Peske et al., 2005; Rodnina et al., 1997; Seo et al., 2004). Another model suggests that EF-G promotes mRNA release by GTP hydrolysis (Chen et al., 2017).

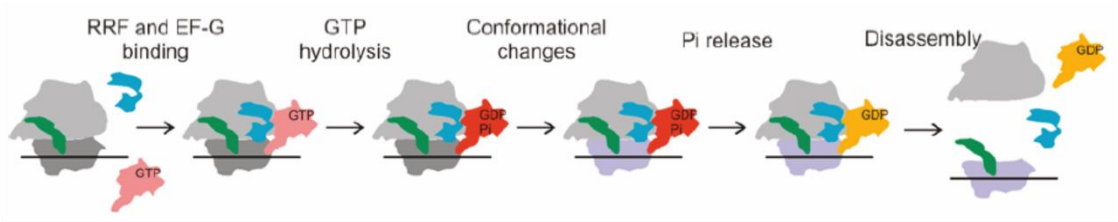

Figure 2.10. A model of ribosome recycling. RRF (blue) and GTP-bound EF-G (pink) bind to the post-termination ribosome. GTP-hydrolysis (GDP•Pi-bound EF-G is shown in red) and Pi release (GDP-bound EF-G is shown in yellow) promote ribosome splitting (Rodnina et al., 2011).

Recycling marks the end of one round of protein synthesis, and ensures the availability of ribosomal subunits. However, during each stage of translation, a number of events can occur that cause the ribosome to pause or completely stall on mRNA, effectively rendering them inactive. This is highly detrimental to cell viability (Chadani et al., 2011b; Feaga et al., 2016), not least because ribosome biogenesis is energetically costly (Davis and Williamson, 2017). Rescue mechanisms are therefore required to maintain a pool of active ribosomes.

2.2 Ribosome pausing and arrest

The speed and progression of translation is modulated by many intrinsic factors, including mRNA secondary structures, poly-proline stretches, stalling peptides, and codon usage (reviewed in (Buskirk and Green, 2017; Rodnina, 2016)). Some of these factors provide opportunities to regulate the synthesis of specific proteins and thereby maintain homeostasis; for example, mRNA secondary structures can influence the kinetics of mRNA selection during translation initiation, resulting in different expression levels between transcripts (Reeve et al., 2014). Furthermore, codon usage affects translation kinetics on stretches of the same transcript, because the cellular concentration of different tRNA isoforms is different (Gorochowski et al., 2015; Tuller et al., 2010). This has been shown to allow the nascent peptide to assume the correct fold co-translationally (Buhr et al., 2016; Yu et al., 2015). In some other cases, the ribosome pauses altogether. For example, the SecM stalling peptide regulates the copy number of certain membrane proteins (Nakatogawa et al., 2004). Pausing in this situation can be resolved, and translation can continue on the same transcript.

There are also cases where ribosomes are stalled in response to stress conditions. The accumulation of these stalled ribosomes is unproductive, and require termination of translation altogether for the ribosome to engage in productive rounds of protein synthesis. This can happen during the bacterial stress response or because of mRNA damage (reviewed in (Starosta et al., 2014)). Termination on these stalled ribosomes results in a ribosome free to undergo initiation, as well as the release of an unfinished translation product. In the following section, examples of pausing resolved by continued elongation and of stalling resolved by premature termination are discussed.

2.2.1 Ribosome pausing resolved by elongation

The availability of aminoacylated tRNAs is a key element effecting elongation rates. In bacteria, this plays a role in attenuation of gene expression: operons encoding genes involved in amino acid biosynthesis often have a segment in the 5’ end of the open reading frame containing codons for the amino acid regulated by that operon (Yanofsky, 1981). Scarcity of the amino acid in question leads to fewer aminoacyl-tRNAs that correspond to those codons, leading to ribosomes pausing. Translational pausing allows secondary structures to form downstream of the paused ribosome, which eliminates a transcription termination signal, allowing the transcribing RNA polymerase to complete the transcript. Similar coding sequence

characteristics have been identified in operons for the biosynthesis of tryptophan, histidine, threonine, isoleucine, leucine, and phenylalanine. Upon biosynthesis of the amino acid, the paused ribosome can resume translation, triggering transcription termination downstream and reducing production of amino acid biosynthesis components (reviewed in (Kolter and Yanofsky, 1982)).

Ribosomes also pause on mRNAs encoding consecutive proline residues. Proline is a secondary amine, making it a poor peptidyl acceptor; its cyclic side chain affects the positioning of Pro-tRNA^{Pro} in the peptidyl-transferase center, making it also a poor peptidyl-donor (Doerfel et al., 2015). To resolve pausing on poly-proline stretches, the ribosome employs the dedicated factor EF-P (Doerfel et al., 2013). Structural studies have shown that EF-P binds between the ribosomal P site and E site and interacts with the CCA end of the P-site tRNA (**Figure 2.11**) (Huter et al., 2017a). Kinetic studies revealed that this interaction serves to steer the P site and A site tRNAs into an orientation more favorable for the peptidyl-transfer reaction (Doerfel et al., 2015).

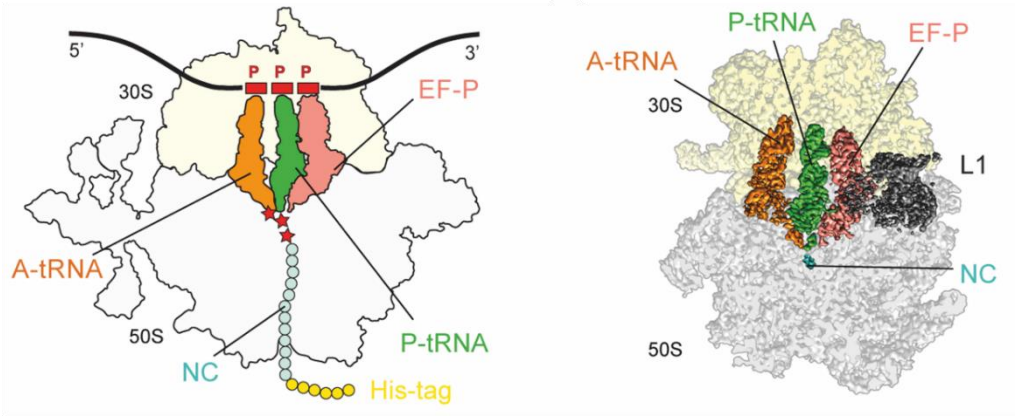

Figure 2.11. Schematic (left) and structural model (right) of EF-P bound to a ribosome stalled on a poly-proline sequence (prolines are indicated as red stars) (adapted from (Huter et al., 2017a)).

Finally, certain nascent peptide sequences also pause translation. The SecM peptide causes stalling during elongation on an RxGP motif, which is due to distortions in the peptidyl-transferase center caused by interactions with rRNA residues in the peptide exit tunnel (**Figure 2.12**) (Bhushan et al., 2011; Gumbart et al., 2012). The resulting stalled ribosomal complexes are very stable. The stalling is relieved by SecA, a protein encoded downstream of SecM. It has been proposed that SecA "pulls" SecM out of the peptide exit tunnel, allowing elongation to

proceed (Bhushan et al., 2011; Gumbart et al., 2012). This is an elegant mechanism to maintain the stoichiometry of bacterial secretion machinery: the Shine-Dalgarno sequence of SecA is exposed as a consequence of SecM stalling, and an abundance of SecA relieves SecM stalling which in turn downregulates SecA expression (Nakatogawa et al., 2004). Another example is the TnaC peptide, which is encoded upstream of genes tryptophanase and tryptophan permease genes. When tryptophan is abundant in the cell, free tryptophan binds to the ribosome and inhibits TnaC release by RF2 (Gong and Yanofsky, 2002; Martinez et al., 2014). This stalling prevents Rho-dependent transcription termination and results in expression of the downstream genes that facilitate breakdown of tryptophan. At low cellular tryptophan levels, translation termination can proceed on the TnaC peptide unimpeded.

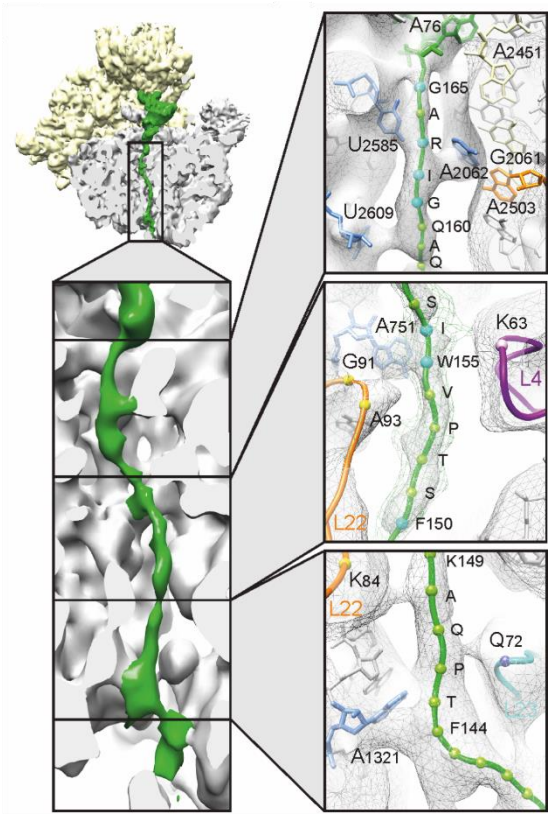

Figure 2.12. SecM (green) stalls the ribosome via interactions with the peptide exit tunnel (grey) (Bhushan et al., 2011).

One key similarity between proline-induced stalling and nascent peptide-induced stalling is the occupancy of the ribosomal A site. When the ribosome stalls on consecutive proline residues, the ribosomal A site is occupied by a Pro-tRNA^{Pro} (Huter et al., 2017a); the same can be said for SecM-induced stalling (Bhushan et al., 2011). On the other hand, ribosomes stalled by the TnaC peptide have a release factor in the ribosomal A site (Cruz-Vera et al., 2005). The

presence of either aminoacyl-tRNA or release factor ensures that these stalled ribosomes are not targeted for rescue by premature termination (Buskirk and Green, 2017).

2.2.2 Ribosome stalling resolved by premature termination

In the previous section, reversible instances of ribosome stalling are described. These cases are reversible in the sense that binding of an aminoacyl-tRNA or action of another protein factor relieves stalling and allows the ribosome to complete elongation and termination on an otherwise undamaged transcript (Buskirk and Green, 2017). In other instances, the ribosome can translate until the 3' end of the mRNA and stall due to the lack of an in-frame stop codon, resulting in a stalled ribosome that has an unoccupied A site. To resolve these non-stop stalled ribosomal complexes, premature termination allows the ribosome to be recycled while releasing an incompletely synthesized translation product (reviewed in (Starosta et al., 2014)).

Non-stop stalling can be caused by errors in decoding. Stop codon read-through, where the ribosome fails to decode the stop codon and continues translating into the 3'UTR of the transcript, has been shown to produce non-stop stalled ribosomes, for example when suppressor tRNAs that decode stop codons are expressed (Ueda et al., 2002). Aminoglycoside antibiotics bind to the 16S rRNA of the 30S subunit and interfere with the function of the decoding center (reviewed in (McCoy et al., 2011)). They often induce decoding errors that can lead to stop codon read-through or loss of the correct reading frame, moving the stop codon out of frame and thereby creating non-stop stalled ribosomes (Abo et al., 2002; Holberger and Hayes, 2009).

Another cause of non-stop stalling is the truncation of mRNAs. The lack of mRNA surveillance in bacteria, particularly mechanisms that monitor the 3' end of mRNAs, means that the ribosome cannot avoid initiating on damaged transcripts, as is discussed in section 2.1.2. In bacteria, mRNA turnover is mediated by 3'-5' cleavage by the exoribonuclease RNase II (Deutscher and Reuven, 1991), but this is commonly preceded by endonucleolytic cleavage in the 5' end of transcripts mediated by RNase E (Hui et al., 2014). Because translation initiation depends on sequence featured in the 5' UTR of mRNA, it is unlikely that regular mRNA turnover contributes significantly to non-stop stalling.

One source of truncated mRNAs is premature transcription termination. One example is the *E. coli lac* repressor LacI. LacI binds to two operator sites overlapping with the promoter,

thereby repressing transcription of the *lacZYA* gene. At high levels of LacI, it will also bind to a third operator site at the 3' end of the *lacI* gene itself, inducing premature transcription termination and regulating its own expression (Abo et al., 2000). Because translation in bacteria occurs co-transcriptionally, this can occur while there are translating ribosomes on the growing *lacI* transcript, and results in non-stop stalled ribosomes. Similar modes of transcription regulation have been identified in other organisms, for example the catabolite control protein CcpA in *B. subtilis* (Ujiie et al., 2009).

Furthermore, some early studies have suggested that translational pausing can lead to cleavage of the codon in the ribosomal A site (Hayes and Sauer, 2003; Sunohara et al., 2004). This has been observed in the context of consecutive proline residues, where both peptide bond formation and peptide release are slow (Hayes et al., 2002a; Roche and Sauer, 2001). Similarly, ribosomes stalled at rare codons were found to go through A-site mRNA cleavage (Hayes et al., 2002b; Roche and Sauer, 1999); these studies deal in particular with consecutive rare arginine codons. It should be mentioned that in most of these studies, mRNA truncation was inferred by studying SsrA-tagging, a product of tmRNA-SmpB mediated ribosome rescue that will be discussed in a later section. The mechanism of A-site mRNA cleavage is unclear; studies have found that in the absence of mRNA interferases such as RelE, MazF, ChpBK, YoeB, YafQ, and YhaV, ribosome pausing-induced mRNA cleavage is still observed (Garza-Sanchez et al., 2009; Hayes and Sauer, 2003). It has been proposed that RNase II plays a role, however further cleavage of the transcript in the ribosomal A site is required for SsrA-tagging (Garza-Sanchez et al., 2009), pointing to the involvement of other mRNA interferases.

2.2.3 mRNA truncation by toxin-antitoxin systems

An important source of truncated mRNAs is through the action of bacterial toxin-antitoxin systems. The toxin is usually a globular protein, the activity of which is inhibited when the labile antitoxin protein wraps around it. The two proteins are often encoded together on a plasmid or in the bacterial chromosome, so that the toxin is constitutively bound by the antitoxin and therefore inactive. The antitoxin is degraded under specific conditions such as stress, which frees the toxin to take part in the stress response (reviewed in (Yamaguchi et al., 2011)). It has been proposed that toxin-antitoxin systems function in programmed cell death (Gerdes et al., 1997) and nutritional stress (Gerdes, 2000). There are several types of toxin-antitoxin systems, of which type II toxin-antitoxins target the ribosome, and produce

truncated mRNAs in response to certain stress conditions (reviewed in (Starosta et al., 2014)). In this section, mRNA interferases, or type II toxin-antitoxin systems that cleave mRNAs, are discussed.

The MazEF toxin-antitoxin system differs from other mRNA interferases in that it cleaves mRNA independently of the ribosome. The toxin MazF cleaves mRNA at 3-, 5-, and 7-nucleotide motifs (Cook et al., 2013), and is inactivated by the antitoxin MazE, which blocks the mRNA binding site on MazF (**Figure 2.13a**) (Simanshu et al., 2013). Degradation of MazE is triggered by heat stress, starvation, oxidative stress, DNA damage (Hazan et al., 2004). Some studies have found that MazEF cleaves ACA sequences upstream of start codons (**Figure 2.13b**), effectively creating leaderless mRNAs (Vesper et al., 2011). Concurrently, it was suggested that MaxF cleavage also targets the ribosomal 16S rRNA, which removes the anit-Shine-Dalgarno sequence (Moll and Engelberg-Kulka, 2012). These findings led to the hypothesis that MazF activates an alternative translation program in which specialized ribosomes translate leaderless mRNAs. However, a subsequent study used ribosome profiling to construct a global analysis of MaxF-mediated mRNA cleavage, and found no preference for either the 5' UTR or the anti-Shine-Dalgarno sequence (Culviner and Laub, 2018). It was instead proposed that MazF reduces overall translation activity by cleaving multiple sites in mRNA, and by targeting transcripts encoding ribosomal proteins as well as rRNA. Notably, Culviner and colleagues also found that ribosome footprints increased by ~8 fold on the mRNA-like domain of tmRNA, indicating that MazF activity produces non-stop stalled ribosomes that require rescue by tmRNA-SmpB.

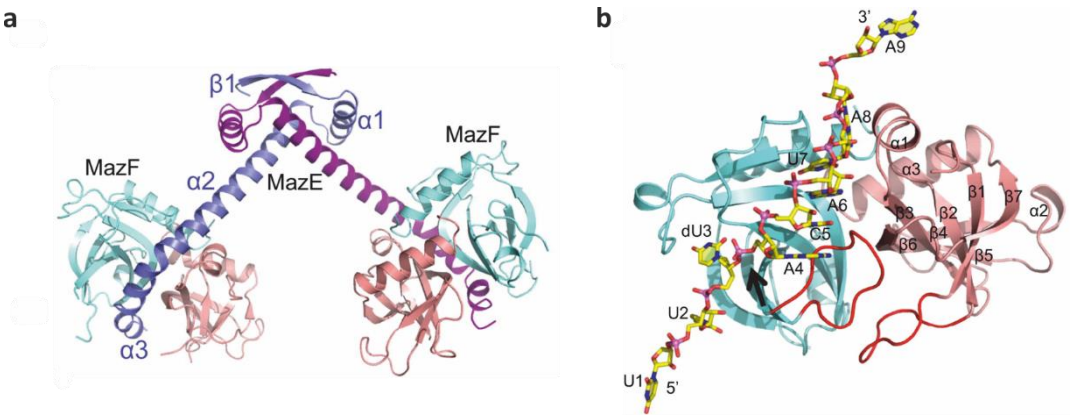

Figure 2.13. Structure of *Bacillus subtilis* toxin MazF dimers (cyan and red) **(a)** in complex with the antitoxin MazE (blue and purple) and **(b)** bound to the target mRNA sequence (yellow) (adapted from (Simanshu et al., 2013)).

In contrast to the MazEF system, the RelBE toxin-antitoxin system is ribosome-dependent. The mRNA cleavage activity of RelE is only active when RelE is bound to the ribosome (Pedersen et al., 2003). To inactivate RelE, RelB wraps around the toxin (**Figure 2.14a**), reaching into the active site and at the same time preventing RelE from entering the ribosomal A site (Boggild et al., 2012; Neubauer et al., 2009). RelE is believed to be activated in response to amino acid starvation (Christensen et al., 2001; Pedersen et al., 2002), upon which Lon protease digests the antitoxin RelB, freeing RelE to bind to ribosomes stalled with an unoccupied A site (Christensen et al., 2001; Neubauer et al., 2009) (**Figure 2.14c**). In previous studies, it was proposed that RelBE targets the stop codons UAG and UGA, as well as the sense codons UCG and CAG (Pedersen et al., 2003). However, a more recent ribosome profiling study, RelBE was found to have a general preference for cleavage after C and before G (Buskirk and Green, 2017). The same study also revealed that RelE cleavage most often occurs after the second codon of in the vacant A site, leaving ribosomes stalled with two nucleotides extending past the ribosomal P site (Buskirk and Green, 2017). RelE activity stops translation in its tracks, allowing the cell to divert resources towards pathways that overcome stress. Resolving the resulting non-stop stalled ribosomes, however, requires the action of rescue mechanisms.

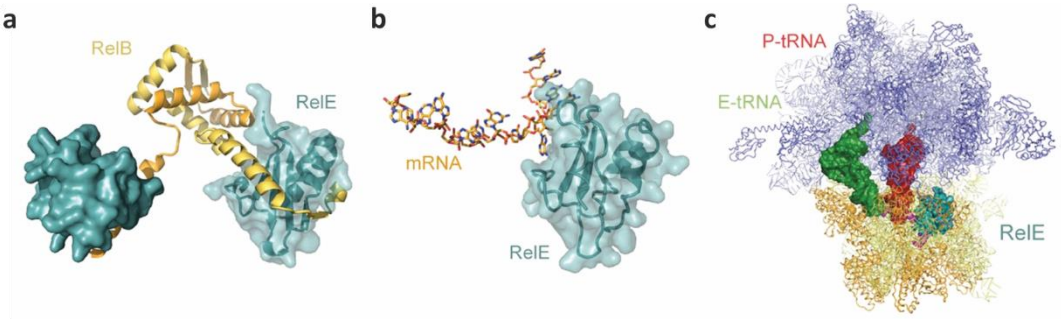

Figure 2.14. Structure of the *E. coli* toxin RelE **(a)** in complex with the antitoxin RelB, **(b)** bound to mRNA, and **(c)** bound to the A site of the 70S ribosome (adapted from (Starosta et al., 2014)).

Other ribosome-dependent type II toxin-antitoxin systems in *E. coli* include YefM/YeoB, DinJ/YafQ, YafNO, and YgjNM, most of which are also activated by amino-acid starvation (reviewed in (Starosta et al., 2014)). Like RelE, YoeB catalyzes the cleavage of mRNA in the ribosomal A site in the absence of YefM (Feng et al., 2013). A recent study proposed that YoeB is activated during heat shock, although global protein synthesis is not inhibited by YoeB-induced mRNA cleavage (Janssen et al., 2015). The authors therefore argue that instead of slowing down translation, the primary function of YoeB is to target stalled ribosomes and

digest the associated transcript, effectively creating more ideal substrates for ribosome rescue mechanisms so that the ribosomes can be recycled. The YafQ toxin in the DinJ/YafQ toxin-antitoxin system, on the other hand, binds to the 50S subunit of the ribosome and cleaves mRNA. It is believed that the antitoxin DinJ is degraded in response to DNA damage (Armalyte et al., 2012; Prysak et al., 2009).

2.2.4 Beyond non-stop stalling

Stalling of the 70S ribosome has thus far been discussed. However, it has been shown that heat shock in bacteria causes translating ribosomes to dissociate into the 30S subunit and the peptidyl-tRNA-bound 50S subunit (Korber et al., 2000). For these 50S subunits to participate in translation initiation, the peptidyl-tRNA must be hydrolyzed. It has been proposed that the protein Hsp15, which is upregulated upon heat shock, plays a role in the rescue of these subunits (Jiang et al., 2009). Hsp15 interacts with both the 23S rRNA and with the peptidyl-tRNA, stabilizing the peptidyl-tRNA in the P site (Jiang et al., 2009). This allows the A site to remain vacant. Jiang and colleagues postulated that factors with peptidyl-tRNA hydrolysis activity can then bind to the A site and release the nascent peptide (**Figure 2.15**). Given that canonical release factor activity is contingent on stop codon recognition (Jin et al., 2010; Korostelev et al., 2008; Laurberg et al., 2008; Weixlbaumer et al., 2008), it was proposed that hydrolysis could be catalyzed by stop codon-independent release factors such as ArfB (Jiang et al., 2009).

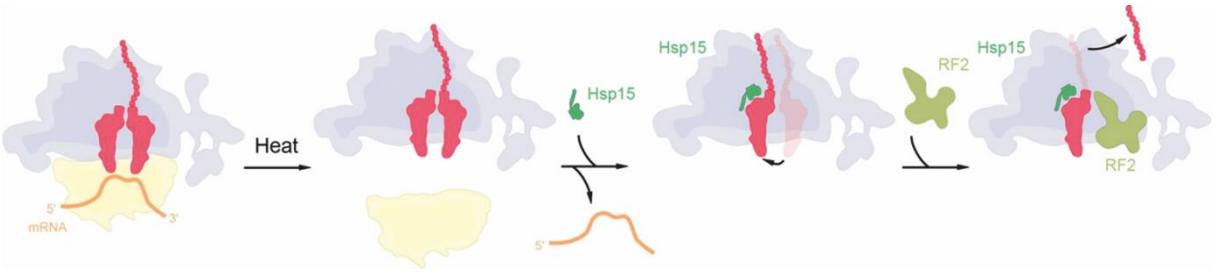

Figure 2.15. Model of peptidyl-tRNA (pink) translocation mediated by Hsp15 (green). The vacated ribosomal A site is a potential binding site for rescue factors or release factors that can hydrolyze the peptidyl-tRNA. RF2 is shown in olive green (Starosta et al., 2014).

2.3 Rescue mechanisms for non-stop stalling

The rescue of non-stop stalled ribosomes requires hydrolysis of the peptidyl-tRNA in the P site, after which the ribosome recycling machinery (described in section 2.1.5) can recycle the ribosomal subunits for subsequent rounds of translation. In bacteria, this is accomplished in two ways: rescue factors tmRNA-SmpB (the components of the *trans*-translation pathway) (**Figure 2.16a**) and ArfA (**Figure 2.16b**) effectively serve as interfaces between the stalled ribosome and canonical release factors, either by introducing a stop codon (tmRNA-SmpB) (Keiler et al., 1996), or by facilitating release factor binding (ArfA) (Chadani et al., 2010). Alternatively, ArfB (**Figure 2.16c**) is a peptidyl-tRNA hydrolase that acts as a stop codon-independent release factor (Chadani et al., 2011b; Handa et al., 2011).

It has been reported that in *E. coli*, 0.4% of all synthesized peptides are tagged with the ssrA degradation tag of the tmRNA-SmpB system (Moore and Sauer, 2005). More recently, analysis of nascent polypeptides showed that an estimated 2-4% of translation events result in non-stop stalling (Ito et al., 2011). It appears that non-stop stalling is a common occurrence in the cell, and recue mechanisms play an important role in maintaining the cell's capacity for protein synthesis.

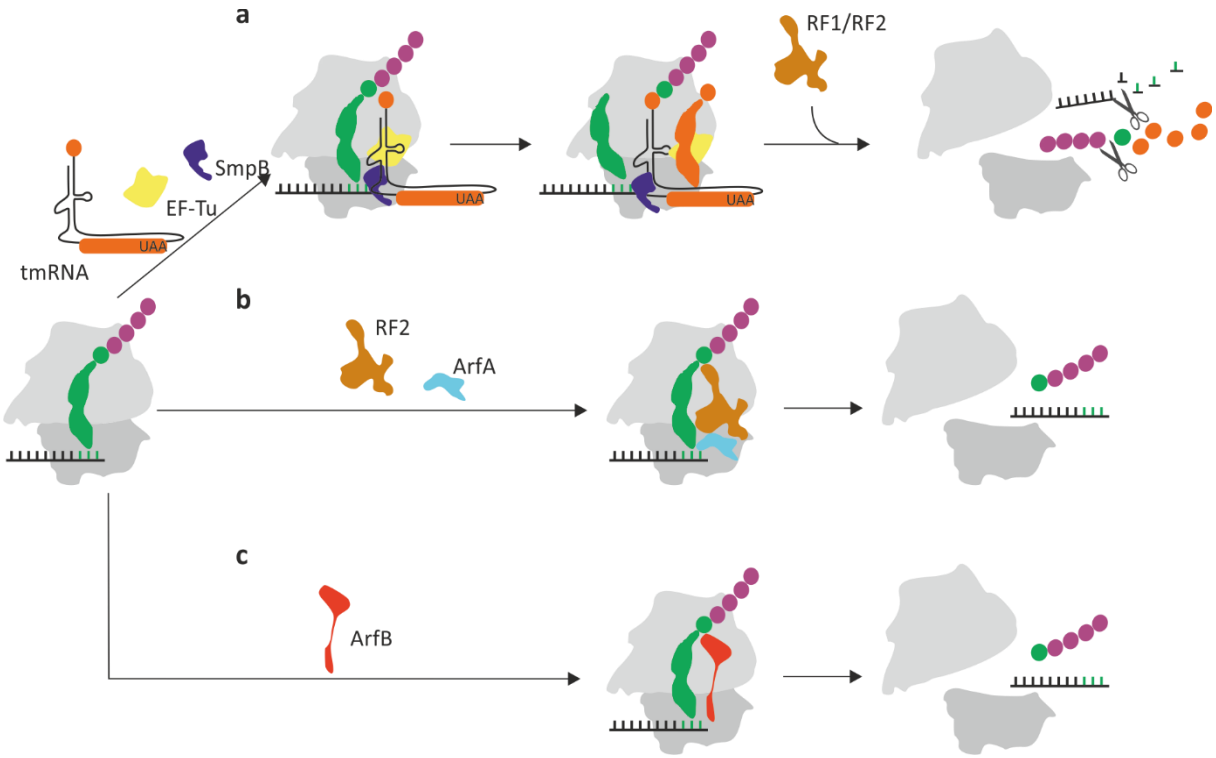

Figure 2.16. Three rescue mechanisms for non-stop stalled ribosomes in *E. coli*: **(a)** tmRNA-SmpB-mediated *trans*-translation, **(b)** ArfA, and **(c)** ArfB.

2.3.1 *Trans*-translation

Trans-translation is the most well-studied bacterial rescue mechanism for resolving non-stop stalled ribosomal complexes. It involves restarting translation by switching from the truncated mRNA template to the coding sequence on the tmRNA molecule, which ends with a stop codon that allows translation to be terminated by canonical release factors. Importantly, the coding sequence of tmRNA encodes a peptide degradation tag, which marks the released nascent peptide for degradation by the ClpXP protease (reviewed in (Janssen and Hayes, 2012)).

The main components that perform trans-translation are the RNA molecule tmRNA and the small protein SmpB, along with elongation factors EF-Tu, EF-G, and release factors RF1 or RF2 (reviewed in (Himeno et al., 2014)). The 5' and 3' ends of tmRNA form the tRNA-like domain (**Figure 2.17**), which is similar to the acceptor stem of canonical tRNA. Alanyl-tRNA synthetase recognizes the G:U wobble base pair and charges it with alanine (Komine et al., 1994). Outside of the tRNA-like domain, E. coli tmRNA contains 4 pseudoknots, the function of which is unknown (Nameki et al., 2000) (**Figure 2.17**). However in between pseudoknots 1 and 2 is a small reading frame that encodes the peptide sequence AANDENYALAA followed by the stop codon UAA (Keiler et al., 1996).

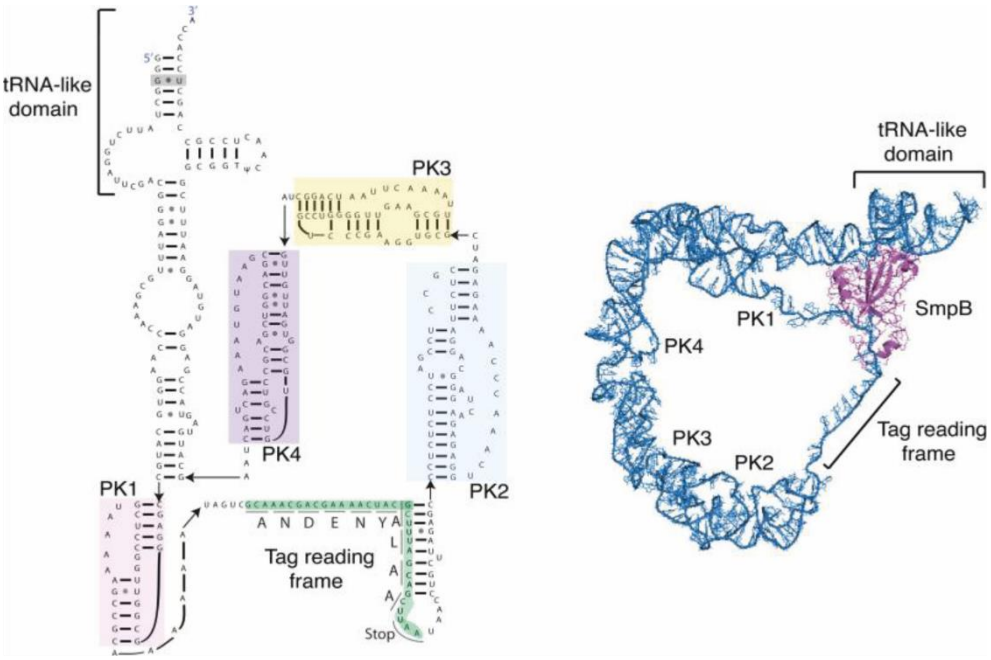

Figure 2.17. The secondary structure (left) and atomic model (right) of tmRNA. PK1 to PK4 indicate the location of the four pseudoknots. The ssrA tag is indicated in green, and the GU base pair involved in aminoacylation is shaded (Keiler and Ramadoss, 2011).

In the first step of *trans*-translation, the small protein SmpB binds to the tRNA-like domain of tmRNA, taking the place where the anticodon loop of a tRNA would be (**Figure 2.17**), suggesting that the tRNA-like domain and SmpB together mimic tRNA (Bessho et al., 2007; Kurita et al., 2007). SmpB has a globular core and a C-terminal tail rich in positive amino acids, which renders it unstructured in solution (Dong et al., 2002; Someya et al., 2003). Studies have shown that binding of SmpB protects tmRNA from degradation, and plays an important role in facilitating the aminoacylation with Ala (Barends et al., 2001; Hanawa-Suetsugu et al., 2002; Shimizu and Ueda, 2002). Following aminoacylation, tmRNA-SmpB forms a quaternary complex with EF-Tu and GTP and binds to the ribosomal A site. A crystal structure of tmRNA-SmpB on the *Thermus thermophilus* ribosome revealed that Y126 of SmpB stacks with the decoding center nucleotide G530, and the decoding bases A1492 and A1493 are ”flipped out” (**Figure 2.18**) (Neubauer et al., 2012). While the conformation of these bases differ from canonical decoding during translation elongation (see section 2.1.3), they still induce a closed conformation of the 30S subunit, which triggers GTP hydrolysis by EF-Tu, allowing the aminoacylated tmRNA to accommodate into the A site (Neubauer et al., 2012).

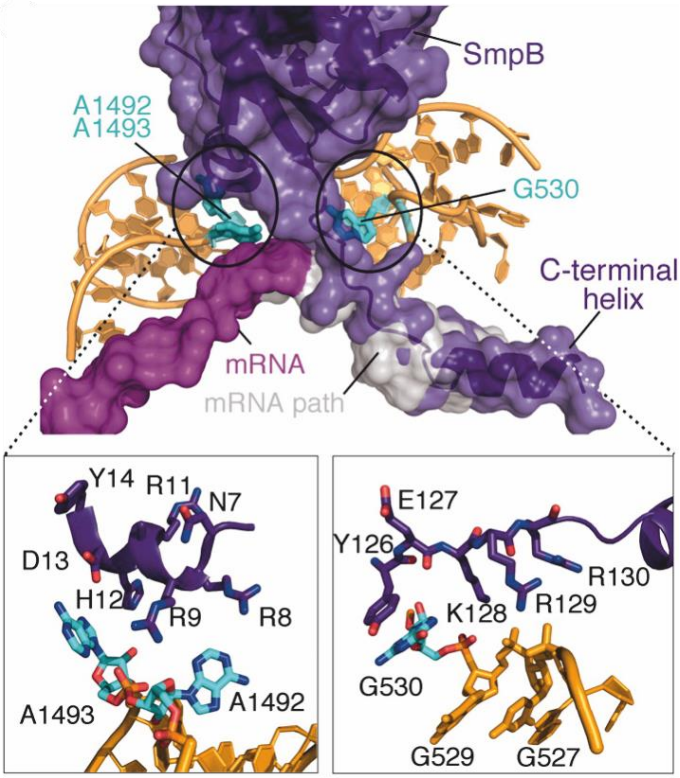

Figure 2.18. Conformation of the *T. Thermophilus* ribosome decoding center in the presence of SmpB (adapted from (Neubauer et al., 2012)).

A recent, high-resolution cryo-EM structure of the *E. coli* tmRNA-SmpB in several states during *trans*-translation showed that during accommodation, the globular domain of SmpB rotates into the A site, and the acceptor arm of the tRNA-like domain moves into the peptidyl-transferase center (Rae et al., 2019). This motion mimics the distortion of tRNA during the accommodation step of canonical elongation (Reviewed in (Rodnina et al., 2005)).

With tmRNA-SmpB occupying the ribosomal A site, peptide bond formation transfers the nascent chain from the P-site tRNA to tmRNA. In the following steps, tmRNA must be translocated into the P site, and the first codon of the tag sequence must be presented in the A site. This process is facilitated by EF-G (Ramrath et al., 2012); it has been shown that EF-G promotes the release of deacylated tRNA and the truncated mRNA from the ribosome (Ivanova et al., 2005).

Notably, the mRNA features such as a Shine-Dalgarno sequence that establish a reading frame for the ribosome are not present on the mRNA-like domain of tmRNA. Only recently did high resolution cryo-EM structures reveal that the final couple of residues of the SmpB C-terminal tail interacts with the first few nucleotides of the mRNA-like domain (Rae et al., 2019). Previous studies had shown that the nucleotides preceding the first codon of the tag sequence are essential for positioning the first codon (Konno et al., 2007; Lee et al., 2001); together, these findings suggest that the SmpB C-terminal tail is important for maintenance of the tmRNA reading frame.

Through each cycle of elongation, tmRNA-SmpB moves stepwise from the A site through the P site, and finally past the E site (**Figure 2.19**) (Rae et al., 2019). The switch from the truncated mRNA to the coding sequence on tmRNA is mediated by the flipping of the SmpB C-terminal tail. During accommodation, the C-terminal tail is folded into an α-helix in the mRNA entry channel in the A site (**Figure 2.19** steps 2 and 3) (Rae et al., 2019; Ramrath et al., 2012). Following accommodation, the α-helix flips into the mRNA entry channel in the E site, with glycine 132 acting as a hinge during this dramatic structural rearrangement (**Figure 2.19** step 5) (Rae et al., 2019). This frees up the mRNA entry channel in the A site, allowing the mRNA-like domain of tmRNA to bind. *Trans*-translation requires truncated mRNA to function (Ivanova et al., 2004; Kurita et al., 2014), which can be explained by the central role of the C-terminal tail in binding to the A site and E site parts of the mRNA path. When mRNA is present in the mRNA entry channel it would compete with the SmpB C-terminal tail for binding, allowing

SmpB to discriminate between non-stop stalled ribosomes and ribosomes on intact mRNA (Miller and Buskirk, 2014).

As translation of the tmRNA coding sequence progresses, the head of SmpB is displaced not into the E site, but towards the solvent side of the ribosome, so that it does not clash with the deacylated E site tRNA (**Figure 2.19** steps 8 and 9)(Rae et al., 2019). Throughout this process, pseudoknot 2 of tmRNA maintains contact with ribosomal protein S3, which coordinates the position of tmRNA (Rae et al., 2019).

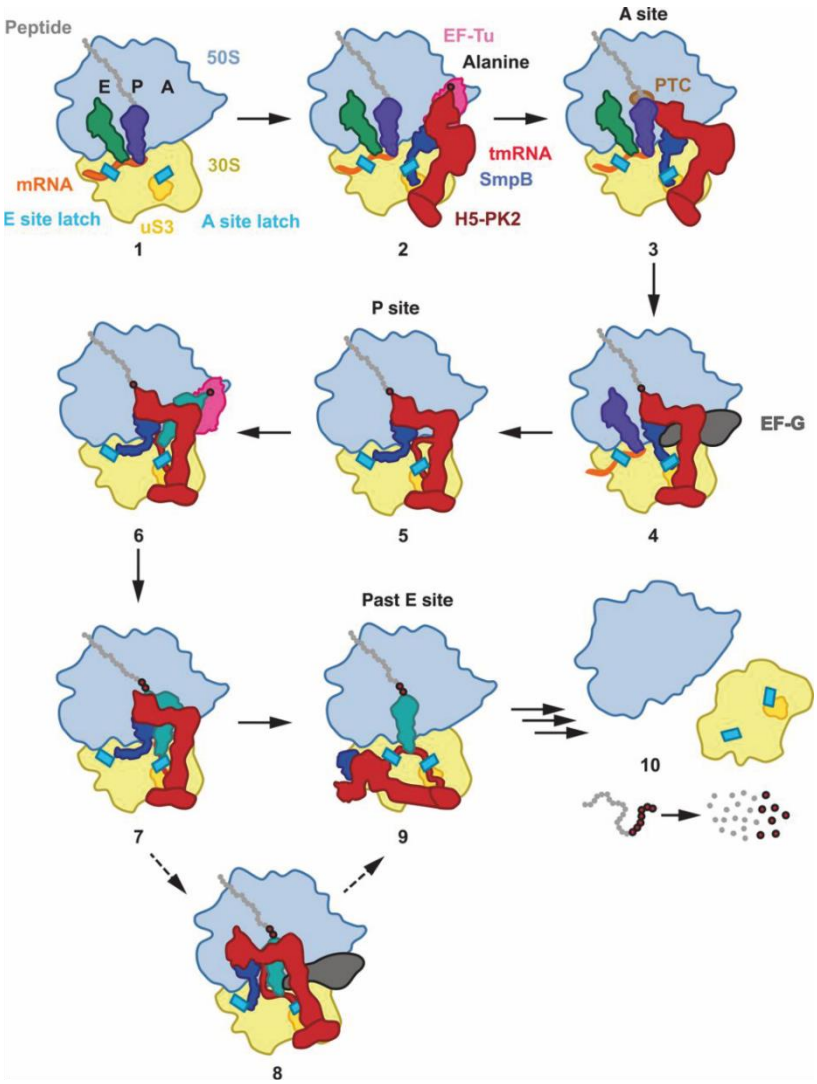

Figure 2.19. Mechanism of tmRNA-SmpB-mediated *trans*-translation according to recently published cryo-EM structures (Rae et al., 2019).

The coding sequence of tmRNA ends with the stop codon UAA, which can be recognized by both RF1 and RF2 (see section 2.1.4). Termination occurs just as during regular translation, and the ribosome is recycled. The released nascent peptide, which is the truncated translation

product tagged with the ssrA sequence AANDENYALAA (Keiler et al., 1996), is targeted by cellular proteases for degradation. In *E. coli*, these include proteases FtsH and Lon, which consume ATP in order to unfold proteins and translocate them into the protease lumen (Choy et al., 2007; Herman et al., 1998). Within one mechanism, tmRNA-SmpB rescues non-stop stalled ribosomes, and also ensures the degradation of the unfinished translation product.

Trans-translation seems to be the most universally utilized ribosome rescue system in bacteria; tmRNA and SmpB gene sequences have been annotated in almost all sequenced bacterial genomes. While the consistent level of non-stop ribosome stalling points to tmRNA-SmpB being a translational quality control system under all conditions (Ito et al., 2011; Moore and Sauer, 2005), in certain bacterial species it also plays specific physiological roles. In *Bacillus subtilis* and *Strepomyces coelicolor*, for example, tmRNA-SmpB regulates sporulation (Abe et al., 2008; Barends et al., 2010). In *Salmonella typhimurium* and *Yersinia pestis*, which causes typhoid fever and plague, respectively, deletion of tmRNA-SmpB leads to reduction of virulence (Julio et al., 2000; Okan et al., 2010), suggesting a role for *trans*-translation in bacterial pathogenesis.

Interestingly, recent studies have also implicated *trans*-translation in the monitoring of co-translational protein folding. While investigating ssrA-tagged substrates, Hayes and colleagues found that overexpressed large multidomain proteins are tagged in various sites (Hayes and Keiler, 2010). This tagging activity was not correlated with RNase activity or rare codons, but is increased upon heat shock and deletion of the ribosome-associated DnaK chaperone (Calloni et al., 2012; Hayes and Keiler, 2010). One possible explanation is that heat shock and loss of DnaK increases the probability of misfolding of the nascent peptide during translation, however because DnaK is involved in many processes in the cell, this connection is somewhat tenuous. Rather, it serves to highlight the need to further investigate ssrA-tagged peptides, in order to understand the wider physiological roles of *trans*-translation.

2.3.2 ArfA

The importance of ribosome rescue has been known for over two decades, but until relatively recently it was unclear why deletion of tmRNA-SmpB is not lethal in many bacteria, for example in *E. coli* (Komine et al., 1994). Chadani and colleagues performed mutagenesis on *ΔssrA* strains and identified mutants that required tmRNA-SmpB for growth (Chadani et al., 2010). In a subsequent suppressor assay, the researchers discovered that supplying these

mutants with plasmids carrying the gene *ydhL* rescued the growth defect (Chadani et al., 2010). *ydhL* was renamed *arfA*, for alternative ribosome rescue factor.

ArfA is a small protein of approximately 70 amino acids, with only the first 47 essential for its function (Garza-Sanchez et al., 2011). Notably, ArfA alone did not exhibit peptidyl-tRNA hydrolysis activity on stalled ribosomes *in vitro*, but could rescue stalled ribosomes when supplemented with *E. coli* S30 extract, indicating that additional factors are required for ArfA-mediated ribosome rescue (Chadani et al., 2011b). Subsequent studies using the PURE system, which is an *in vitro* coupled transcription and translation reaction mix, identified RF2 as the necessary and sufficient component that facilitates ArfA-mediated rescue (Chadani et al., 2012; Shimizu, 2012). Since RF2 is the component carrying the GGQ-motif that hydrolyzes peptidyl-tRNA, it was hypothesized that ArfA recapitulates the interaction between RF2 and stop codons, allowing RF2 to catalyze peptide release despite the absence of a stop codon (Chadani et al., 2012; Shimizu, 2012).

Several recent structural studies have clarified how ArfA recruits RF2 and facilitates peptidyl-tRNA hydrolysis (Demo et al., 2017; Huter et al., 2017b; James et al., 2016; Ma et al., 2017; Zeng et al., 2017). ArfA binds to the small subunit of the ribosome (**Figure 2.20a**). While its C-terminal residues reach into the mRNA entry channel, the N-terminal and middle portion of the protein interacts extensively with secondary structure elements of domain 3 and domain 2 of RF2. It was suggested that the binding of the C-terminal residues in the mRNA entry channel causes ArfA to reject ribosomes stalled with mRNA extending past the P site (Kurita et al., 2014). Interestingly, no interaction between ArfA and the SPF motif of RF2 was observed. The SPF motif, as described in section 2.1.4, is responsible for stop codon recognition during canonical termination (Korostelev et al., 2008; Korostelev et al., 2010; Laurberg et al., 2008). This finding made it apparent that ArfA does not recruit RF2 by mimicking stop codons. Rather, the interactions between ArfA and RF2 serve to directly stabilize a specific conformation of the RF2 switch loop (Demo et al., 2017; Huter et al., 2017b; James et al., 2016; Ma et al., 2017; Zeng et al., 2017). This conformation of the switch loop stabilizes RF2 in its open conformation (**Figure 2.20b**). Similar to canonical termination, the open conformation of RF2 places the GGQ motif in the optimal position in the peptidyl-transferase center for peptidyl-tRNA hydrolysis (Korostelev et al., 2008; Laurberg et al., 2008).

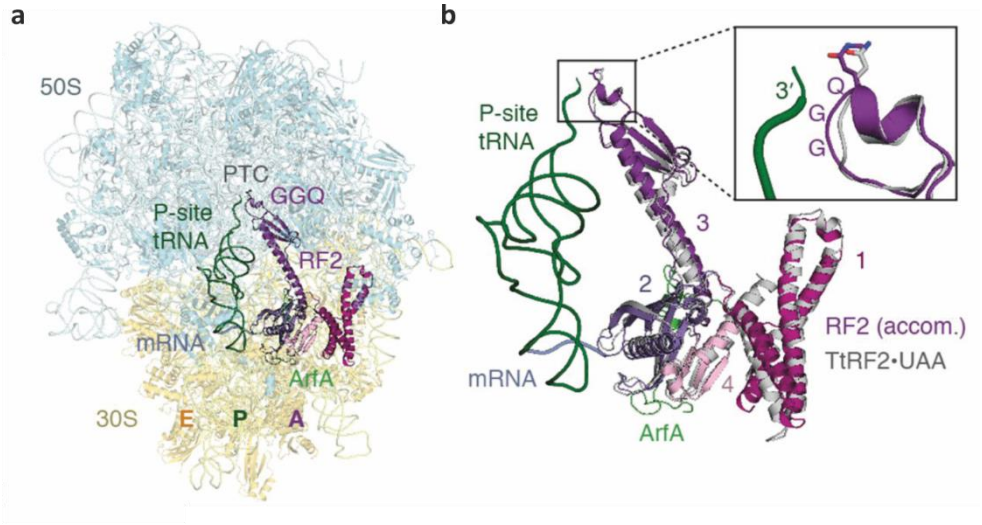

Figure 2.20. Cryo-EM structure of ArfA on the 70S *E. coli* ribosome. **(a)** ArfA and RF2 bound to the ribosome. **(b)** Close up view of the interaction between the P-site tRNA (green), ArfA (pink), and accommodated RF2 (purple) (Adapted from (James et al., 2016)).

During canonical termination, the switch loop of release factors interacts with the decoding center residues A1492, A1493, G530, and A1913, which contributes to the stabilization of the open conformation of the release factors (Korostelev et al., 2008; Laurberg et al., 2008). However, these interactions do not occur between RF2 and the ribosome with ArfA present. Instead, Glu 30 of ArfA stacks with G530 (**Figure 2.21a**), maintaining G530 in the same *anti* conformation as is observed during stop codon recognition (**Figure 2.21b**). Meanwhile, A1493 is flipped out, and A1492 stacks with A1913 of the 16S rRNA (Demo et al., 2017; Huter et al., 2017b; James et al., 2016; Ma et al., 2017; Zeng et al., 2017). This conformation is reminiscent of what was observed in tmRNA-SmpB bound ribosomes (Neubauer et al., 2012).

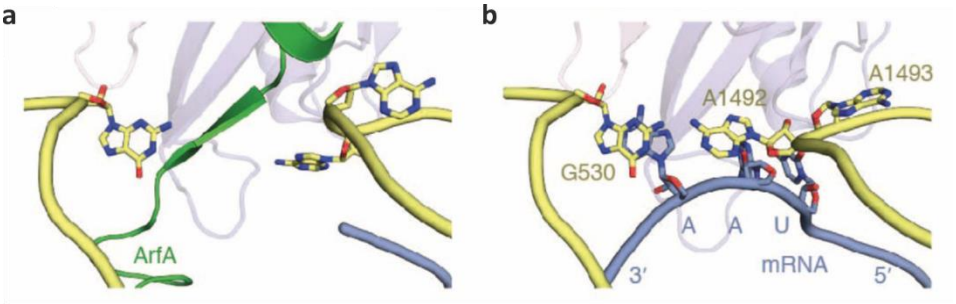

Figure 2.21. Conformation of decoding center residues during **(a)** ArfA-mediated ribosome rescue and **(b)** canonical termination (James et al., 2016).

Beyond certain structural similarities, there is a strong physiological connection between ArfA and tmRNA-SmpB. The *arfA* transcript contains a stem loop structure that is cleaved by

RNaseIII, resulting in a non-stop mRNA (Garza-Sanchez et al., 2011; Schaub et al., 2012). When tmRNA-SmpB is present, non-stop stalling on the truncated *arfA* transcript is resolved via *trans*-translation (discussed in section 2.3.1), leading to ssrA-tagging and degradation of ArfA. In the absence of tmRNA, the truncated form of ArfA is expressed (Chadani et al., 2011a; Garza-Sanchez et al., 2011; Schaub et al., 2012). In this scenario, it is unclear which mechanism releases ArfA from the non-stop stalled ribosomes. The regulation of ArfA by tmRNA-SmpB strongly suggests that ArfA acts as a back-up rescue mechanism to *trans*-translation; only when the tmRNA-SmpB is overwhelmed does ArfA come into play.

While tmRNA-SmpB is found in most sequenced bacterial genomes, ArfA has only been identified in some species of β- and γ-proteobacteria (Schaub et al., 2012). It is possible that in other species, mechanisms similar to that of ArfA exist; one ArfA-like factor was recently discovered in *Francisella tularensis*. The factor in question was named ArfT, and it rescues non-stop stalled ribosomes by recruiting RF1 (Goralski et al., 2018). Like ArfA, ArfT has positively charged residues on its C-terminal end that may mediate binding to the mRNA entry channel. Further studies are required to elucidate how it interacts with the ribosome and with RF1, and structural comparisons between ArfA and ArfT could shed light on why these factors only recruit one release factor and not the other.

2.3.3 ArfB

ArfB, the third non-stop rescue factor, was first identified as a putative peptidyl-tRNA hydrolase because its sequence bore strong similarities to domain 3 of release factors, and because it contains the GGQ motif that in release factors catalyzes peptidyl-tRNA hydrolysis (Handa et al., 2011; Korostelev et al., 2008; Laurberg et al., 2008). When added to non-stop stalled ribosomes assembled using the PURExpress system, ArfB exhibited peptidyl-tRNA hydrolysis activity (Handa et al., 2011).

In a subsequent study, ArfB was found to be a multicopy suppressor of synthetic lethality in a *ΔssrA ΔarfA E. coli* strain. When supplied with multiple copies of plasmids carrying various *E. coli* genes, a plasmid carrying the *yaeJ*, the gene that encodes ArfB, was found to restore cell growth in this strain (Chadani et al., 2011b). While it should be noted that endogenous levels of ArfB expression was not sufficient to rescue the synthetic lethality phenotype, this confirmed that ArfB has ribosome rescue activity *in vivo*.

ArfB consists of 140 amino acids. Mutagenesis studies revealed that it is indeed the GGQ motif in the N-terminal domain that mediates peptidyl-tRNA hydrolysis (Chadani et al., 2011b; Handa et al., 2011). It was also shown that the last 40 C-terminal residues are essential for the ribosome rescue activity of ArfB (Chadani et al., 2011b). Furthermore, based on sucrose gradient centrifugation assays, whereby polysomes, 70S ribosomes, and ribosomal subunits were separated based on their sedimentation rate, it was postulated that ArfB is a 70S ribosome-bound factor (Chadani et al., 2011b; Handa et al., 2011).

The redundancy of ArfB in *E. coli*, as well as the apparent lack of a direct regulatory relationship with tmRNA-SmpB and ArfA (discussed in section 2.3.2), led to speculation on the function of ArfB. In the early biochemical characterization studies of ArfB, it was shown that ArfB catalyzed peptidyl-tRNA hydrolysis when incubated with ribosomes stalled on rare codon clusters in the PUREsystem, which have mRNA extending past the P site (Handa et al., 2011; Shimizu, 2012). Since both tmRNA-SmpB and ArfA show marked decrease in rescue activity on ribosomes stalled with mRNA within the mRNA entry channel (Ivanova et al., 2004; Kurita et al., 2014), these results led to the hypothesis that ArfB is less sensitive to mRNA length and serves to also rescue ribosomes stalled in the middle of mRNA (Handa et al., 2011; Shimizu, 2012).

In a crystal structure of ArfB bound to the *Thermus thermophilus* ribosome, it was shown that ArfB has a globular N-terminal domain, a long flexible linker that spans approximately 40 Å on the ribosome, and a C-terminal tail that forms an α-helix (**Figure 2.22a**) (Gagnon et al., 2012). Crucially, the C-terminal tail is unstructured in an NMR structure (Kogure et al., 2014), but in its bound form is folded within the mRNA entry channel (**Figure 2.22b**). It is worth noting that C-terminal tails rich in positively charged residues that bind in the mRNA entry channel is a common feature among the tmRNA-SmpB, ArfA, and ArfB rescue systems. Gagnon and colleagues observed that binding of the C-terminal tail would clash sterically with mRNA extending past the P site, casting into doubt how ArfB might mediate rescue of ribosomes stalled on rare codon clusters. Based on this structure, it was proposed that the C-terminal tail of ArfB probes the mRNA entry channel, and if the channel is empty, it moves the N-terminal domain through the flexible linker, thereby positioning the GGQ motif next to the CAA end of the P-site tRNA for peptidyl-tRNA hydrolysis (Gagnon et al., 2012).

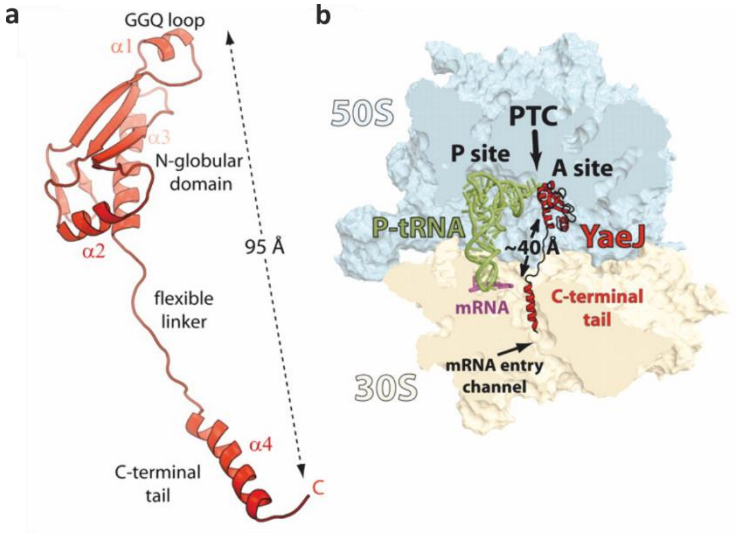

Figure 2.22. Crystal structure of **(a)** ArfB bound to the **(b)** *Thermus thermophilus* ribosome (adapted from (Gagnon et al., 2012)).

The crystal structure also provided insights into the decoding center of the ribosome during ArfB-mediated ribosome rescue. In this model, G530 stacks with Arg 118 of ArfB (**Figure 2.23a**), while A1492 is partially flipped out (**Figure 2.23b**) (Gagnon et al., 2012). Pro 110 of ArfB stacks with A1493 and A1913, which may serve as an anchor for the flexible linker. The conformation of these decoding center residues avoids steric clashes with the ArfB C-terminal tail (**Figure 2.23b**) (Gagnon et al., 2012). Intriguingly, the final 10 residues of ArfB were not resolved in this structure, even though they were shown to be essential for ribosome binding (Handa et al., 2011).

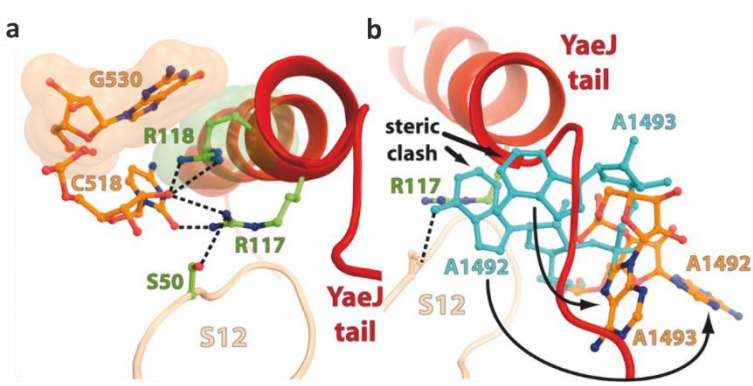

Figure 2.23. Configuration of the decoding center residues **(a)** G530, **(b)** A1493 and A1492 with ArfB bound to the ribosome (in orange). ArfB is labeled as YaeJ in the graph, and the blue nucleotides indicate the orientations of A1493 and A1492 when a tRNA occupies the ribosomal A site (adapted from (Gagnon et al., 2012)).

While not as widely found in bacteria as tmRNA-SmpB, ArfB is conserved in more species than ArfA, with 34% of sequenced bacterial species containing ArfB homologs. Despite the strong evolutionary conservation, ArfB does not appear to be essential in bacteria (Feaga et al., 2014). In eukaryotes, on the other hand, ArfB homologs exist in all species from yeast to humans (Duarte et al., 2012). These homologs are targeted to mitochondria, which according to the endosymbiotic theory, could indicate that ArfB was present in alphaproteobacteria that were engulfed to form mitochondria (reviewed in (Martin et al., 2015)).

The best-studied ArfB homolog is ICT1, which is a nuclear-encoded protein present in human mitochondria (Richter et al., 2010). Solution structures of ICT1 show striking similarities to ArfB (**Figure 2.24**). In addition to a very similar catalytic domain (Handa et al., 2010), ICT1 also has a C-terminal tail rich in positive residues; many of the residues in this region that are highly conserved in ArfB are also conserved in ICT1 (Akabane et al., 2014; Kogure et al., 2014). Homology modeling using the crystal structure of ArfB and the cryo-EM structure of ICT1 also suggested that the C-terminal tail of ICT1 folds into an α-helix bound in the mRNA entry channel (Lind et al., 2013). Based on these structural comparisons and sequence analyses, it is tempting to assume that these ICT1 residues interact with the mitoribosome in a similar way to how the ArfB C-terminal tail interacts with the bacterial ribosome.

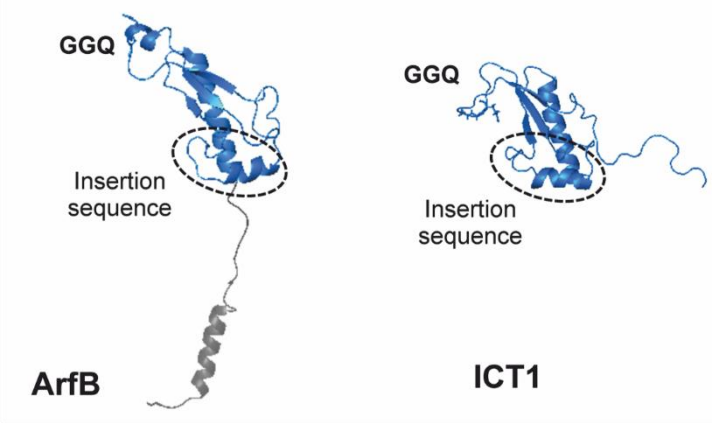

Figure 2.24. Comparison of the ArfB crystal structure and the ICT1 solution structure (adapted from (Akabane et al., 2014)).

ICT1 is essential for cell viability (Richter et al., 2010), though its exact function in human mitochondria is still unclear. Studies in which ICT1 was added to bacterial translation systems show that similarly to ArfB, it can catalyze peptidyl-tRNA hydrolysis on ribosomes stalled on non-stop mRNAs, and expressing ArfB could rescue the lethal phenotype in ICT1-deficient

human cells (Feaga et al., 2016). However, cryo-EM structures of the human mitochondrial ribosome cast doubt on the functional role of ICT1. The structures showed that ICT1 is incorporated into the mitoribosomal large subunit, and it is named mL62 (formerly MRPL58) (Amunts et al., 2015; Brown et al., 2014). The position of mL62 on the large subunit is more than 80 Å away from the A site, where release factors typically bind (Brown et al., 2014). It was subsequently suggested that while ICT1 plays a structural role as a large ribosomal subunit protein, a fraction of ICT1 in mitochondrial remains unbound and can function as a stop codon-independent release factor (Akabane et al., 2014), though there is as yet no definitive evidence of this unbound fraction of ICT1. More compelling is the finding that mutating the GGQ motif of ICT1 is detrimental to cell viability, which indicates that the hydrolytic activity of ICT1 is important for the cell (Richter et al., 2010).

Of the ribosome rescue mechanisms that target non-stop stalling that have been discussed so far, only homologs of ArfB have been found in mitochondria (Duarte et al., 2012). It is possible that while ArfB is not essential in certain bacterial species such as *E. coli*, which have tmRNA-SmpB as well as ArfA, its homologs have a much more significant role in mitochondrial translation.

2.3.4 Coupled folding and binding mechanisms

A common feature of tmRNA-SmpB, ArfA, and ArfB is the presence of positively charged amino acid sequences at the C terminus that bind within the mRNA entry channel of non-stop stalled ribosomes (Demo et al., 2017; Gagnon et al., 2012; Huter et al., 2017b; James et al., 2016; Ma et al., 2017; Neubauer et al., 2012; Rae et al., 2019; Zeng et al., 2017). Furthermore, NMR studies of SmpB and ArfB have shown that their positively charged C-terminal tails are unstructured in solution (Dong et al., 2002; Someya et al., 2003). It has been suggested for all three mechanisms that the unstructured regions facilitate recognition of the empty mRNA-entry channel, thereby selecting stalled ribosomes for rescue (Gagnon et al., 2012; Kurita et al., 2014; Miller and Buskirk, 2014).

Intrinsic disorder is a feature of many proteins involved in regulation of gene expression and signaling pathways (reviewed in (Dyson and Wright, 2005)). Intrinsically disordered domains do not have stable three-dimensional structures, and are defined by repetitive sequences of charged amino acids and the lack of bulky hydrophobic residues (Romero et al., 2001). While many such sequences have been identified *in silico*, it has also been confirmed that intrinsic

disorder persists under cellular solvent conditions (Theillet et al., 2016). The behavior of these dynamic and flexible regions differ greatly from that of folded protein domains, and have important implications on binding interactions in the cell. It has long been postulated that the advantage of intrinsic disorder is fast association, high specificity, and low affinity, all of which enable regulatory networks to activate and deactivate signaling cascades very quickly, in particular when cellular concentrations of these regulatory proteins are low (reviewed in (Dyson and Wright, 2005; Mollica et al., 2016)).

In their bound state, intrinsically disordered proteins (IDPs) often assume a secondary structure; the association of an IDP and its binding partner is therefore a "coupled binding and folding reaction", with the enthalpy of binding compensating for the entropic cost of folding (reviewed in (Dyson and Wright, 2002)). IDPs typically have many charged residues, and electrostatics have been shown to play a role in increasing k_{ON} through electrostatic steering (Ganguly et al., 2012). However, electrostatic steering alone does not appear to account for diffusion controlled association rates, where binding so fast that it is limited by the rate of diffusion (Shammas et al., 2013). It has been proposed that intrinsic disorder itself accelerates association through a "fly-casting" mechanism (Shoemaker et al., 2000). Fly-casting refers to the extended, flexible configurations of IDPs in solution, which allows them to first form weak interactions with their binding partners over long distances, thereby increasing the "capture radius" of an IDP. These interactions lower the free energy of folding, allowing specific short-range interactions to form, so that the binding partner effectively "reels in" the IDP (Shoemaker et al., 2000).

Experimental evidence of the fly-casting hypothesis is scarce, mostly due to technical constraints. In fact, in some studies, stabilizing transient secondary structures of the IDP in solution was found to increase the rate of binding (k_{ON}) for some proteins (Arai et al., 2015; Iesmantavicius et al., 2014). This led to another outstanding question regarding the coupled binding and folding of IDPs: whether the association goes through a conformational selection or an induced fit mechanism. In the former, IDPs where transient secondary structures have formed are preferentially bound, which drives the equilibrium towards IDPs with pre-formed structures. In the latter, folding occurs on the binding partner following binding of the fully unfolded IDP (Mollica et al., 2016).

While these theories on the role of intrinsic disorder in protein binding have been in place for many years, experimental validation is still a developing field. The commonly used methods to study IDP binding include NMR spectroscopy and rapid kinetics techniques, and kinetic models have been proposed that can potentially differentiate between the conformational selection and induced fit mechanisms (Shammas et al., 2016). However, recent studies show that IDP binding mechanisms are diverse and resist simple categorization. For example, measured k_{ON} values range from 10^7 $M^{-1}s^{-1}$ for the KIX domain of CREB-binding protein (CBP) and its ligands (Shammas et al., 2013), to 630 $M^{-1}s^{-1}$ for spectrin tetramerization (Shammas et al., 2012). K_d values have also been measured from nanomolar range to micromolar range, refuting the assumption that all IDPs form low affinity complexes with their binding partners (Shammas et al., 2016). Additionally, experimental data suggests that IDP binding mechanisms can combine aspects of both conformational selection and induced fit, in which pre-formed structures play a role in initial binding, but folding of the IDP is only completed after binding (Mollica et al., 2016).

The role of intrinsic disorder in protein-protein interactions appear to vary between different IDPs, and careful consideration of structural information as well as kinetic data is necessary to understand specific binding interactions. In the case of ArfB and ICT1, the positively-charged C-terminal tail could facilitate electrostatically-enhanced binding to the ribosome via interactions with the negatively charged rRNA backbone (Handa et al., 2010; Kogure et al., 2014). Rapid association could compensate for low expression levels of ArfB in *E. coli* (Taniguchi et al., 2010). Current theories on the binding of intrinsically disordered proteins provide a framework for understanding ArfB-ribosome interactions, and a detailed investigation into the kinetics of ArfB-mediated rescue could give additional insight into these highly dynamic association reactions.

2.4 Ribosome rescue in mitochondria

ArfB is set apart from the other known bacterial ribosome rescue systems by its ability to catalyze peptidyl-tRNA hydrolysis without external factors (Chadani et al., 2011b; Handa et al., 2011), and by its evolutionary conservation in the mitochondria of all eukaryotes while tmRNA-SmpB and ArfA are entirely absent (Duarte et al., 2012). While eukaryotic translation has many significant differences from prokaryotic translation (reviewed in (Dever et al., 2018; Hellen, 2018; Merrick and Pavitt, 2018)), mitochondrial translation bears some structural and biochemical similarities to bacterial translation (reviewed in (Greber and Ban, 2016; Ott et al., 2016)), to the extent that certain bacterial and mitochondrial factors are interchangeable (Feaga et al., 2016). These similarities allow us to infer the function of bacterial translation factor homologs in human mitochondria, in particular the ArfB homolog ICT1.

2.4.1 Comparison of mitochondrial and bacterial ribosomes

The mammalian 55S mitoribosome is composed of a 28S small subunit with a 12S rRNA and 30 proteins, and a 39S large subunit with a 16S rRNA, 52 proteins, and the CP-tRNA (**Figure 2.25a**) (Greber and Ban, 2016). The CP-tRNA is a tRNA molecule ($tRNA^{Phe}$ in porcine mitoribosome structures and $tRNA^{Val}$ in human mitoribosome structures) that takes the place of bacterial 5S ribosomes in the central protuberance (Brown et al., 2014; Greber et al., 2014). Mitochondrial rRNAs are significantly shortened compared to bacterial rRNAs. Indeed, recent cryo-EM structures of mammalian mitoribosomes show that while the surface of the bacterial ribosome (**Figure 2.25b**) mostly consists of rRNA, the surface of the mitochondrial ribosome is covered in proteins (**Figure 2.25c**). (Amunts et al., 2015; Brown et al., 2014; Greber et al., 2015; Greber et al., 2014). The increased protein content in mammalian mitochondrial ribosomes compensates for the structural roles played by bacterial rRNA, and confer mitochondrial-specific functions to the mitoribosome such as membrane attachment and mRNA recruitment (Amunts et al., 2015; Greber et al., 2015; Greber et al., 2014). The 13 components of the oxidative phosphorylation pathway synthesized by the mitochondrial ribosome are all targeted to the mitochondrial membrane, therefore many of the additional mitoribosomal proteins facilitate the translation of these highly hydrophobic proteins (Ott et al., 2016).

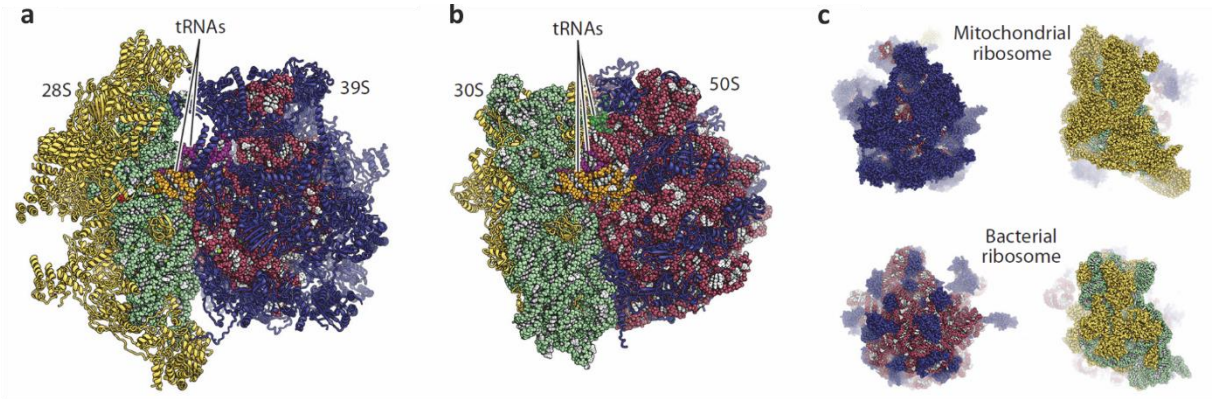

Figure 2.25. Structures of the **(a)** human mitochondrial 55S ribosome and the **(b)** bacterial 70S ribosome. **(c)** The exterior of the mitochondrial ribosome is covered with protein (yellow and blue), while the bacterial ribosome exterior is covered with rRNA (red and green) (adapted from (Greber and Ban, 2016)).

Extensive differences in composition from the bacterial ribosome notwithstanding, the functional core of the mitochondrial ribosome is highly conserved. The peptidyl-transferase center is conserved, and structures that capture a nascent peptide in the peptide exit tunnel of the mammalian mitoribosome show that it is very similar to that of the bacterial ribosome; the residues lining the mitochondrial tunnel are however more hydrophobic, likely an adaptation that allows the mitoribosome to specialize in synthetizing membrane proteins (Brown et al., 2014; Greber et al., 2014). The reduction in mitoribosomal rRNA length eliminated a number of residues that contact A site and P site tRNAs in bacteria, however the key interactions with the CCA acceptor end and the anticodon stem loop of tRNAs are conserved (Amunts et al., 2015; Greber et al., 2015).

In the decoding center, the nucleotides A918, A919, and G256 correspond to A1492, A1493, and G530 of the bacterial decoding center (**Figure 2.26a**) (Greber et al., 2015). Relevant to the binding of ArfB-like proteins, the mRNA entry channel is well conserved in the A and P sites (**Figure 2.26b**), while the channel opening is remodeled. The opening of the mRNA entry channel lacks proteins that have helicase activity (S3 and S4 in bacteria), but includes mS39, which could facilitate the recruitment of leaderless mRNAs through the RNA-binding PPR motif (Amunts et al., 2015; Greber et al., 2015).

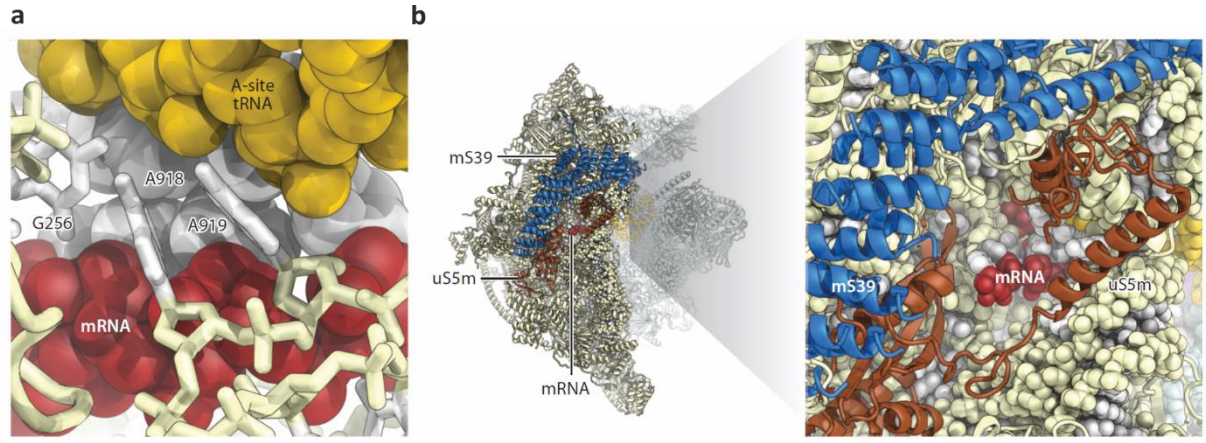

Figure 2.26. The conserved functional core of the mammalian mitochondrial ribosome. **(a)** The decoding center. **(b)** The mRNA path (adapted from (Greber and Ban, 2016)).

2.4.2 mRNA processing in mitochondria

Since the rescue of ribosomes stalled on truncated mRNAs is a proposed function of ICT1 (Feaga et al., 2016), the structure and processing of mitochondrial mRNAs are of interest. The human mitochondrial genome encodes 13 proteins that make up the core components of oxidative phosphorylation pathway, and mRNA, rRNA as well as a subset of mitochondrial tRNAs are transcribed in mitochondria (reviewed in (Ott et al., 2016)). Mitochondrial primary transcripts are polycistronic, with protein coding sequences interspersed with mitochondrial tRNAs and rRNAs (Anderson et al., 1981). The primary transcripts are cleaved to release tRNAs, rRNA, and mRNA for further maturation (reviewed in (D'Souza and Minczuk, 2018)).

Primary transcripts are cleaved by RNase P from the 5’ end, and RNase Z from the 3’ end (Brzezniak et al., 2011; Holzmann et al., 2008). Mitochondrial mRNAs are subsequently polyadenylated, with the sole exception of *MT-ND6*. In contrast to eukaryotic mRNAs, which are stabilized by polyadenylation, this modification stabilizes some mitochondrial mRNAs and destabilizes others, and is subject to regulation by enzymes such as PDE12 (Nagaike et al., 2005; Rorbach et al., 2011). Furthermore, polyadenylation completes the stop codon of 7 mitochondrial open reading frames (Temperley et al., 2010b).

Cleavage of the primary transcripts, polyadenylation, and removal of the poly(A) sequences create possibilities for the generation of non-stop mRNAs in mitochondria. While it is unclear how prevalent non-stop ribosome stalling is in mitochondria, the conservation of ArfB-like

proteins such as ICT1 and C12orf65 suggest that ribosome rescue may play an important role in mitochondrial translation (Burroughs and Aravind, 2019; Duarte et al., 2012).

2.4.3 Mitochondrial translation termination

As in bacterial translation, mitochondrial translation termination involves release factor-catalyzed peptidyl-tRNA hydrolysis (Ott et al., 2016). ICT1, C12orf65, mtRF1, and mtRF1a were identified as putative release factors based on sequence homology to bacterial release factors, and all four proteins contain the GGQ motif (Duarte et al., 2012; Handa et al., 2010; Kogure et al., 2012). Unlike ICT1 and C12orf65, mtRF1 and mtRF1a have codon recognition domains reminiscent of the PxT domain of bacterial RF1, although only mtRF1a has shown peptidyl-tRNA hydrolysis activity *in vitro* (Korostelev et al., 2010; Lind et al., 2013; Soleimanpour-Lichaei et al., 2007).

In mitochondria, the codon UGA codes for tryptophan, with UAA and UAG utilized as stop codons for most open reading frames (Temperley et al., 2010b). Homology modeling showed that mtRF1a can decode these stop codons similarly to RF1, while it is still unclear why mtRF1 is inactive in *in vitro* assays (Lind et al., 2013). However for the genes *MT-CO1* and *MT-ND6*, the coding sequence ends with AGA and AGG, respectively. It is still unclear how translation termination occurs on these two genes; one hypothesis states that because mitochondria lack the $tRNA^{Arg}$ encoded by these two codons, ribosome stalling induces a -1 frameshift which creates an in-frame UAG stop codon (Temperley et al., 2010a). On the other hand, ICT1 and C12orf65 have also been proposed to terminate translation on AGA and AGG codons, due to their lack of a codon recognition domain (Lind et al., 2013). To understand the role of ArfB-like factors in ribosome rescue and canonical termination in mitochondria, a more detailed mechanistic understanding of how these proteins interact with the ribosome is required.

2.5 Scope and aim of thesis

In this study, we set out to construct a kinetic model of ArfB-mediated ribosome rescue, with the specific aims of establishing substrate specificity and understanding the interplay of the N-terminal and C-terminal domains of ArfB. While previous studies showed the hydrolytic activity of ArfB on non-stop stalled ribosomes and on ribosomes stalled on rare codon clusters, the experiments were carried out under equilibrium conditions and gave limited mechanistic insight. Furthermore, the crystal structure of ArfB bound to the ribosome showed that binding of the ArfB C-terminal tail in the mRNA entry channel should clash sterically with mRNA extending past the P site. This raised question regarding the role of the C-terminal tail: if the C-terminal tail is essential for ArfB activity, how can ArfB catalyze peptidyl-tRNA hydrolysis on ribosomes stalled in the middle of mRNAs?

To address the issue of substrate specificity, we used a fully reconstituted *E. coli* translation system and purified ArfB to conduct both steady-state and pre-steady state experiments. By supplying aminacyl-tRNAs that only encode the first two codons of our model mRNA, we could purify stalled ribosomes that had a quantifiable radioactive dipeptidyl-tRNA in the P site, an empty A site, and variable lengths of mRNA extending into the mRNA entry channel. These model ribosomal complexes allowed us to directly measure the rate of ArfB-mediated peptidyl-tRNA hydrolysis on different potential substrate complexes using the quenched-flow technique. We could also perform classical Michaelis-Menten titrations to obtain specificity constants for different stalled ribosomes.

In addition to the catalytic activity of ArfB, the association and dissociation of ArfB from stalled ribosomes are also of interest. tmRNA-SmpB, ArfA, and ArfB all have unstructured C-terminal domains, and for all three systems it has been suggested that they probe the mRNA entry channel for mRNA and ensure substrate specificity. However, this has yet to be conclusively shown due to the lack of kinetic data on the binding of rescue factors. While the crystal structure shows the ArfB C-terminal tail as an α-helix in the mRNA entry channel, the atomic model could not explain the importance of several C-terminal residues according to mutational experiments, and it is not known what role the folding of the C-terminal domain plays in ArfB activity.

By incorporating fluorescence labels into our model ribosomal complexes as well as into purified ArfB, we were able to monitor and dissociation of ArfB in real time using Förster

resonance energy transfer (FRET) and the stopped flow technique. Fluorimetric titrations provided further thermodynamic parameters of binding; both FRET and anisotropy were used to confirm the results. Experiments were carried out at 37°C and at 20°C with the goal of eventually modeling ArfB behavior at one of these temperatures. The interpretation of kinetic data was aided by atomic models obtained by cryo-electron microscopy of ArfB-bound ribosome complexes. Cryo-EM experiments and analysis were performed by Claudia Müller and Daniel Wilson (Institute for Biochemistry and Molecular Biology, University of Hamburg), and by Valentyn Petrychenko and Niels Fischer (Department of Structural Dynamics, Max Planck Institute for Biophysical Chemistry).

Finally, the question remains of the physiological significance of ArfB. To study factors that potentially interact with ArfB in the cell, we used the pKOV vector to generate *E. coli* strains in which chromosomally encoded ArfB is tagged with a 3xFLAG tag. This enables us to pull down endogenously expressed ArfB using immunoprecipitation, and submit the protein and potential interacting proteins for analysis by mass spectrometry.

3 MATERIALS AND METHODS

3.1 Materials

3.1.1 Chemicals

Table 3.1. List of chemicals

Chemical	Manufacturer
[^{3}H]-N-formylmethionine	Perkin Elmer
[^{14}C]-phenylalanine	Perkin Elmer
Acrylamide, 40% w/v solution, 29:1	SERVA Electrophoresis
Agarose	SERVA Electrophoresis
Ammonium chloride	Merck Millipore
Ammonium persulfate (APS)	Merck Millipore
ATTO 540-Q maleimide	ATTO-TEC
β-mercaptoethanol	Sigma-Aldrich
Boric acid	Carl Roth
Bromophenol Blue sodium salt	Merck Millipore
Chloramphenicol	Sigma-Aldrich
cOmplete protease inhibitor cocktail tablets	Roche
DMSO	Merck Millipore
DNaseI	Jena Bioscience
DNA Stain G	SERVA Electrophoresis
dNTP mix	New England Biolabs
Dpn1	New England Biolabs
DTT	AppliChem
EDTA	Sigma-Aldrich
Ethanol (EtOH)	Merck Millipore
Fluorescein-5-maleimide	Thermo Fischer
Glycerol	Merck Millipore
GTP	Sigma-Aldrich
HEPES	Sigma-Aldrich
HF buffer, 5x	New England Biolabs
Imidazole	Carl Roth
IPTG	Carl Roth
IRGASAFE scintillation cocktail	Perkin Elmer
Kanamycin sulfate	SERVA Electrophoresis
Ni-IDA resin	Macherey-Nagel
Magnesium chloride hexahydrate	Merck Millipore

Methylene blue	Merck Millipore
Perfect Protein Markers, 15-150kDa	EMD Millipore
Phosphoenolpyruvate	Sigma-Aldrich
Phusion polymerase	New England Biolabs
Potassium acetate	Merck Millipore
Potassium chloride	Merck Millipore
Potassium hydroxide	Merck Millipore
Pyruvate kinase from rabbit muscle	Roche
SmartLadder MW 1700-10	Eurogentec
Sodium chloride	Merck Millipore
Sodium dodecylsulfate (SDS)	SERVA Electrophoresis
TEMED	Sigma-Aldrich
Trichloroacetic acid (TCA)	Merck Millipore
Tris-HCl	Merck Millipore
Tryptone	Carl Roth
Yeast extract	Carl Roth

3.1.2 Buffers

Table 3.2. Buffer composition

	Buffer name and pH	Composition
ArfB purification	Lysis buffer (pH 7.5)	Tris-HCl 20 mM NaCl 500 mM Glycerol 10% v/v β-mercaptoethanol 1 mM
	Buffer SA (pH 7.0)	HEPES 40 mM KCl 300 mM $MgCl_2$ 7 mM β-mercaptoethanol 10 mM
	Buffer SB (pH 7.0)	HEPES 40 mM KCl 1000 mM $MgCl_2$ 7 mM β-mercaptoethanol 10 mM
mRNA purification	Buffer FA (pH 6.0)	BisTris 30 mM EDTA 1 mM NaCl 300mM
	Buffer FB (pH 6.0)	BisTris 30 mM EDTA 1 mM NaCl 1.5 M
Reaction buffers	$HAKM_7$ (pH 7.4)	HEPES 50 mM NH_4Cl 70 mM KCl 30 mM $MgCl_2$ 7 mM
	$HAKM_{20}$ (pH 7.4)	HEPES 50 mM NH_4Cl 70 mM KCl 30 mM $MgCl_2$ 20 mM
	HKM_7 (pH 7.4)	HEPES 50 mM KCl 30 mM $MgCl_2$ 7 mM
Affinity purification coupled mass spectrometry	LB broth	NaCl 1% w/v Tryptone 1% w/v Yeast extract 0.5% w/v
	SDS-PAGE sample buffer (pH 6.8)	Tris-HCl 50 mM SDS 2% Glycerol 10% v/v

	Bromophenol blue 0.1% v/v
Sonication buffer (pH 7.9)	Tris-HCl 20 mM NaCl 150 mM EDTA 0.2 mM Glycerol 10%
AFC buffer (pH 7.0)	Tris-HCl 10 mM NaCl 150 mM Triton X-100 0.1%

3.1.3 Primers and sequences

Table 3.3. Primers for mutagenesis

Mutation	Primer sequence
ArfB(K96C)	GTTAATTCTGTAATCATAGCCACCAGCCGGGC
	GCCCGGCTGGTGGCTATGATTACAGAATTAAC
ArfB(R112C)	CACGCGGCCCACCTGTGCATCGAAAGAG
	CTCTTTCGATGCACAGGTGGGCCGCGTG
$ArfB_{GAQ}$	GGGCGCGGGCGCGCAGCATGTTA
	TAACATGCTGCGCGCCCGCGCCC
$ArfB_{Nterm}$	TAACTCGAGCACCACCACCACCACC
	TTCTGTTGTTAATTCACAAATCATAGCCACCAGCC
$ArfB_{Cterm}$	AAAAAAGCCCGACGACCCACGC
	CATACCACCAATCTGTTCTCTGTGAGCCTCA
lepB A2F	GGGCAAACATATTGAACATATTAGAATTCTCC
	GGAGAATTCTAATATGTTCAATATGTTTGCCC

Single mutated codons are shown in red.

Table 3.4. Model mRNA sequences

Name	Sequence
P+0	UAAUACGACUCACUAUAGGGCGAAUUGGAGCUCACAACGGUUUCCCUCUAGAA AUAAUUUUGUUUAACUUUAAGAAGGAGAAUUCUAAUAUGUUC
P+3	UAAUACGACUCACUAUAGGGCGAAUUGGAGCUCACAACGGUUUCCCUCUAGAA AUAAUUUUGUUUAACUUUAAGAAGGAGAAUUCUAAUAUGUUCAAU
P+6	UAAUACGACUCACUAUAGGGCGAAUUGGAGCUCACAACGGUUUCCCUCUAGAA AUAAUUUUGUUUAACUUUAAGAAGGAGAAUUCUAAUAUGUUCAAUAUG
P+9	UAAUACGACUCACUAUAGGGCGAAUUGGAGCUCACAACGGUUUCCCUCUAGAA AUAAUUUUGUUUAACUUUAAGAAGGAGAAUUCUAAUAUGUUCAAUAUGUUU
P+12	UAAUACGACUCACUAUAGGGCGAAUUGGAGCUCACAACGGUUUCCCUCUAGAA AUAAUUUUGUUUAACUUUAAGAAGGAGAAUUCUAAUAUGUUCAAUAUGUUU GCC
P+15	UAAUACGACUCACUAUAGGGCGAAUUGGAGCUCACAACGGUUUCCCUCUAGAA AUAAUUUUGUUUAACUUUAAGAAGGAGAAUUCUAAUAUGUUCAAUAUGUUU GCCCUG
P+24	UAAUACGACUCACUAUAGGGCGAAUUGGAGCUCACAACGGUUUCCCUCUAGAA AUAAUUUUGUUUAACUUUAAGAAGGAGAAUUCUAAUAUGUUCAAUAUGUUU GCCCUGAUUCUGGUG
P+30	UAAUACGACUCACUAUAGGGCGAAUUGGAGCUCACAACGGUUUCCCUCUAGAA AUAAUUUUGUUUAACUUUAAGAAGGAGAAUUCUAAUAUGUUCAAUAUGUUU GCCCUGAUUCUGGUGAUUGCC

P+99	UAAUACGACUCACUAUAGGGCGAAUUGGAGCUCACAACGGUUUCCCUCUAGAA AUAAUUUUGUUUAACUUUAAGAAGGAGAAUUCUAAUAUGUUCAAUAUGUUU GCCCUGAUUCUGGUGAUUGCCACACUGGUGACGGGCAUUUUAUGGUGCGUGG AUAAAUUCUUUUUCGCACCUAAACGGCGGGAACGUCAG

The start codon AUG is indicated in blue.

Table 3.5. List of vectors

Vector	Use	Source
pBSKII	Standard cloning vector for model mRNAs	Addgene
pSUMO	Protein expression vector for ArfB	Addgene
pKOV	Vector for inserting tag sequences in *E. coli* chromosomal DNA (**Figure 3.1**)	Addgene

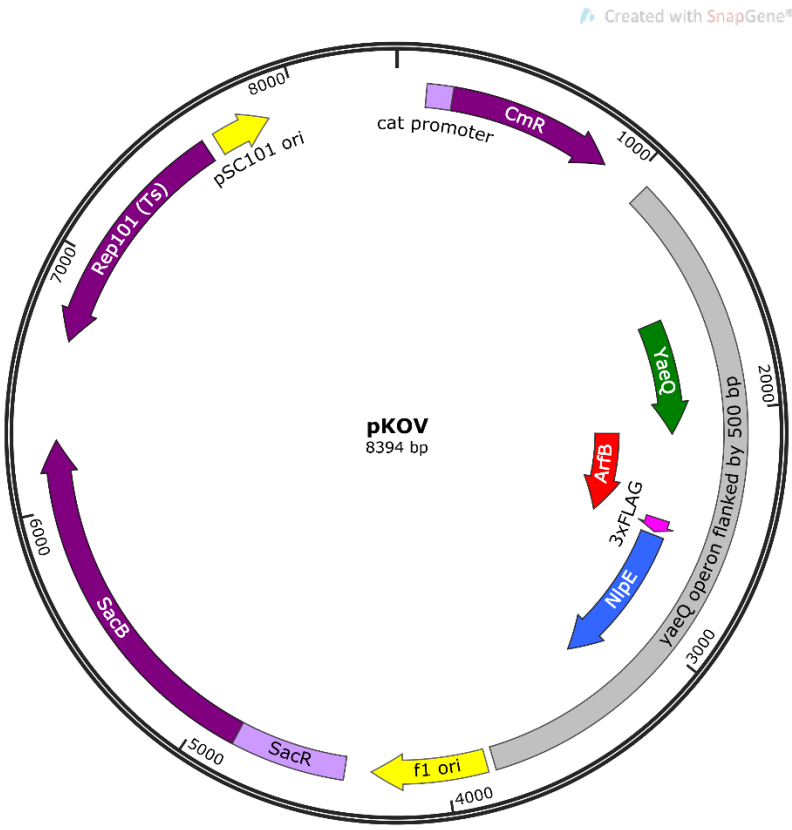

Figure 3.1. Map of the plasmid used to generate *E. coli* strains. The *yaeQ* operon carrying ArfB was cloned including its flanking 500 base pairs (grey), and a 3xFLAG tag (pink) was inserted into the C terminus of ArfB (red).

3.2 Methods

3.2.1 ArfB overexpression and purification

The *arfB* gene from *E. coli* strain K12 (UniProt ID: P40711) was cloned into a pSUMO vector with an N-terminal 6x His-tag followed by a cleavable SUMO tag. The vector contained an IPTG-inducible promoter and a kanamycin resistance cassette. The resulting plasmid was transformed into *E. coli* strain BL21 DE3 cells. Protein overexpression was induced with 250 mM IPTG in 500 mL bacterial cultures at A_{600} 0.6, after which the cultures were shaken for 6 hours at 30°C. The cells were harvested by centrifugation (6000 xg for 20 min at 4°C) and the pellets were flash frozen in liquid nitrogen. The harvested cells were thawed in lysis buffer (Gagnon et al., 2012) supplemented with protease inhibitors (1 tablet of cOmplete EDTA-free Protease Inhibitor Cocktail per 10 g cells, Roche Diagnostics) and DNase1 (40 units per 10 g cells, Jena Bioscience), and lysed using the Emulsiflex C3 (Avestin). Cell lysates were clarified by centrifugation at 25,000 rpm for 1 h at 4°C (Avanti J-30I, rotor JA 30.50Ti, Beckman Coulter).

6xHis-SUMO-tagged ArfB was enriched by incubating the clarified lysate with Ni-IDA resin (2 g per 10 g cells, Macherey Nagel) for 1 h at 4°C, and eluted with buffer SA supplemented with 600 mM imidazole. Imidazole was removed from the solution by dialysis overnight into buffer SA at 4°C (D-Tube dialyzer, 3.5 kDa molecular weight cutoff, EMD Millipore), while simultaneously incubating the mixture with Ulp1 protease (4000 pmol per 10 g cells, purified in-house by Franziska Hummel) to cleave the 6xHis-SUMO tag. Untagged ArfB was purified by ion-exchange chromatography over a 5 mL HiTrap HP SP column (GE Healthcare). Briefly, the column was charged with 100% buffer SB (1000 mM KCl) and equilibrated with buffer SA (300 mM KCl). A gradient from 300 mM to 1000 mM KCl was then run over 12 column volumes (approximately 60 mL). 0.75 mL fractions were collected. The cleaved 6xHis-SUMO tag does not bind to the column, and untagged ArfB elutes at approximately 550 mM KCl. Fractions containing ArfB were identified by 15% SDS-PAGE, and ArfB concentration was determined using IF3 as a standard on SDS-PAGE gels. Protein band intensities were quantified using MiBio (Microtek).

ArfB single-cysteine variants and slowly hydrolyzing ArfB ($ArfB_{GAQ}$) were purified for fluorescence labeling. Wildtype ArfB does not contain cysteines, so positions 96 (lysine) or 112 (arginine) were mutated to cysteine using the QuikChange mutagenesis protocol, while

position 27 (glycine) was mutated to generate $ArfB_{GAQ}$. The resulting ArfB variants ArfB(K96C), ArfB(R112C), and $ArfB_{GAQ}$ were purified as described previously.

The N-terminal domain of ArfB ($ArfB_{Nterm}$), truncated at position 101, was expressed using the same pSUMO vector described above. The overexpression and purification was performed as described above for full-length ArfB, with the exception of the tag cleavage and ion-exchange chromatography steps. The 6xHis-SUMO tag on $ArfB_{Nterm}$ was first cleaved, then removed by incubation with Ni-IDA resin. $ArfB_{Nterm}$ was further purified over a 5 mL HiTrap Q HP anion exchange chromatography column (GE Healthcare); $ArfB_{Nterm}$ does not bind to the resin and was collected from the flow-through and concentrated.

The C-terminal domain of ArfB ($ArfB_{Cterm}$) was truncated at position 106. The overexpression and purification was performed as described above for full-length ArfB.

3.2.2 *in vitro* translation and purification of stalled ribosomes

The non-stop mRNAs used in this project contain a ribosome binding site and a start codon followed by 1 to 34 additional codons. The sequences were derived from the *E. coli lepB* gene (UniProt ID: P00803), with the second codon mutated by site-directed mutagenesis to UUC (phenylalanine) for fluorescence labeling purposes. The modified DNA sequence was cloned into a pBSKII vector containing a T7 promoter. DNA templates for *in vitro* translation were generated by polymerase chain reactions (PCRs) with a T7 primer and a reverse primer that defined the length of the transcript. The PCR mixtures contained 0.02 u/µL Phusion polymerase (Thermo Fischer), 0.2 mM dNTP, 0.2 µM of each primer, 100 ng of the template plasmid, and 1x HF buffer. *In vitro* transcription was carried out in water for 3 h at 37˚C with 10 ng DNA template, 1x transcription buffer, 10 mM DTT, 3 mM NTP mix, 5 mM GMP, 0.005 u/µL pyrophosphatase (Lucigen), 1.6 u/µL T7 RNA polymerase, and 0.004 u/µL RNAse Inhibitor (Molox). DNA products and RNA products were verified by agarose gel electrophoresis and urea polyacrylamide gel electrophoresis, respectively.

mRNA was purified by ion exchange chromatography over a 5 mL HiTrap HP SP column (GE Healthcare). The column was charged with 10 mL buffer FB (1.5 M NaCl) and equilibrated with buffer FA (300 mM NaCl). A gradient from 300 mM to 1.5 M NaCl was run over 100 mL. Fractions of 2 mL were collected; mRNA eluted at approximately 40% buffer FB. Fractions containing mRNA were identified by A260 peaks and precipitated overnight at -20°C in 1/10

volume potassium acetate and 2.5x volume ice-cold ethanol. Precipitated mRNA was pelleted at 4000 xg for 1 hour at 4°C and resuspended in nuclease-free water. Final concentration of the mRNA was calculated using the equation $A=\varepsilon*b*c$, where A is A260, ε is the extinction coefficient of the mRNA (1232.5 mM-1cm-1, predicted using the Extinction Coefficient Calculator, The Scripps Research Institute), b is the path length (1 cm), and c is the concentration.

For the translation reaction, 70S ribosomes from *E. coli* strain MRE600, initiation factors, EF-Tu, EF-G, RRF, RF3, f[^{3}H]Met-tRNA^{fMet}, [^{14}C]Phe-tRNA^{Phe}, and [^{14}C]Phe-tRNA^{Phe}(Flu) were prepared as previously described (Milon et al., 2007; Rodnina and Wintermeyer, 1995) by Sandra Kappler, Olaf Geintzer, Cristina Kothe, and Michael Zimmermann. Stalled ribosome complexes were prepared by translating the first two codons on the mRNA. To initiate translation, 70S ribosomes were mixed with a 1.5 fold excess of initiation factors, 3 fold excess f[^{3}H]Met-tRNA^{fMet}, and 3 fold excess mRNA in HAKM$_7$ buffer (50 mM HEPES, 30 mM KCl, 70 mM NH_4Cl, 7 mM $MgCl_2$, pH 7.4) supplemented with 1 mM dithiothreitol (DTT) and 1 mM GTP. This mixture was incubated for 45 min at 37°C. 3 pmol ribosomes were filtered over nitrocellulose filters and quantified by scintillation counting to assess initiation efficiency, which was >90% for all mRNA lengths. Ternary complexes were formed for 15 min at 37°C with 3 fold excess of [^{14}C]Phe-tRNA^{Phe} over ribosomes and 1.5 µM EF-G, and 2 fold excess of EF-Tu pre-incubated with 1 mM GTP, 3 mM phosphoenolpyruvate (PEP), and 0.5 mg/mL pyruvate kinase in HAKM$_7$ buffer. For fluorescence-labeled ribosomal complexes used in FRET experiments, fluorescein-labeled tRNA ([^{14}C]Phe-tRNA^{Phe}(Flu), provided by Olaf Geintzer) was used.

Initiation complexes (IC) were mixed with 3x fold ternary complexes (TC) according to Phe-tRNA^{Phe} concentration. Dipeptide formation occurred for 2 min at room temperature. All ribosomes, regardless of the length of the associated mRNA, were supplied with the same ternary complex so that the P site was occupied by a radiolabeled dipeptidyl-tRNA. Consequently, varying lengths of mRNA extend past the P site to form P+0 complexes (0 nucleotides past the P-site) and P+n complexes (n = 3, 6, 9, 12, 15, 24, 30, 99). Complexes were purified by ultracentrifugation for 2 hours at 55,000 rpm (Optima MAX XP Ultracentrifuge, TLS-55 rotor, Beckman Coulter) over a cushion of 1.1 M sucrose in HAKM$_{20}$ buffer (HAKM$_7$ buffer containing 20 mM $MgCl_2$). The pellets were resuspended in HKM$_7$ buffer (HAKM$_7$ buffer

without NH_4Cl) and quantified by liquid-liquid scintillation counting, then flash frozen and stored at -80°C. Dipeptide formation under these conditions was > 80%.

3.2.3 Pre-steady state hydrolysis assays

All experiments were performed in HKM_7 buffer (50 mM HEPES, 30 mM KCl, 7 mM $MgCl_2$, pH 7.4). Single round peptidyl-tRNA hydrolysis reactions were monitored by rapidly mixing P+0 complexes and ArfB in a quenched-flow apparatus at 37°C and by hand at 20°C. For the quenched-flow experiments, equal volumes of P+n complex (0.3 µM) and ArfB (0.4, 0.6, 0.9, 1.2, 3, 4 µM) were rapidly mixed in the appropriate reaction loop. At the desired time point, the reaction was quenched with a solution of 10% trichloroacetic acid (TCA) and 50% ethanol. The samples were kept on ice for 30 min, then the precipitated ribosomes and peptidyl-tRNA were spun down for 15 min at 16,000 x *g* at 4°C. The supernatant, which contains released peptides, were quantified by liquid-liquid scintillation counting. For each time course, 15-18 time points were sampled. The resulting radioactivity counts were plotted against the corresponding reaction time, and the curve was fit with a one exponential or two exponential equation. The two exponential function is as follows:

$$f(x) = A + B * exp^{-cx} + D * exp^{-ex}$$

Where A is the final plateau, B is the amplitude of the first phase, c is the rate constant of the first phase, D is the amplitude of the second phase, and e is the rate constant of the second phase. The one exponential function is as follows:

$$f(x) = A * (1 - exp^{-bx})$$

where A is the final plateau and b is the rate constant. All hydrolysis time courses were normalized by the plateau extrapolated from the exponential fit to give the fraction of peptide released at each time point.

3.2.4 Steady state hydrolysis assays

Endpoint peptidyl-tRNA hydrolysis assays were performed by mixing stalled ribosome complexes with 10 fold excess of release factor (ArfB or $ArfB_{GAQ}$, where applicable) at 37°C. The reactions were quenched and released peptides were quantified with the method described above.

Multiple turnover peptidyl-tRNA hydrolysis was measured at 20°C and 37°C by incubating ArfB with at least 10 fold excess of stalled ribosomal complex. ArfB concentration was 0.02 µM for P+0 complexes and 0.05 µM for P+9 complexes. At each time point, an aliquot of the mixture was quenched as described above. At each stalled ribosomal complex concentration, the linear fit of the time course gave the initial velocity of the reaction. Background peptide dropoff, measured in a parallel reaction without ArfB, was subtracted. Michaelis-Menten constants K_M and k_{cat} were calculated from the hyperbolic fit of initial velocity plotted against substrate concentration.

The effect of translation factors on ArfB turnover was assayed by measuring initial velocity in the presence of 0.5 µM ribosome recycling factors RRF and EF-G. Because subunit splitting is a GTP-dependent process, the HKM_7 buffer was supplemented with 3 mM PEP, 1 mM GTP or GTP-γS, and 1 mg/mL pyruvate kinase.

3.2.5 Competition between ArfB and ternary complex

The effect of ternary complex on ArfB-mediated ribosome rescue was measured by simultaneously incubating 0.5 µM P+3 or P+33 complex (ribosomes initiated on an mRNA with two codons, with phenylalanine as the second, untranslated codon) with ArfB and cognate ternary complex of EF-Tu – GTP – [^{14}C]Phe-tRNA^{Phe} (0.25 µM). After incubation at 37°C for 20 and 120 s, two aliquots were taken. One was quenched with 0.1 x sample volume 5M potassium hydroxide (KOH) then hydrolyzed for 30 min at 37°C for subsequent quantification of dipeptide formation. The other was quenched in a solution of 10% TCA and 50% EtOH for quantification of released [^{3}H]fMet, using the protocol described in section 3.2.3.

Dipeptides were quantified using a previously published protocol (Doerfel et al., 2013). Briefly, the samples quenched with KOH were neutralized with acetic acid and analyzed by reversed phase HPLC (Chromolith RP8 100-4.6 mm column, Merck), over a 0-65% acetonitrile gradient in 0.1% TFA. Fractions were analyzed by scintillation counting, with the fractions containing both ^{3}H and ^{14}C counts identified as dipeptide-containing fractions. Fraction dipeptide formed was calculated by normalizing the dipeptide peak with total amino acids detected, as calculated by the sum of all peaks.

The effect of non-cognate ternary complex was assayed by measuring time courses of ArfB-mediated peptidyl-tRNA hydrolysis on 0.5 µM P+3 and P+33 complexes at 37°C. Non-cognate

ternary complex (TC) was formed with 10 µM EF-Tu, 5 µM Val-tRNA^{Val}, 0.5 mg/mL pyruvate kinase, 1.5 mM PEP, and 0.5 mM GTP. TC was mixed with an equal volume of purified P+0 IC or P+30 IC in the presence of 0.1 µM ArfB and 2 µM ArfB, respectively. To assess the effect of translocation on hydrolysis, 2 µM EF-G was also added to a set of samples. Aliquots were taken at time points up to 5 min, then processed as previously described to quantify the released peptides. The resulting curves were fit with a hyperbolic equation.

3.2.6 Fluorescence labeling of ArfB

Single-cysteine variants of ArfB, ArfB(K96C) and ArfB(R112C), were purified as described previously. Single-cysteine mutants were found to be identical to the wildtype in terms of hydrolytic activity, as shown by single-round hydrolysis reaction time courses.

Fluorescence labeling was carried out using previously published protocols (Milon et al., 2007). Briefly, purified ArfB was exchanged into SA buffer without β-mercaptoethanol through a PD-10 desalting column (GE Healthcare). 10x excess thiol-reactive fluorescent dye (fluorescein or ATTO-540Q) was then added to the protein drop-by-drop, and the mixture was incubated in the dark at room temperature for 2 hours. The labeling reaction was stopped by adding 1 µL 1.4 M β-Mercaptoethanol.

Free dye was removed using a PD-10 desalting column. Labeling efficiency, estimated by absorbance measurements of the dye by SDS-PAGE based protein concentration determination, was approximately 60% in most cases.

3.2.7 Stopped-flow measurements of ArfB binding

All stopped flow experiments were performed in HKM_7 buffer, with an excitation wavelength of 465 nm and a KV500 cutoff filter (Schott), and using an SX-20MV stopped flow machine (Applied Photophysics, United Kingdom). For the association reaction, equal volumes of ArfB(540Q) and P+0(Flu) complex (P+0 complex with a fluorescein-labeled [^{14}C]Phe-tRNA^{Phe} in the ribosomal P site) were rapidly mixed at 20°C for a final concentration of 0.05 µM, 0.1 µM, 0.2 µM, 0.3 µM, 0.4 µM, and 0.5 µM ArfB, and 0.015 µM P+0(Flu) complex. Fluorescence change upon FRET between the fluorescein dye on the P+0(Flu) complex and the ATTO(540Q) quencher was recorded over time. The resulting traces were fit with the three exponential equation:

$$f(x) = A + B * exp^{-cx} + D * exp^{-ex} + F * exp^{-gx}$$

Where A is the final plateau, B, D, and F are the amplitudes of each phase, and c, e, and g are the rate constants of each phase. Exponential fitting was performed using the GraphPad Prism software.

Chase experiments were performed at 20°C to measure the dissociation rate (k_{OFF}) of ArfB from the ribosome. For the post-hydrolysis dissociation reaction, 0.2 µM ArfB(540Q) was pre-incubated with 0.03 µM P+0(Flu) complex for 5 min at 37°C, then rapidly mixed with an equal volume of 2 µM unlabeled P+0 complex. For the pre-hydrolysis dissociation reaction, 0.2 µM $ArfB_{GAQ}$(540Q) was pre-incubated with 0.03 µM P+0(Flu) for 1 min at room temperature, then rapidly mixed with an equal volume of 2 µM unlabeled P+0 complex. Recovery of fluorescence following dissociation of the quencher-labeled ArfB variants was recorded over time. The resulting fluorescence traces were fit with the following two exponential equation using GraphPad Prism:

$$f(x) = A + B * exp^{-cx} + D * exp^{-ex}$$

Where A is the final plateau, B is the amplitude of the first phase, c is the rate of the first phase, D is the amplitude of the second phase, and e is the rate of the second phase. All fluorescence traces were normalized by the highest level of fluorescence as extrapolated by the fit.

3.2.8 Fluorimeter measurements of ArfB binding

Binding affinity of ArfB for stalled ribosomes was measured by monitoring anisotropy in a spectrofluorometer (Horiba, Japan). The excitation wavelength was 465 nm and emission was measured at 520 nm, with slit width of 5 nm. Sub-stoichiometric amounts of P+0 complex were added to 10 nM ArfB(Flu) (ArfB labeled with fluorescein). At each data point, the cuvette was vortexed to ensure equilibrium was reached before measuring anisotropy. The anisotropy value at each point was the average of 10 measurements. The anisotropy value of the unbound protein was subtracted to obtain anisotropy change (Δ Anisotropy). Δ Anisotropy was plotted against P+0 concentration for an equilibrium binding curve, which was fit with a hyperbolic equation:

$$f(x) = (A * x)/(K_d + x)$$

Where A is the maximal binding and K_d is the concentration of ligand required to reach half-maximal binding.

To assess the effect of salt concentration on ArfB binding, 50 nM ArfB(Flu) was mixed with 150 nM P+0 complexes in $HK_{50}M_7$ buffer (HKM_7 buffer with 50 mM KCl). Then, KCl or $MgCl_2$ was titrated into the sample, and the anisotropy value at each concentration was recorded. To account for light scattering caused by the ribosome, polarized light intensities of P+0 complexes at each KCl or $MgCl_2$ concentration were also subtracted. Anisotropy (r) was then calculated using the equation:

$$r = \frac{I_{VV} - G * I_{VH}}{I_{VV} + 2G * I_{VH}}$$

Where I_{VV} = intensity of vertically excited vertical emission, I_{VH} = intensity of vertically excited horizontal emission. Grating factor (G) was calculated as follows:

$$G = \frac{I_{HH}}{I_{HV}}$$

Where I_{HH} = intensity of horizontally excited horizontal emission, and I_{HV} = horizontally excited vertical emission.

A titration of the unbound protein was performed in parallel and the anisotropy values subtracted to give an anisotropy change value at each salt concentration. The resulting curve was fit with the following equation:

$$f(x) = A + (B - A)/(1 + 10^{(\log(IC50 - x) * k^1)})$$

Where A = minimum value; B = maximum value; x = log of total ion concentration in M; IC_{50} = inhibitory concentration corresponding to 50% of the amplitude change; k^1 = Hill slope factor.

Binding affinities were also measured using a FRET pair of the fluorescein on P+0(Flu) complexes, and the non-emitting fluorescence acceptor ATTO540Q on ArfB(540Q). Sub-stoichiometric amounts of ArfB(540Q) were titrated into P+0(Flu) complexes, and fluorescence of the donor fluorophore was monitored by excitation at 488 nm and detection at 520 nm, with a slit width of 7 nm. The decrease in the fluorescence of fluorescein was

recorded using a spectrofluorometer. The resulting curve was fit with a quadratic equation to account for ligand depletion:

$$f(x) = -[A + B * \frac{D + x + K_d - \sqrt{(-D - x - K_d)^2 - 4 * D * x}}{2}]$$

Where A is the fluorescence at no binding, B is the amplitude, D is the ribosome complex concentration, and K_d is the concentration of ligand required to reach half-maximal binding.

3.2.9 Sample preparation for cryo-electron microscopy

Cryo-electron microscopy samples were prepared using purified P+0 and P+9 complexes. Because complexes were purified over a sucrose cushion, traces of sucrose were removed from P+9 complexes using Zeba Spin Desalting Columns (7K MWCO, ThermoFisher). The complexes (0.4 µM) were then incubated with ArfB (1.5 µM) and Api137 (50 µM) for 10 min at 37°C.

Cryo-EM analysis was performed by Claudia Müller (Institute for Biochemistry and Molecular Biology, University of Hamburg) and Niels Fischer (Department of Structural Dynamics, Max Planck Institute for Biophysical Chemistry). Data analysis and model construction were performed by Niels Fischer and Valentyn Petrychenko (Department of Structural Dynamics, Max Planck Institute for Biophysical Chemistry).

3.2.10 Circular dichroism measurements

Circular dichroism (CD) spectra of ArfB and $ArfB_{Nterm}$ were measured at 20°C and 37°C with spectral scans from 180 nm to 260 nm, at 1 nm intervals in a Chirascan circular dichroism spectrometer (Applied Photophysics, UK) . ArfB and $ArfB_{Nterm}$ were diluted to 8 µM in CD buffer (20 mM Na_2HPO_4, 100 mM NaF) for each measurement.

3.2.11 Directed tag insertion in chromosomal ArfB

Endogenous ArfB was enriched for mass spectrometry analysis by immunoprecipitation. A 3xFLAG tag was inserted at the C terminus of chromosomally encoded ArfB using a previously published method (Link et al., 1997). Briefly, a segment of the *E. coli* BW25113 sequence containing the *yaeQ-arfB-nlpE* operon and 500 flanking base pairs were cloned into the pKOV vector using Gibson Assembly of three fragments. The 3xFLAG tag (amino acid sequence

DYKDHDGDYKDHDIDYKDDDDK) was inserted at the C terminus by appending the sequence to the amplification primers.

Gene replacement was performed in an electrocompetent BW25113 strain. The pKOV vector carrying the modified *arfB* gene was transformed into BW25113 cells using electroporation, then grown overnight at 30°C. The resulting cells were re-plated on LB agar supplemented with chloramphenicol and incubated overnight at 43°C for plasmid integration, then again incubated overnight at 30°C on LB agar supplemented with sucrose (5% w/v, no NaCl) for plasmid excision. Replica plating was performed on LB agar plates supplemented with chloramphenicol to screen for loss of the plasmid. Positive clones were confirmed by PCR.

3.2.12 Immunoprecipitation of endogenous ArfB

The *E. coli* strain containing 3xFLAG-tagged chromosomal *arfB* was cultured until O.D. 0.6 (log-phase), and the cells were stored by flash-freezing in liquid nitrogen. Cells were thawed in sonication buffer supplemented with protease inhibitor (cOMPLETE EDTA free, 1 tablet per 50 mL buffer) and DNaseI (10 µL per 50 mL buffer). Lysis was performed by sonicating on ice for 10 min at 25% amplitude, 10 s pulse with 10 s break. The lysate was clarified by centrifugation at 35,000 g for 30 min. The supernatant was flash-frozen and stored for further steps.

3xFLAG-tagged ArfB was enriched using anti-FLAG M2 beads. The beads were equilibrated in AFC buffer supplemented with 1 protease inhibitor tablet per 50 mL buffer. 10% Triton X-100 was added to the clarified lysate for a final concentration of 0.1%, then the lysate was the incubated with 100 µL anti-FLAG M2 beads for 1 hour at 4°C while rotating. The beads were washed with a total of 1 mL AFC buffer, then bound proteins were eluted by incubating for 3 min at 95°C in SDS sample buffer without reducing agents. The eluted proteins were loaded on 4-20% SDS-PAGE gradient gels (BioRad), and bands corresponding to the size of ArfB (14 kDa) were excised for mass spectrometry analysis.

3.2.13 Targeted mass spectrometry

Isolated endogenous ArfB was digested using the protease ArgC in order to obtain a peptide containing the GGQ motif. Targeted mass spectrometry analysis was performed using the Q Exactive HF (Thermo Fischer); data analysis was carried out in the software Skyline (University of Washington, USA) by Dr. Ingo Wolgemuth (Department of Physical Biochemistry, Max Planck Institute for Biophysical Chemistry).

4 RESULTS

4.1 Substrate specificity of ArfB

The issue of substrate specificity of ArfB can be simplified to one of the interplay between ArfB and mRNA extending past the ribosomal P site. In the case of ribosomes stalled on truncated mRNAs, the A site is unoccupied by aminoacyl-tRNA, and the mRNA entry channel is empty. In the case of ribosomes stalled on rare codon clusters, however, the A site may still be unoccupied due to a lack of cognate ternary complex corresponding to the rare codon in question, but the mRNA in the mRNA entry channel extends beyond the P site. According to biochemical studies using purified ArfB and stalled ribosomes assembled in the PURE system, ArfB can resolve the latter type of stalling (Handa et al., 2011).

To accurately measure the activity of ArfB on ribosomes stalled in the middle of mRNAs, we purified ribosomal complexes stalled on mRNAs of varying length, translating only the first two codons so all ribosomal complexes would have the same radioactive fMet-Phe dipeptide in the P site, but have increasing lengths of mRNA extending past the P site (**Figure 4.1a**).This was achieved by providing only the ternary complexes for the first codon in the translation reaction. We then proceeded to measure the effect of mRNA length on the ArfB-mediated peptidyl-tRNA hydrolysis reaction (**Figure 4.1b**).

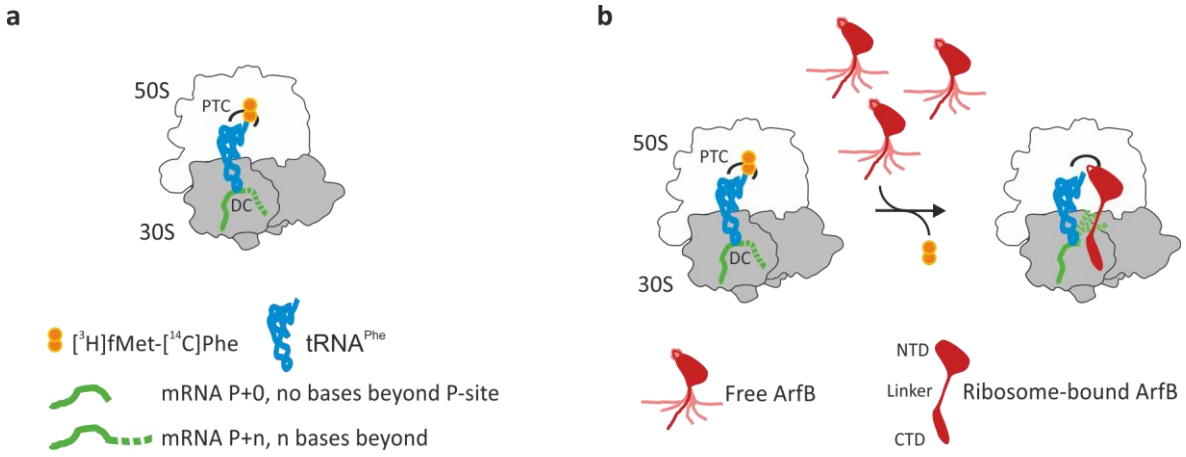

Figure 4.1. Schematic of the single-round hydrolysis experiment. **(a)** P+n complexes. **(b)** P+n complexes were mixed with excess ArfB, and released dipeptides were quantified.

4.1.1 Single-round ArfB-mediated hydrolysis on P+n complexes

We measured pre-steady state time courses of ArfB-mediated peptidyl-tRNA hydrolysis on stalled ribosomes with increasing lengths of mRNA extending past the P site. Using the quenched flow apparatus, we rapidly mixed excess ArfB with P+n complexes (n = 0, 3, 6, 9, 12, 15, 24, 30, 99 nucleotides extending past the ribosomal P site). The resulting curves were fit with single-exponential equations (**Figure 4.2a**), which in turn gave the apparent rate constant of the hydrolysis reaction ($k_{hydrolysis}$).

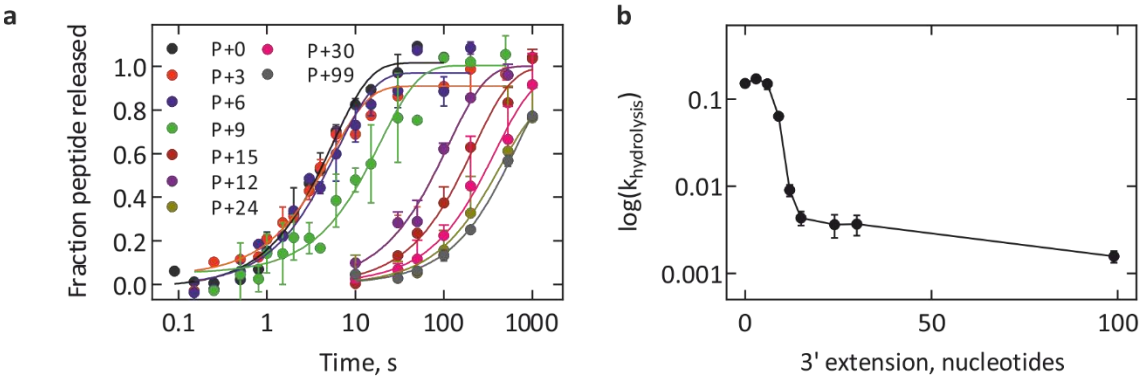

Figure 4.2. ArfB preferentially hydrolyzes peptidyl-tRNA on stalled ribosomes with less than 6 nucleotides extending past the P site. **(a)** Time course of single-round peptidyl-tRNA hydrolysis. P+n complexes (0.15 µM) were rapidly mixed with ArfB (1 µM). Error bars represent the range of values of two biological replicates. **(b)** The apparent rate of peptidyl-tRNA hydrolysis on P+n complexes. Error bars show the standard error of the fit.

The apparent rate constant of the single-round hydrolysis reaction decreases dramatically on stalled ribosomes with more than 6 nucleotides extending past the P site, decreasing by more than 2 fold from P+0 to P+9 complexes (**Figure 4.2b**). On P+99 complexes, hydrolysis occurs at approximately 0.0016 s^{-1}, two orders of magnitude slower than on of P+0 complexes (approximately 0.15 s^{-1}). It is worth noting that while slow, the hydrolysis reaction still reaches saturation after more than 20 min incubation, which is in line with previous reports of steady-state measurements that show ArfB-mediated rescue of ribosomes stalled on longer mRNAs (Handa et al., 2011). Our pre-steady state measurements, however, show that this hydrolysis occurs at a very slow rate.

4.1.2 Competition between ArfB and cognate ternary complex

The slow rate of ArfB-mediated peptidyl-tRNA hydrolysis calls into question whether its activity on ribosomes stalled on longer mRNAs is physiologically relevant. With a codon presented in the A site, there are A-site binding translation factors that may compete with ArfB for a binding site, with the most abundant being elongation factor EF-Tu (Jacobson and Rosenbusch, 1976). To test if this affects ArfB activity, we performed competition experiments to measure ArfB-mediated hydrolysis in the presence of cognate ternary complex (TC) EF-Tu – GTP – [^{14}C]Phe-tRNA^{Phe}.

We incubated P+3 or P+33 complex with ArfB and TC simultaneously, and monitored dipeptide formation and fMet release at concurrent time points (**Figure 4.3a**). Unlike those used in previously described single-round hydrolysis experiments, the ribosomal complexes were stalled with a single [^{3}H]fMet-tRNA^{Met} in the ribosomal P site. The ternary complex was formed with [^{14}C]Phe-tRNA^{Phe}, in cognate to the A-site codon on the stalled ribosomal complexes. We find that dipeptide formation dominates when ArfB concentration is low, with over 50% dipeptide formation as opposed to less than 40% fMet release at 20 and 120 s, levels consistent with control experiments where no ArfB was added (**Figure 4.3b**). At high ArfB concentration, however, fMet hydrolysis is the dominant reaction on P+3 complexes (**Figure 4.3c**). Furthermore, we also find that dipeptide formation is the main reaction occurring on P+33 complexes, regardless of ArfB concentration.

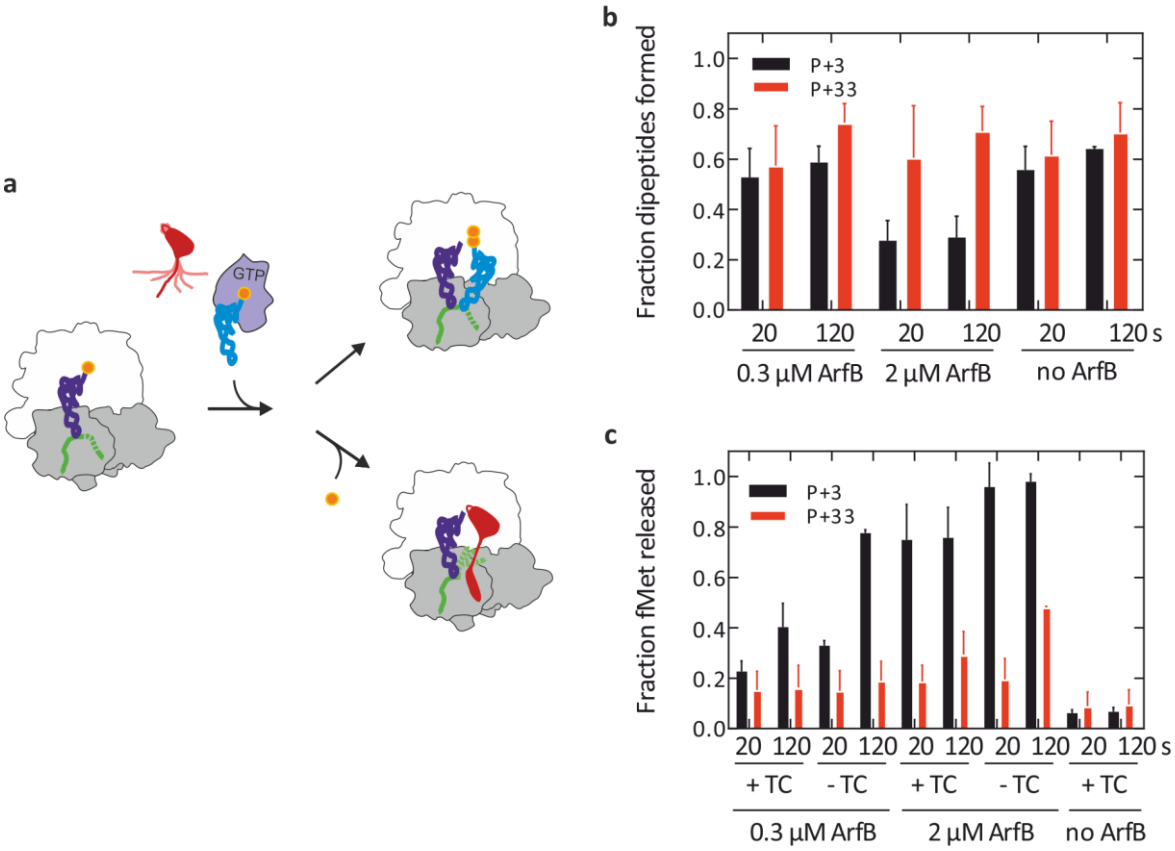

Figure 4.3. Cognate ternary complex competes with ArfB. **(a)** Schematic of the competition experiment. P+n complexes are mixed with both ArfB and cognate ternary complex, and dipeptide formation and fMet release are quantified. **(b)** Dipeptide formation on P+n complexes (0.5 µM) in the presence of ArfB (0.3 or 2 µM) and cognate ternary complex EF-Tu-GTP-[^{14}C]Phe-tRNA^{Phe} (0.25 µM). **(c)** ArfB-mediated fMet release on P+33 complexes in the presence of cognate ternary complex. Error bars indicate the range of values of two biological replicates.

This experiment shows that in the presence of cognate ternary complex, ArfB-mediated peptidyl-tRNA hydrolysis is precluded on ribosomes stalled in the middle of an mRNA. As ArfB expression levels are low under experimentally tested conditions (Schmidt et al., 2016; Taniguchi et al., 2010), it seems unlikely that the ArfB rescue pathway can compete with translation elongation, even on ribosomes with only 3 nucleotides extending past the P site.

4.1.3 Competition between ArfB and non-cognate ternary complex

In the case of ribosomes stalled on rare codon clusters, cognate ternary complexes are by definition scarce, whereas non-cognate ternary complexes (where the associated aminoacyl-tRNA does not correspond to the codon presented in the ribosomal A site) may still transiently bind to the ribosome (Rodnina et al., 1995). To assess if this transient binding of non-cognate

TC can affect ArfB-mediated ribosome rescue, we performed peptidyl-tRNA hydrolysis time courses in the presence of non-cognate ternary complex EF-Tu – GTP – Val-tRNA^{Val}.

We incubated P+3 and P+33 with ArfB and non-cognate ternary complex which was formed with Val-tRNA^{Val} (**Figure 4.4a**) The codon presented in the ribosomal A site encoded Phe, and a higher ArfB concentration was selected for P+33 to ensure a readout that could be reliably quantified. fMet release was monitored over time. The resulting curves overlap under all conditions, indicating that the presence of non-cognate ternary complex does not affect ArfB-mediated peptidyl-tRNA hydrolysis, regardless of mRNA length (**Figure 4.4b** and **Figure 4.4c**).

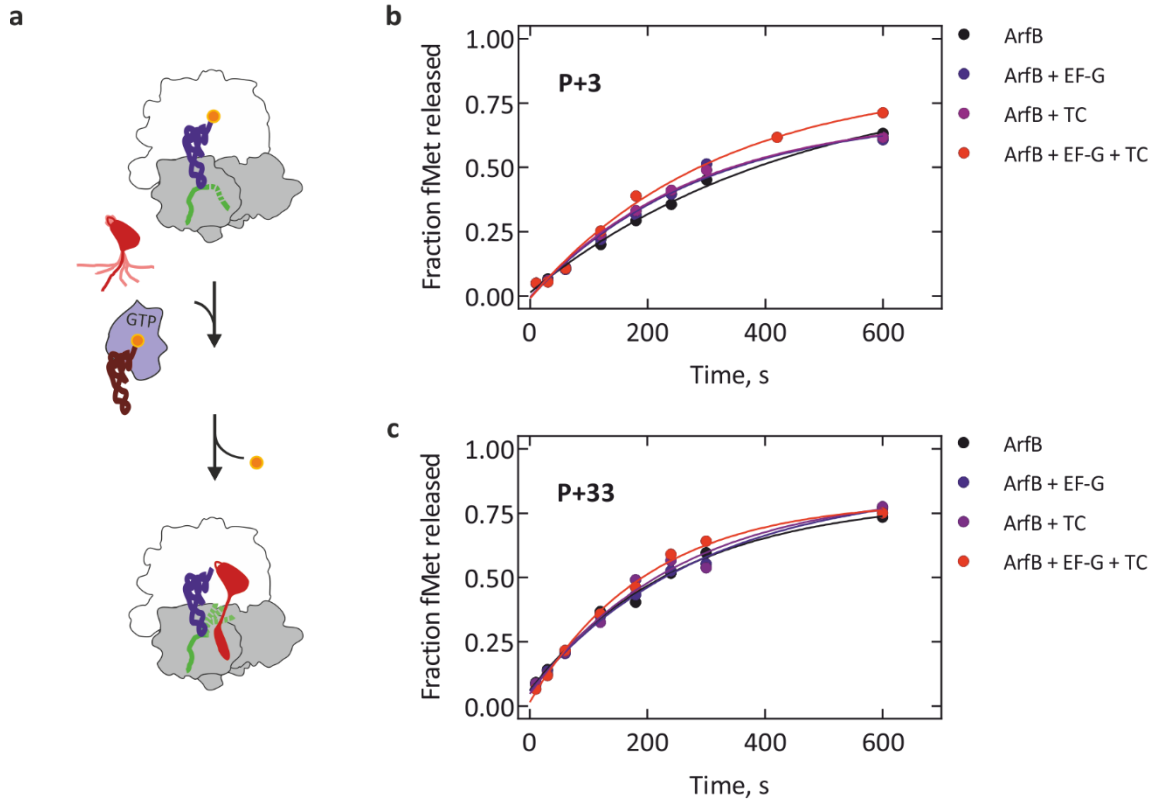

Figure 4.4. Non-cognate ternary complex does not affect ArfB-mediated ribosome rescue. **(a)** Schematic of the competition experiment. P+n complexes are mixed with both ArfB and non-cognate ternary complex, and fMet release is quantified. fMet release at 37°C in the presence of ternary complex (TC, 10 µM EF-Tu, 5 µM Val-tRNA^{Val}, 0.5 mM GTP) on **(b)** P+3 complexes (0.5 µM) incubated with ArfB (0.1 µM) and **(c)** P+33 complexes (0.5 µM) incubated with ArfB (2 µM).

4.1.4 Mechanism of inhibition by mRNA

To understand how mRNA in the mRNA entry channel inhibits ArfB-mediated ribosome rescue, we performed Michaelis-Menten titrations to determine the values of the constants K_M and k_{cat}. Time courses of ArfB-mediated peptidyl-tRNA hydrolysis were measured at increasing concentrations of P+0 and P+9 complex. P+9 complex was chosen because it was shown to be the mRNA length at which the apparent rate of hydrolysis significantly decreased, but is still reliably quantifiable by our methods.

The resulting curves were fit with hyperbolic equations, from which we could compute K_M, or the concentration at which the reaction velocity reaches its half-maximum value. The K_M for P+0 is 0.25 ± 0.09 μM, and k_{cat}, the maximum velocity of the reaction divided by total ArfB concentration, is approximately 0.01 s^{-1} (**Figure 4.5a**). We could not titrate the curve for P+9 to saturation, due to the infeasibility of using ribosomal complexes at concentrations higher than 2 μM; the specificity constant k_{cat}/K_M is therefore reported (**Figure 4.5b**).

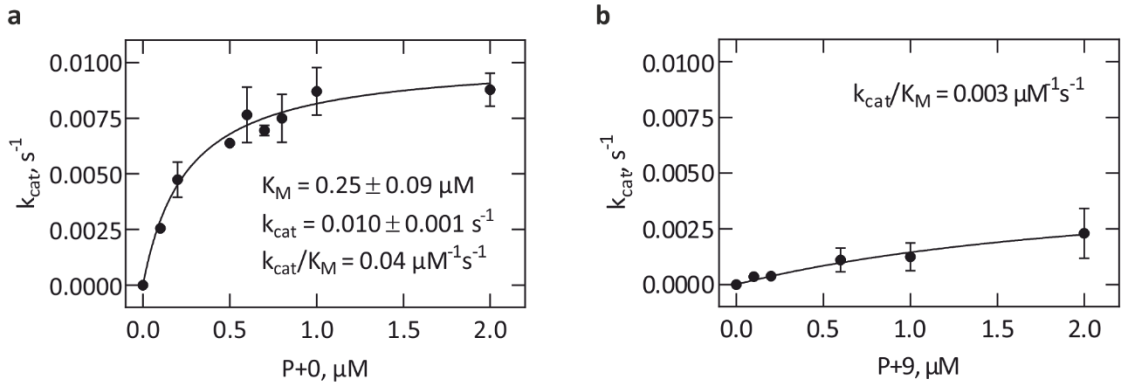

Figure 4.5. mRNA inhibits ArfB-mediated ribosome rescue. **(a)** Michaelis-Menten curve of ArfB-mediated peptidyl-tRNA hydrolysis on P+0 complexes. ArfB (0.02 μM) was incubated with increasing concentrations of P+0 complex. **(b)** Michaelis-Menten curve of ArfB-mediated peptidyl-tRNA hydrolysis on P+9 complexes. ArfB (0.05 μM) was incubated with increasing concentrations of P+9 complex. Error bars represent the SEM of three biological replicates.

k_{cat}/K_M, called the "specificity constant", can be used to compare the two substrates P+0 and P+9. For P+0, the specificity constant is 0.04 s μM^{-1}, whereas for P+9 it is 0.003 s μM^{-1}. This approximately 13 fold difference shows that ArfB is more specific for P+0 than for P+9. The low k_{cat}, however, also shows that ArfB is a catalytically inefficient enzyme, with its turnover likely limited by dissociation.

4.1.5 Effect of recycling factors on ArfB turnover

The low k_{cat} of ArfB creates an interesting conundrum regarding its physiological role. Under experimentally tested conditions, the expression of ArfB in *E. coli* is very low (Taniguchi et al., 2010), and while the low cellular concentration can be compensated for by high binding affinity, the slow turnover would make ArfB a very inefficient release factor. The question remains if there are factors that assist ArfB dissociation and accelerate turnover. To answer this question, we tested known factors associated with ribosome recycling using turnover assays.

While the detailed mechanism is still under debate, it is known that EF-G and RRF together facilitate the dissociation of deacylated tRNA and mRNA, as well as ribosome splitting (Gao et al., 2005; Peske et al., 2005). We therefore performed the initial velocity measurements described in section 4.1.4 in the presence of EF-G and RRF.

When the buffer was supplemented with GTP, we observe a moderate increase in initial velocity with EF-G and RRF present (**Figure 4.6a**). The addition of EF-G and RRF individually also produced an increase in initial velocity to a lesser extent. The same trend is observed in an experiment where the buffer was supplemented with the slow-hydrolyzing GTP analog GTP-γS (**Figure 4.6b**). In the absence of nucleotide altogether, the additions of EF-G and RRF also increase initial velocity to a small degree (**Figure 4.6c**).

By taking the concentration of peptides released at the 5-min time point and dividing it by the enzyme concentration, we calculate the average number of times each ArfB molecule hydrolyzed the dipeptide (**Figure 4.6d**). The addition of RRF and EF-G increases this number by almost 30%. This suggests that the presence of ribosome recycling machinery moderately accelerates ArfB turnover, a phenomenon that may be independent of GTP hydrolysis.

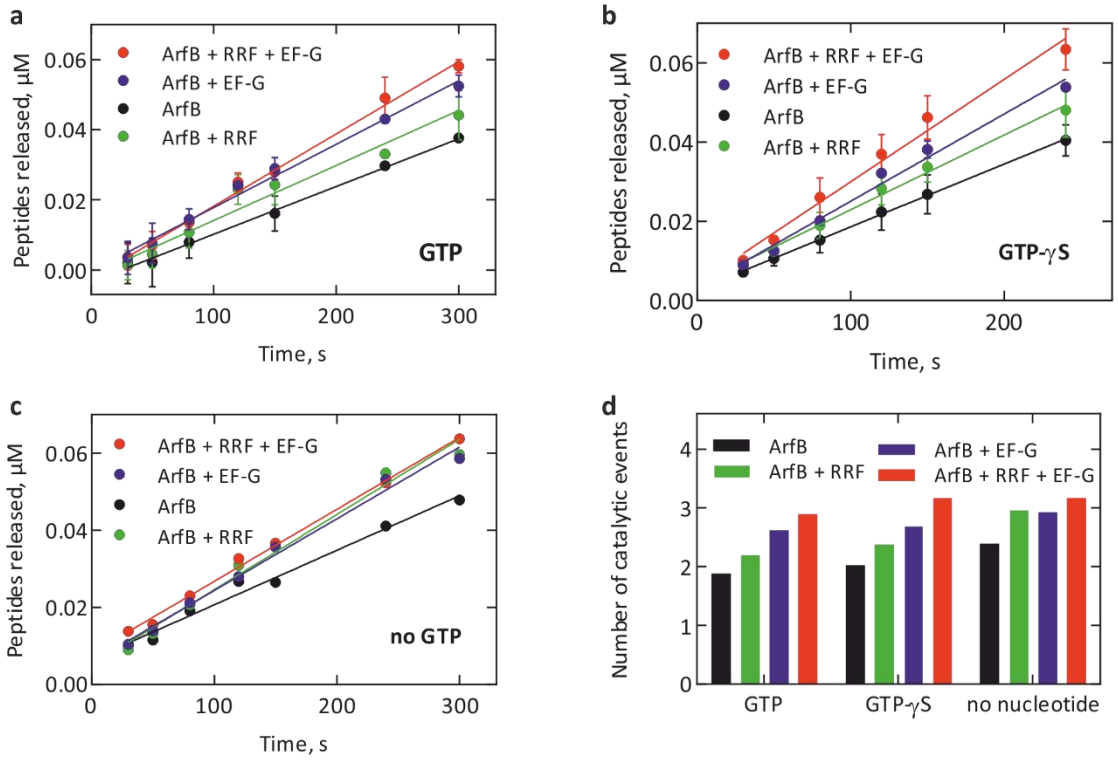

Figure 4.6. Recycling factors accelerate ArfB turnover. ArfB (0.02 μM) was incubated with P+0 complex (0.2 μM) in the presence of RRF (0.5 μM) and EF-G (0.5 μM) in the presence of **(a)** GTP (1 mM), **(b)** GTP-γS, and **(c)** no nucleotide. Solid lines represent the linear fit of the time course, and error bars represent the SEM of three independent experiments. **(d)** Number of catalytic events per ArfB molecule, calculated as peptides released divided by ArfB concentration.

4.2 Initial binding of ArfB

The crystal structure of ArfB shows the C-terminal tail occupying the mRNA entry channel, which should clash with mRNA extending past the P site (Gagnon et al., 2012). This suggests that the specificity of ArfB for ribosomes stalled on truncated mRNA may arise from binding. To evaluate the effect of mRNA on ArfB interactions with the ribosome, we developed a Förster resonance energy transfer (FRET) pair to report on binding events (Lakowicz, 1988). Briefly, FRET occurs between an excited donor fluorophore and an acceptor fluorophore when they come into a close distance that is comparable to the size of proteins (30 – 60 Å). The fluorescence change of the donor fluorophore and of the acceptor fluorophore therefore reports on changes of distance between two labeled proteins. We labeled stalled ribosomal complexes with a donor fluorophore, and attached an acceptor fluorophore to ArfB to directly monitor ArfB binding over time (**Figure 4.7**).

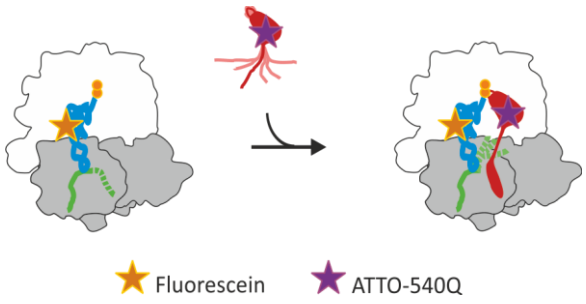

Figure 4.7. Schematic of the ArfB binding experiment. Fluorescein-labeled P+n complexes are rapidly mixed with ATTO-540Q-labeled ArfB and fluorescence change is monitored over time.

4.2.1 Activity of labeled ArfB and ribosomal complexes

We prepared P+0, P+9, and P+30 complexes with [^{14}C]Phe-tRNA^{Phe}(Flu), which is labeled with fluorescein on position 8 of the tRNA^{Phe}. This resulted in stalled ribosomal complexes with a fluorescent P-site tRNA. ArfB was labeled with the fluorescence quencher ATTO-540Q on positions 96 and 112, on the globular N-terminal domain and the C-terminal tail, respectively.

The activity of the labelled ArfB and ribosomal complexes was tested by single-round peptide release as described in section 4.1.1. All the components show comparable activity to their wild-type counterparts (**Figure 4.8a, Figure 4.8b**). We can therefore use fluorescence-labeled ArfB and P+n complexes to study ArfB binding.

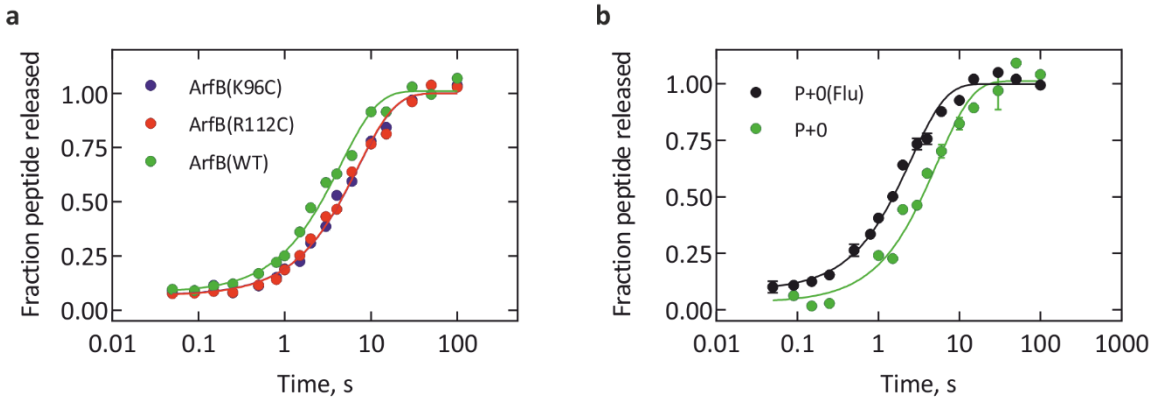

Figure 4.8. The activity of fluorescence-labeled P+0 complex and quencher-labeled ArfB is comparable to unlabeled, wild-type components. **(a)** ATTO-540Q labeled ArfB(K96C) and ArfB(R112C) (1 µM) have similar activity ($k_{hydrolysis}$ = 0.14 ± 0.01 s^{-1} for both variants) on P+0 complexes (0.15 µM) as unlabeled wild-type (WT) ArfB ($k_{hydrolysis}$ = 0.23 ± 0.02 s^{-1}) in the single-round hydrolysis time course. **(b)** P+0 complex (0.15 µM) with a fluorescein-labeled P site tRNA (P+0(Flu)) has a similar activity ($k_{hydrolysis}$ = 0.40 ± 0.02 s^{-1}) as the unlabeled complex in the hydrolysis reaction with ArfB (1 µM).

4.2.2 Activity of the hydrolysis-deficient ArfB mutant

To measure ArfB binding to pre-hydrolysis P+n complexes, we used a hydrolysis-deficient variant in some binding experiments. Previous studies have shown that mutating the second residue in the catalytically active GGQ motif can reduce the hydrolytic activity of ArfB (Chadani et al., 2011b). We therefore purified $ArfB_{GAQ}$, where Gly 27 is mutated to Ala.

The hydrolytic activity of the hydrolysis-deficient variant was tested by incubating $ArfB_{GAQ}$ with stalled ribosomal complex at 37°C (**Figure 4.9a**). $ArfB_{GAQ}$ is active on all complexes at 37°C, to the extent that after 40 min incubation, at least 25% of P+30 complex will be in the post-hydrolysis state, creating heterogeneous conditions that would make interpretation of binding experiments difficult.

We then repeated the time courses of peptidyl-tRNA hydrolysis on P+0 complexes at 20°C. P+0 was incubated with $ArfB_{GAQ}$ or ArfB (**Figure 4.9b**). The results show that at 20°C, peptidyl-tRNA hydrolysis by $ArfB_{GAQ}$ is comparable to that of the background where no ArfB was added for up to 2 hours. Using $ArfB_{GAQ}$ at this temperature, we are able to measure ArfB binding to stalled ribosomes exclusively in the pre-hydrolysis state.

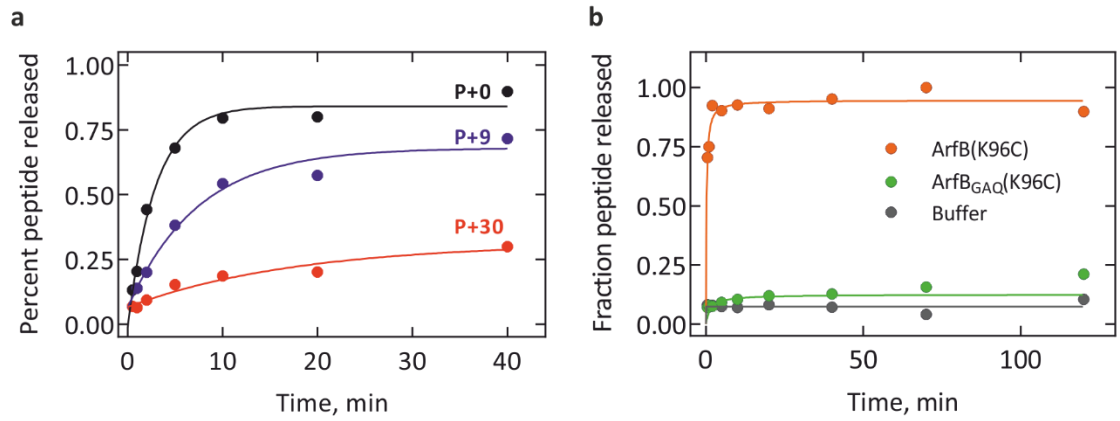

Figure 4.9. Hydrolytic activity of $ArfB_{GAQ}$. **(a)** Time courses of peptidyl-tRNA hydrolysis by $ArfB_{GAQ}$ (1 µM) on P+0, P+9, and P+30 (0.1 µM) complexes at 37°C. **(b)** Peptidyl-tRNA hydrolysis by ATTO-540Q labeled ArfB(K96C) and $ArfB_{GAQ}$(K96C) (1 µM) on P+0 complexes (0.1 µM) at 20°C.

4.2.3 Binding of $ArfB_{GAQ}$ to ribosomes in real time

To measure the binding of ArfB to ribosomes in real time, we rapidly mixed quencher-labeled $ArfB_{GAQ}$(K96C) with P+0(Flu) in the stopped flow apparatus at 20°C. Upon ArfB binding, the two fluorescent dyes come into close contact and the fluorescence of the donor fluorophore, fluorescein, is quenched by the acceptor fluorophore, ATTO-540Q. The decrease in donor fluorescence over time reports on the binding of ArfB.

At 20°C, ArfB binds to the ribosome very rapidly, so that at higher concentrations of ArfB, the reaction occurs in the dead-time of the stopped flow (1 – 1.5 ms) (**Figure 4.10a**). The fluorescence traces of the binding reaction can be described with three exponents, suggesting a multi-step interaction following initial binding, or that we are monitoring more than a single binding event. By plotting the apparent rate constants against ArfB concentration, we determine the rate-concentration relationship for each exponent (**Figure 4.10b**). The apparent rate of the three phases show a linear dependence on ArfB concentration, which is a hallmark of bimolecular association reactions, indicating that the three phases most likely do not show consecutive steps on a multistep pathway. The slope given by the linear fit of apparent rates is the k_{ON} of each phase, while the y-intercept gives the k_{OFF} (**Table 4.1**). For the first phase, which is also the dominant phase according to its amplitude, the k_{ON} is 960 ± 70 μM^{-1} s^{-1}; the k_{OFF} is 43 ± 16 s^{-1}. This suggests that initial binding of ArfB is limited by diffusion; the binding

affinity K_d, calculated from the ratio of k_{off}/k_{on}, is 45 ± 18 nM for the majority of molecules in the population.

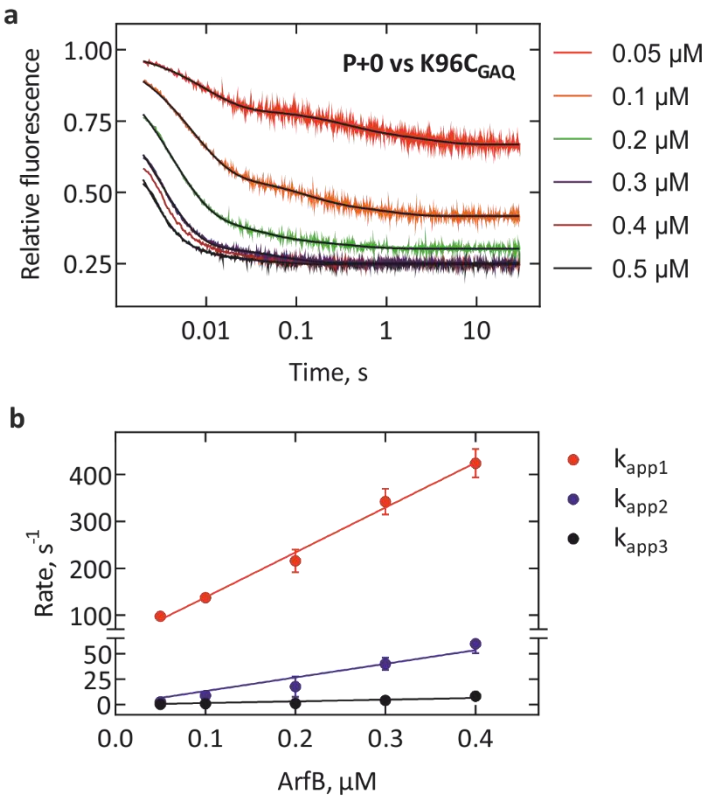

Figure 4.10. ArfB$_{GAQ}$ binds to P+0 complexes rapidly. **(a)** Time courses of quencher-labeled ArfB$_{GAQ}$(K96C) (0.05-0.5 μM) binding to P+0(Flu) (0.015 μM) at 20°C. **(b)** Apparent rate constants of ArfB binding to P+0 complexes, derived from the three exponential fit of the binding traces. Error bars represent the range of values of two independent experiments.

Table 4.1. Association and dissociation rates of ArfB$_{GAQ}$ to P+0 complexes

	k_{app1}	k_{app2}	k_{app3}
k_{ON}, μM^{-1} s^{-1}	960 ± 70	130 ± 10	17 ± 2
k_{OFF}, s^{-1}	43 ± 16	n.s.	n.s.

Association and dissociation rate constants were obtained from the linear fit of the concentration dependence of each apparent rate. Errors are SEM of the fit.

4.2.4 Binding of ArfB to P+0 complexes

Because the binding is very rapid compared to the rate of hydrolysis, we then performed the same binding experiment using catalytically active ArfB(K96C) and P+0(Flu) (**Figure 4.7**). The

resulting traces can be described with three exponents, with the rate constants exhibiting a similar linear dependence on ArfB concentration as with $ArfB_{GAQ}$ (**Figure 4.11b**, **Table 4.2**). For the first exponent, the k_{ON} is 470 ± 40 μM^{-1} s^{-1}, and the k_{OFF} is 110 ± 20 s^{-1}. The calculated K_d is approximately 230 ± 46 nM.

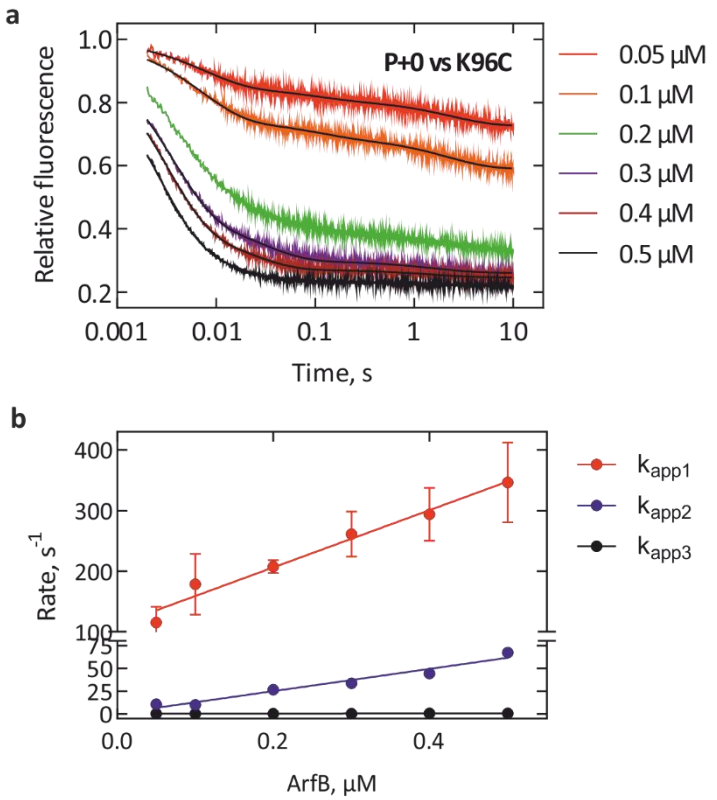

Figure 4.11. ArfB binds to P+0 complexes rapidly. **(a)** Time courses of quencher-labeled ArfB(K96C) (0.05-0.5 µM) binding to P+0(Flu) (0.015 µM) at 20°C. **(b)** Apparent rate constants of ArfB binding to P+0 complexes, derived from the three exponential fit of the binding traces. Error bars represent the range of values of two independent experiments.

Table 4.2. Association and dissociation rates of ArfB to P+0 complexes

	k_{app1}	k_{app2}	k_{app3}
k_{ON}, μM^{-1} s^{-1}	470 ± 40	120 ± 10	1.0 ± 0.2
k_{OFF}, s^{-1}	110 ± 20	n.s.	n.s.

Association and dissociation rate constants were obtained from the linear fit of the concentration dependence of each apparent rate. Errors are SEM of the fit.

4.2.5 Binding of ArfB to P+9 and P+30 complexes

To understand whether the mRNA in the mRNA entry channel affects ArfB binding, we performed binding assays with P+9(Flu) and P+30(Flu) (**Figure 4.12a** and **Figure 4.12b**). The resulting traces can be described with three exponential terms, and the apparent rates show linear dependence on ArfB concentration (**Figure 4.12c**). For P+9(Flu) complexes, the k_{ON} is 280 ± 30 μM^{-1} s^{-1}, and the k_{OFF} is 140 ± 10 s^{-1}. For P+30(Flu) complexes, the k_{ON} is 320 ± 40 μM^{-1} s^{-1}, and the k_{OFF} is 120 ± 10 s^{-1}. The results suggest that binding is also rapid on ribosomes stalled on longer mRNAs, and the association rate constant does not change significantly between the different complexes. Notably, the second and third apparent rate constants also show a linear dependence on ArfB concentration (**Figure 4.12d**, **Table 4.3**). This is an indication that instead of a single binding event followed by a series of conformational changes, we could be observing several binding events in parallel.

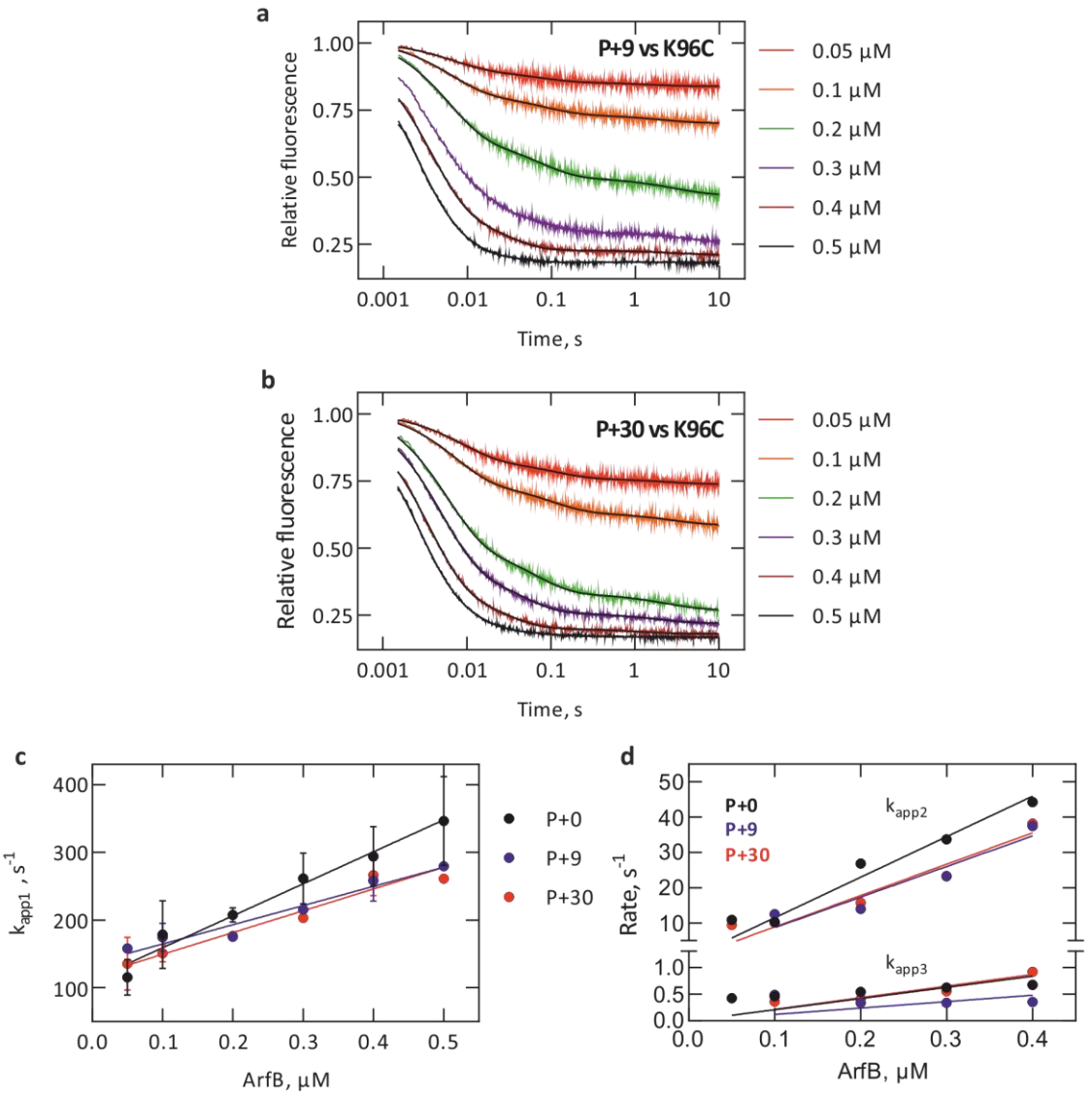

Figure 4.12. ArfB binds to P+9 and P+30 complexes rapidly. **(a)** Time courses of quencher-labeled ArfB(K96C) (0.05-0.5 µM) binding to P+9(Flu) (0.015 µM) at 20°C. **(b)** Time courses of quencher-labeled ArfB(K96C) (0.05-0.5 µM) binding to P+30(Flu) (0.015 µM) at 20°C. **(c)** Concentration dependence of the first apparent rate constant, derived from the three exponential fit of the binding traces. **(d)** Concentration dependence of the second and third rate constants, derived from the three exponential fit of the binding traces. Error bars represent the range of values of two independent experiments.

Table 4.3. Association and dissociation rates of ArfB to P+0, P+9, and P+30 complexes

	P+0	P+9	P+30
Fast k_{ON}, μM^{-1} s^{-1}	470 ± 70	280 ± 30	320 ± 40
Fast k_{OFF}, s^{-1}	110 ± 20	140 ± 10	120 ± 10
Medium k_{ON}, $\mu M^{-1} s^{-1}$	94 ± 4	84 ± 20	80 ± 13
Medium k_{OFF}, s^{-1}	7.0 ± 1.2	0.8 ± 6	2.5 ± 3.2
Slow k_{ON}, μM^{-1} s^{-1}	0.7 ± 0.1	0.06 ± 0.01	1.8 ± 0.5
Slow k_{OFF}, s^{-1}	0.4 ± 0.1	0.3 ± 0.1	n.s.

Association and dissociation rate constants were obtained from the linear fit of the concentration dependence of each apparent rate. Errors are SEM of the fit.

4.2.6 Effect of magnesium ions on initial binding

Diffusion-limited association rate constants, especially with highly charged proteins such as ArfB, often indicate a strong electrostatic component in the binding reaction (Schreiber and Fersht, 1996; Wendt et al., 1997). To study whether this is also true for the ArfB-ribosome interaction we performed initial binding experiments at three concentrations of Mg^{2+}. We chose Mg^{2+} because it was previously shown to have a strong effect on the alternative binding interaction between IF3 and the large ribosomal subunit (Goyal et al., 2017).

We measured fluorescence change upon rapid mixing of P+n(Flu) with quencher-labeled ArfB(K96C) at 7 mM, 20 mM, and 30 mM $MgCl_2$ (**Figure 4.13a, b,** and **c**). Rapid binding of ArfB is still observed at high magnesium concentrations across all three ribosomal complexes. The traces were fit with three exponents, and the apparent rate constant of the fast, major phase was plotted against magnesium concentration (**Figure 4.13d**). Increased Mg^{2+} concentration does not cause a significant decrease in the rate of initial binding, which suggests that electrostatic interactions play a limited role in the rapid association of ArfB to the ribosome.

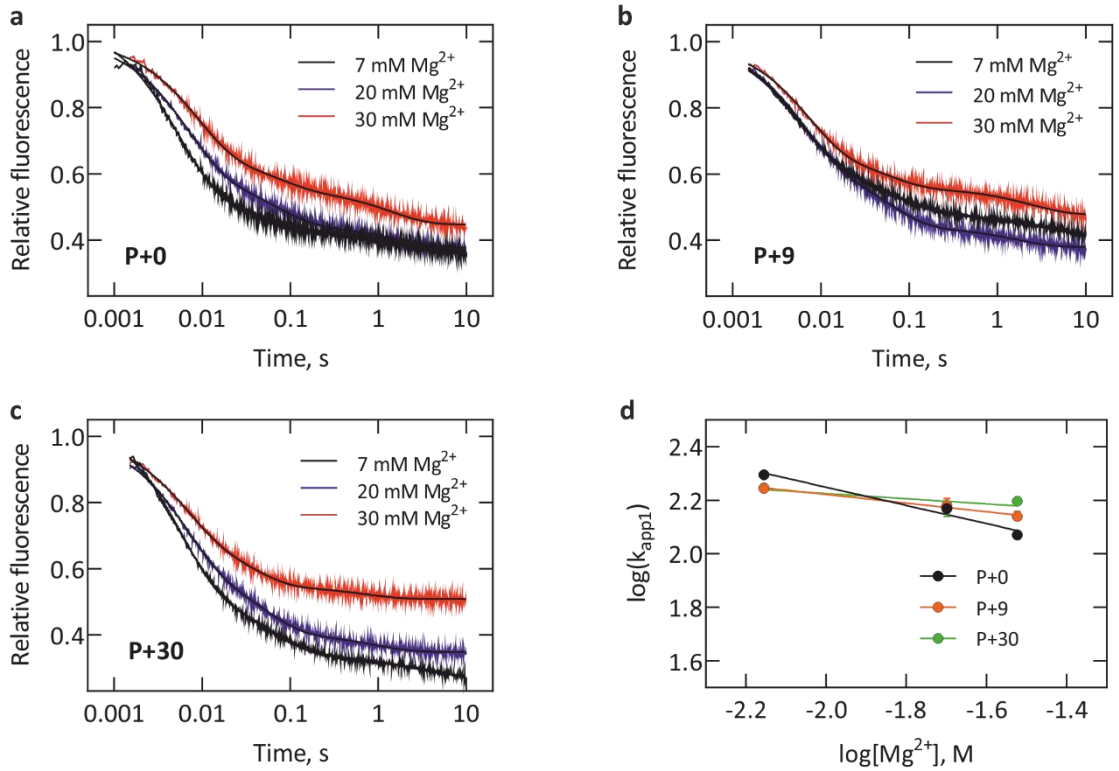

Figure 4.13. Magnesium ions decreases the rate of ArfB initial binding. Time courses of quencher-labeled ArfB(K96C) (0.2 µM) binding to **(a)** P+0(Flu) (0.015 µM), **(b)** P+9(Flu) (0.015 µM), and **(c)** P+30(Flu) (0.015 µM) at 20°C and increasing Mg^{2+} concentrations (7, 20, and 30 mM). **(d)** Effect of Mg^{2+} on the first apparent rate constant, obtained from the three exponential fit of the binding traces. Error bars represent the range of values from two independent experiments.

4.2.7 Dissociation of ArfB from stalled ribosomes

In addition to the association rate constant, our FRET-based stopped flow experimental system allowed us to directly monitor the dissociation of ArfB from the ribosome. This was achieved by pre-incubating ArfB with P+0(Flu), then rapidly mixing in a large excess of unlabeled P+0. The dissociation of ArfB from P+0(Flu) over time is recorded as the recovery of donor fluorescence.

For dissociation from pre-hydrolysis complexes, quencher-labeled $ArfB_{GAQ}$(K96C) was pre-incubated for 10 min at 20°C with P+0(Flu), and the resulting trace can be fit with a two-exponential equation (**Figure 4.14**). The two apparent rates are 0.41 ± 0.01 s^{-1} and 0.04 ± 0.01 s^{-1}. For dissociation from post-hydrolysis complexes, ArfB(K96C) was pre-incubated for 10 min at 37°C with P+0(Flu) to ensure complete peptidyl-tRNA hydrolysis prior to the chase

experiment. The resulting trace was fit with a two-exponential equation (**Figure 4.14**). The apparent rates of dissociation are 0.86 ± 0.02 s^{-1} and 0.04 ± 0.01 s^{-1}.

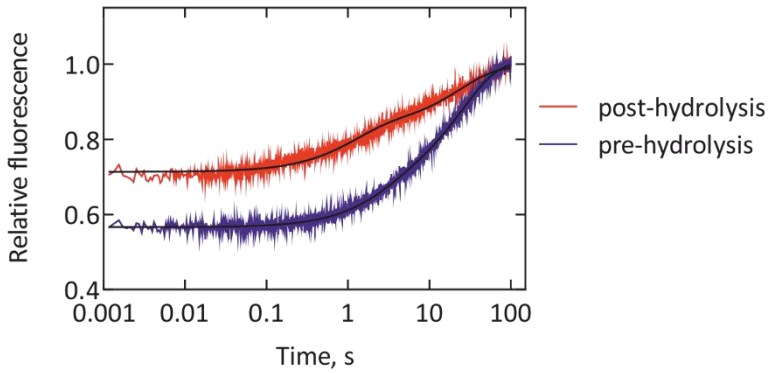

Figure 4.14. Dissociation of ArfB from P+0 complexes. Quencher-labeled ArfB(K96C) or $ArfB_{GAQ}$(K96C) (0.1 µM) was pre-incubated with P+0(Flu) (0.1 µM) then rapidly mixed with P+0 (1 µM).

The effect of mRNA length on dissociation was measured on pre-hydrolysis complexes by chasing quencher-labeled $ArfB_{GAQ}$(K96C) from P+0(Flu), P+9(Flu), and P+30(Flu) complexes. The resulting traces can be fit with two-exponential equations (**Figure 4.15**). For P+9(Flu), the rates are 0.41 ± 0.01 s^{-1} and 0.07 ± 0.01 s^{-1}. For P+30(Flu), the rates are 0.47 ± 0.02 s^{-1} and 0.10 ± 0.01 s^{-1} (**Table 4.4**).

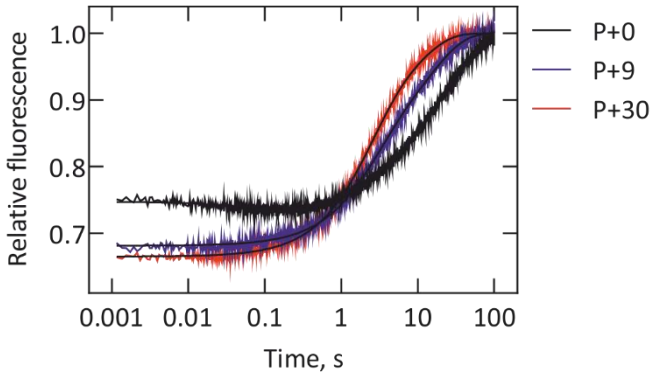

Figure 4.15. Dissociation of ArfB from P+n complexes. Quencher-labeled $ArfB_{GAQ}$(K96C) (0.1 µM) was pre-incubated with P+0(Flu), P+9(Flu), P+30(Flu) (0.1 µM) then rapidly mixed with P+0 (1 µM).

While the dissociation traces are fit with more than one exponent, we can calculate the average rate of dissociation k_{avg} using the following equation:

$$k_{avg} = k_1 * A_1 + k_2 * A_2 + \cdots + k_n * A_n$$

Where k_n is the apparent rate of one exponent, and A_n is the amplitude of the same exponent expressed in fractions of the total amplitude. The resulting average dissociation rates are as shown below in **Table 4.4**.

Table 4.4. Dissociation rates of ArfB.

	k_{app1}, s^{-1}	A_1	k_{app2}, s^{-1}	A_2	k_{avg}
P+0 (post-hydrolysis)	0.86 ± 0.01	0.43 ± 0.01	0.04 ± 0.01	0.57 ± 0.01	0.39 ± 0.01
P+0 (pre-hydrolysis)	0.41 ± 0.01	0.21 ± 0.02	0.04 ± 0.01	0.79 ± 0.02	0.06 ± 0.01
P+9 (pre-hydrolysis)	0.41 ± 0.01	0.47 ± 0.01	0.07 ± 0.01	0.53 ± 0.01	0.23 ± 0.01
P+30 (pre-hydrolysis)	0.47 ± 0.01	0.61 ± 0.01	0.10 ± 0.01	0.39 ± 0.01	0.33 ± 0.01

Dissociation rate constants were obtained from the 3-exponential (for P+0 post-hydrolysis) or 2-exponential (for pre-hydrolysis traces) fit of the traces shown in Figures 4.13 and 4.14. Errors are SEM of the fit. k_{avg} is the average rage of dissociation calculated from the apparent rates.

The vastly slower rate of dissociation measured by chase experiments, in comparison to the k_{OFF} obtained from the binding experiments, suggests that there may be an additional step following binding that makes ArfB more stably bound to the ribosome. We call this potential step “engagement”, and the following designed experiments are aimed at understanding the selectivity of the engagement step.

4.3 ArfB binding to the ribosome is tight and stable

4.3.1 Affinity of ArfB for P+n complexes

If there is indeed an engagement step as the measured ArfB dissociation rates indicate (see section 4.2.7), we would expect the overall affinity constant K_d to differ from the number calculated by the k_{OFF}/k_{ON} of initial binding (see sections 4.2.4 and 4.2.5). Therefore, we turned to steady-state measurements of ArfB binding. Using the FRET pair described above, we titrated P+0(Flu) (2 nM) with sub-stoichiometric amounts of quencher-labeled $ArfB_{GAQ}$(K96C) in the fluorimeter, recording the fluorescence intensity at each ArfB concentration until the binding curve reached saturation. The resulting curve was fit with a quadratic equation to account for ligand depletion. Because relative fluorescence (calculated as $Y = \frac{Y_n}{Y_0}$, where Y_n is the fluorescence intensity at concentration n of ArfB, and Y_0 is the starting fluorescence intensity) corresponds to the fraction of ArfB-bound ribosomes at that particular ArfB concentration, we could convert the curve to show the fraction of ArfB-bound ribosomes with the equation $Y' = Y + (-1) + 1$, where Y' is the fraction of ribosomes bound, and Y is relative fluorescence. The curve fit gives a K_d of 4.3 ± 0.7 nM, an affinity 40 times higher than that calculated from the initial binding experiments (**Figure 4.16a**). The affinity of ArfB to P+9 and P+30 complexes are K_d = 13.2 ± 2.4 nM and 17.8 ± 1.3 nM, respectively (**Figure 4.16b** and **Figure 4.16c**).

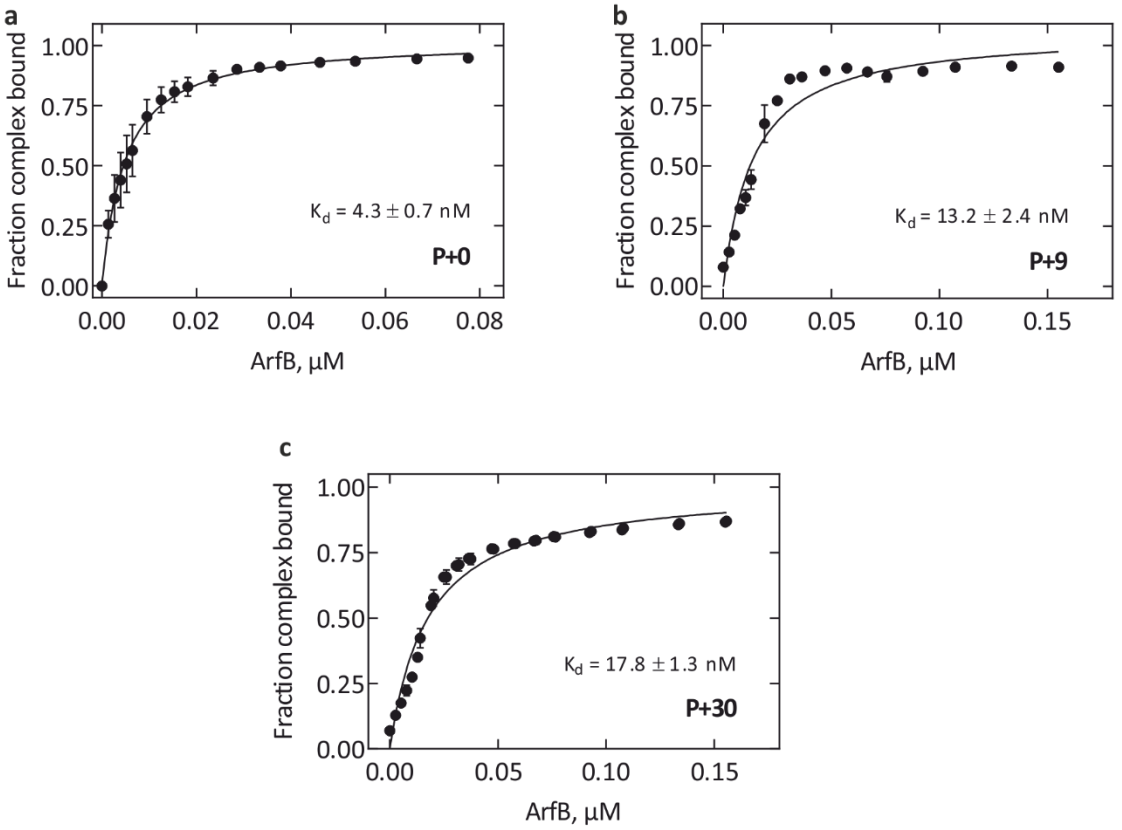

Figure 4.16. ArfB binds tightly to stalled ribosomes. Affinity of ArfB for P+0 complexes. Quencher-labeled $ArfB_{GAQ}$(K96C) was titrated into **(a)** P+0(Flu), **(b)** P+9(Flu), and **(c)** P+30(Flu) (2 nM) and the fluorescence change recorded. Binding curves were fit with a quadratic equation. Error bars represent the SEM of three independent experiments.

Due to the high affinity of ArfB for stalled ribosomes, our FRET-based affinity measurements were performed at low concentrations. To verify our findings, we also performed anisotropy-based affinity titrations using single-cysteine variants labeled with fluorescein (Lakowicz, 1988) (**Figure 4.17a**). The rotational freedom of the dye decreases upon ArfB binding to the ribosome, which is observed as an increase in anisotropy (**Figure 4.17b**).

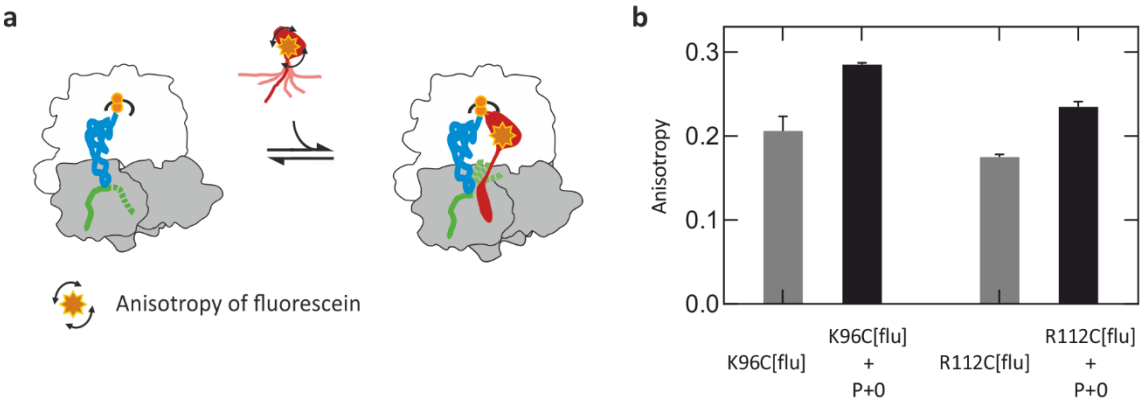

Figure 4.17. Anisotropy change reports on ArfB binding to the ribosome. **(a)** Schematic of anisotropy-based ArfB binding experiments. Fluorescein-labeled ArfB(K96C) is mixed with P+n complexes, and the anisotropy of the dye is recorded. **(b)** Anisotropy of the dye on ArfB increases upon binding to the ribosome. Fluorescein-labeled ArfB(K96C) and ArfB(R112C) (10 nM) were mixed with excess P+0 complex (30 nM). Error bars represent the SEM of three independent experiments.

Fluorescein-labeled ArfB(K96C) and ArfB(R112C) (10 nM) were titrated with unlabeled P+0 and P+12 complexes in the fluorimeter (**Figure 4.18a** and **Figure 4.18b**). The resulting curve was fit with a hyperbolic equation. For P+0 complexes, the K_d values are 2.9 ± 0.7 nM and 1.3 ± 0.3 nM for ArfB(K96C) and ArfB(R112C), respectively. For P+30 complexes, the K_d values are 2.3 ± 0.8 nM and 6.5 ± 1.9 nM for ArfB(K96C) and ArfB(R112C), respectively. Finally, to ensure that the affinity constant we measure is exclusively that of pre-hydrolysis complexes, we repeated the anisotropy-based titration using fluorescein-labeled $ArfB_{GAQ}$(K96C) (**Figure 4.18**). Our titrations with P+0, P+9, and P+30 complexes yield K_d values of 1.8 ± 0.3 nM, 2.3 ± 0.3 nM, and 8.3 ± 0.8 nM, respectively. The K_d values obtained from these titrations are 20 to 50 fold lower than the K_d values calculated as k_{OFF}/k_{ON} as described in section 4.2.4, indicating that subsequent steps following initial binding stabilize ArfB on the stalled ribosome. A comparison of K_d values calculated from initial binding experiments and measured by FRET and anisotropy is shown in **Table 4.5**.

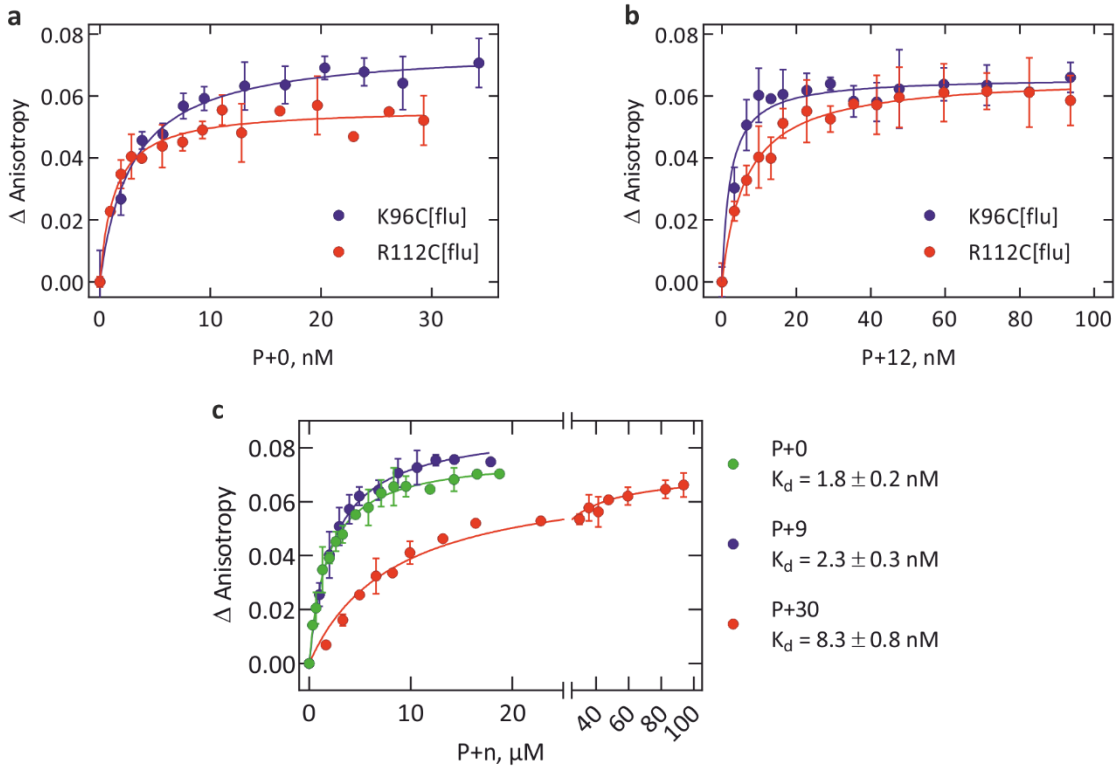

Figure 4.18. ArfB binds tightly to stalled ribosomes. **(a)** Affinity of ArfB for P+0 complexes. ArfB(K96C) (10 nM) and ArfB(R112C) (10 nM) were titrated with P+0. **(b)** Affinity of ArfB for P+12 complexes. ArfB(K96C) (10 nM) and ArfB(R112C) (10 nM) were titrated with P+12 complexes. **(c)** Affinity of $ArfB_{GAQ}$ for P+0, P+9, and P+30 complexes. $ArfB_{GAQ}$(K96C) (10 nM) was titrated with P+n complexes. All single-cysteine ArfB variants were labeled with fluorescein. The anisotropy change at each ribosome concentration was recorded; binding curves were fit with hyperbolic equations, and error bars represent the SEM of three independent experiments.

Table 4.5. Affinity constants of ArfB for stalled ribosomes

	P+0	P+9	P+30
K_d (k_{OFF}/k_{ON}), nM	230 ± 50	470 ± 60	400 ± 60
K_d (FRET), nM	4.3 ± 0.7	13.2 ± 2.4	17.8 ± 1.3
K_d (anisotropy), nM	1.8 ± 0.2	2.3 ± 0.3	8.3 ± 0.8

Apparent rates were obtained by exponential fitting of dissociation traces. Average rates were calculated as the sum of each exponent multiplied by its amplitude.

4.3.2 Effect of buffer ionic strength on ArfB binding

The C-terminal tail of ArfB consists of several positively charged residues, and it is likely that its strong interactions with the ribosome are primarily mediated by electrostatic interactions. To test whether the tight binding of ArfB to the ribosome is mainly due to strong electrostatic interactions, we measured anisotropy change at increased potassium chloride concentrations (**Figure 4.19a**). The resulting dose-response curve shows that the interactions between ArfB and the ribosome are indeed electrostatic, however the IC_{50} or half-maximal inhibitory concentration of approximately 260 mM KCl exceeds the cellular concentration of potassium (180 – 200 mM, (Cayley et al., 1991)), indicating that these interactions are stable under physiological conditions.

As divalent salt concentration is an important factor in ribosome dynamics (Rodnina et al., 2011), we also titrated ArfB-bound P+0 and P+9 complexes with $MgCl_2$ and recorded anisotropy change (**Figure 4.19b**). The IC_{50} is approximately 40 mM and 30 mM for P+0 and P+9 complexes, respectively.

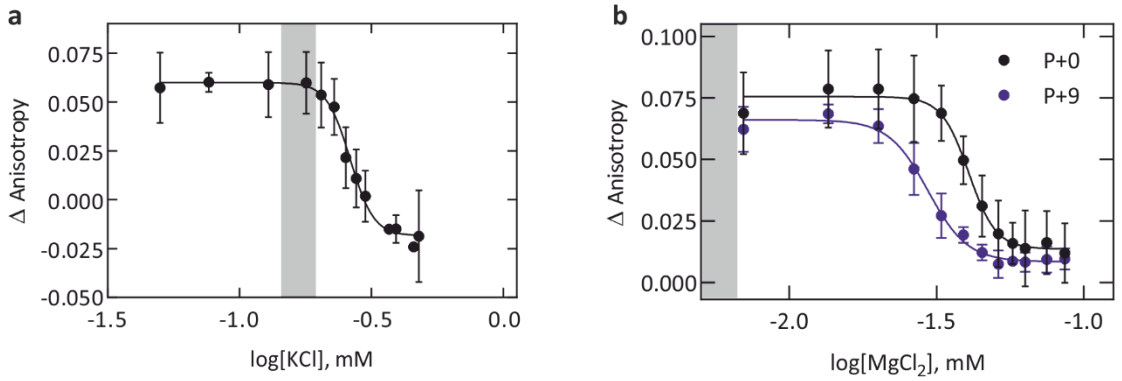

Figure 4.19. ArfB binding remains stable at high salt concentration. **(a)** Effect of monovalent salt on ArfB binding. $ArfB_{GAQ}$(K96C) (50 nM) bound to P+0 (150 nM) was titrated with KCl. **(b)** Effect of divalent salt on ArfB binding. $ArfB_{GAQ}$(K96C) (50 nM) bound to P+0 complex or P+9 complex (150 nM) was titrated with $MgCl_2$. Grey boxes indicate cellular salt concentrations (Cayley et al., 1991). The ArfB variants were labeled with fluorescein. The curves were fit with a dose-response equation and error bars represent the SEM of three independent experiments.

These very high affinity constants show that despite initially labile interactions with the ribosome shown by our binding experiments (see sections 4.2.4 and 4.2.5), engagement increases the affinity of ArfB for the ribosome. The relatively high tolerance for salt suggests

that the interactions between ArfB and stalled ribosomes is specific. It also gives us reason to think that under physiological conditions (Cayley et al., 1991) this interaction is as strong as what we measure *in vitro*.

4.4 Peptidyl-tRNA hydrolysis

Moving further along the pathway of ArfB-mediated ribosome rescue, we measured the apparent rate of peptidyl-tRNA hydrolysis by rapidly mixing ArfB and P+0 and P+9 complexes in the quenched flow at 37°C.

4.4.1 Rates of single-round hydrolysis

We titrated excess ArfB over P+0 complexes. At lower ArfB concentrations (up to 0.6 µM), the curves can be described with two exponents, while at higher concentrations the curve can be described with one exponent (**Figure 4.20a**). The rate of the first phase is 0.15 ± 0.01 s^{-1} and does not show a dependence on ArfB concentration, (**Figure 4.20b**). The two exponential behavior is likely due to non-pseudo first order conditions, with the second exponent describing the second round of hydrolysis (**Figure 4.20c**).

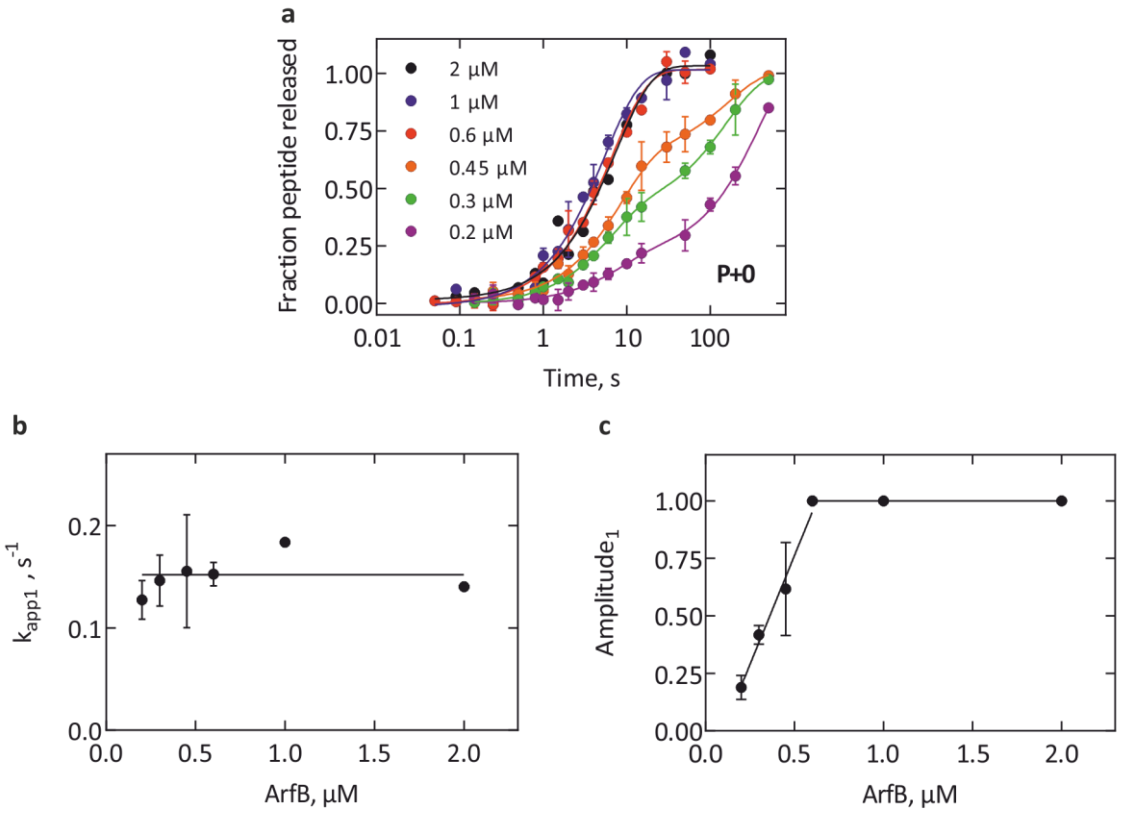

Figure 4.20. ArfB-mediated hydrolysis on P+0 complexes. **(a)** Time courses of peptidyl-tRNA hydrolysis upon rapidly mixing ArfB (0.2-2 µM) with P+0 complexes (0.15 µM). **(b)** The first apparent rate of hydrolysis at different ArfB concentrations. The rates were obtained by fitting the time courses with an exponential equation. **(c)** Amplitudes of the first phase, calculated from the exponential fit of hydrolysis time courses, plotted against ArfB concentration. Error bars represent the range of value of two biological replicates.

To determine whether the hydrolysis rate previously measured for P+9 complexes (**Figure 4.21b**) is also concentration-independent, we performed the same experiment titrating increasing concentrations of ArfB over P+9 complexes (**Figure 4.21a**). We observe a concentration-independent rate of hydrolysis on P+9 complexes of 0.06 ± 0.01 s^{-1} (**Figure 4.21b**).

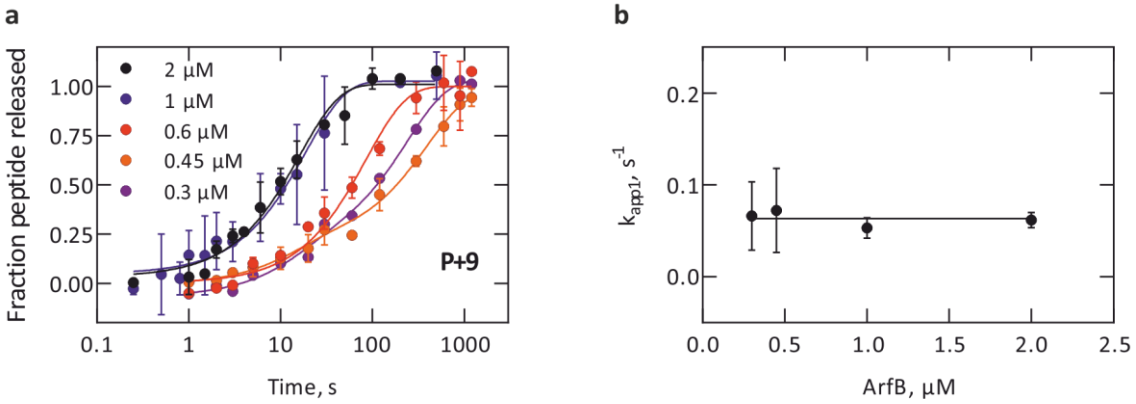

Figure 4.21. ArfB-mediated hydrolysis on P+9 complexes is slow. **(a)** Time courses of peptidyl-tRNA hydrolysis upon rapidly mixing ArfB (0.2-2 µM) with P+9 complexes (0.15 µM). Error bars represent the range of values of two independent experiments. **(b)** The first apparent rate of hydrolysis at different ArfB concentrations. The rates were obtained by fitting the time courses with an exponential equation. Error bars indicate the error of the fit.

4.4.2 ArfB-mediated hydrolysis is pH-independent

The apparent rate of hydrolysis is slow compared to published values of up to 10 s^{-1} for canonical release factors RF1 and RF2 (Kuhlenkoetter et al., 2011; Pierson et al., 2016). It is possible that instead of the catalytic step, we are measuring the preceding, rate-limiting step. Peptidyl-tRNA hydrolysis has previously shown to be highly pH-dependent (Indrisiunaite et al., 2015; Kuhlenkoetter et al., 2011); therefore, we performed single-round hydrolysis experiments at pH 7.8, 7.4, and 8.0 for both P+0 and P+9 complexes (**Figure 4.22a** and **Figure 4.22b**). We find that on both complexes, the hydrolysis rate is identical at all three tested pH levels. We can therefore conclude that with this experiment we determine the rate of a preceding rate-limiting step, which we hypothesize is the engagement step (**Figure 4.22c**). We further speculate that the different rates for P+0 and P+9 indicate that the engagement step is involved in substrate discrimination by ArfB.

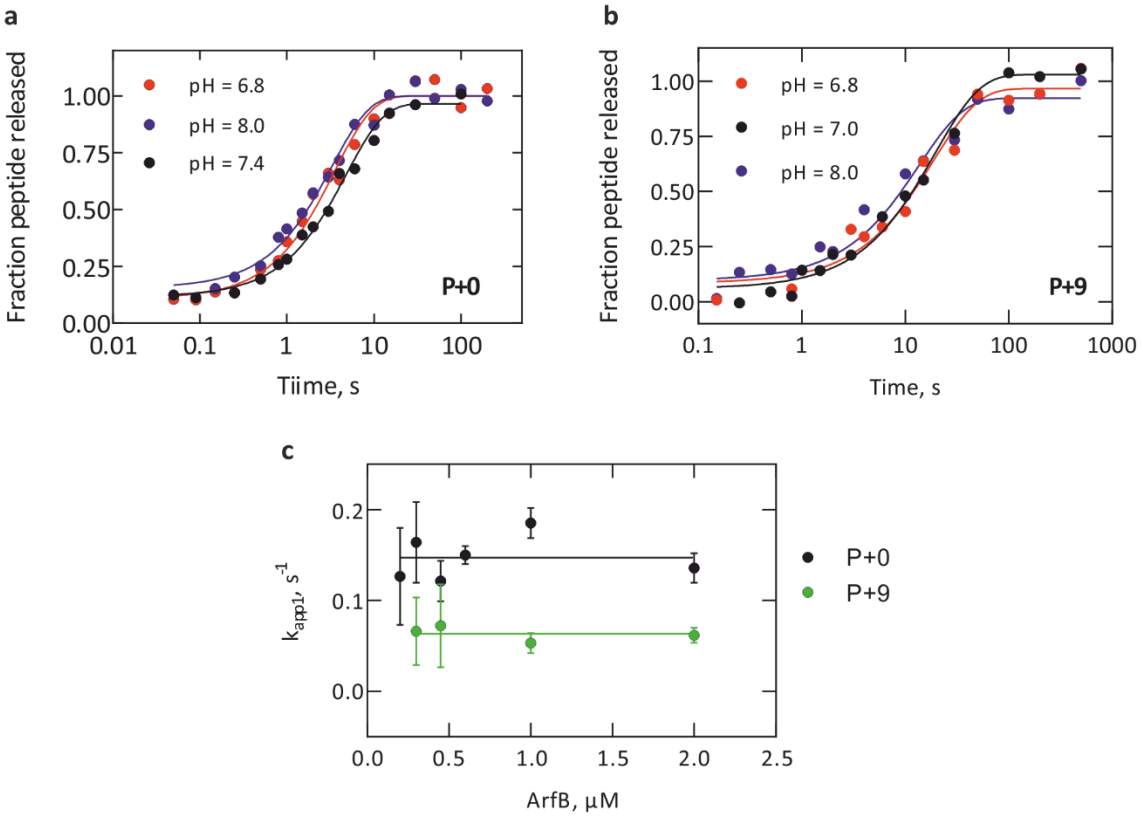

Figure 4.22. ArfB-mediated peptidyl-tRNA hydrolysis is pH-independent. Time courses of peptidyl-tRNA hydrolysis upon rapidly mixing ArfB (1 µM) with **(a)** P+0 complexes and **(b)** P+9 complexes (0.15 µM), at pH = 6.8, 7.4, and 8.0. The time courses were fit with a one exponential equation. **(c)** Comparison of the rate-limiting step on P+0 and P+9 complexes. Average rates were obtained from the exponential fit of single-round hydrolysis time courses. Error bars indicate the error of the fit.

4.5 Structural studies of ArfB

According to our dynamic model of initial binding, the N-terminal domain of ArfB is able to bind in the A site while the C-terminal tail folds and binds in the mRNA entry channel during the following engagement step. Previously, it was suggested that the C-terminal tail positions the N-terminal domain through the long flexible linker (Gagnon et al., 2012); no evidence has yet been presented. There is also evidence that the C-terminal tail is essential for ribosome binding and for peptidyl-tRNA hydrolysis. It is however unclear how the binding and folding of the C-terminal tail activates ArfB.

4.5.1 Interplay of two ArfB domains

Using the isolated N-terminal domain $ArfB_{Nterm}$, we measured the hydrolytic activity in the absence of the C-terminal tail (**Figure 4.23a**). In a hydrolysis assay where P+0 complexes were mixed with ArfB and incubated for five min at 37°C, $ArfB_{Nterm}$ shows no hydrolytic activity. In the stopped flow, we observed no fluorescence change upon mixing quencher-labeled $ArfB_{Nterm}$(K96C) ($ArfB_{Nterm}$ labeled with ATTO-540Q at position 96) with P+0(Flu) (**Figure 4.23b**), indicating that this truncated form of ArfB does not bind to the ribosome.

We then studied binding of the isolated C-terminal domain $ArfB_{Cterm}$; we observe approximately 5% fluorescence change upon mixing quencher-labeled $ArfB_{Cterm}$(R112C) ($ArfB_{Cterm}$ labeled with ATTO-540Q at position 112) with P+0(Flu) complexes (**Figure 4.23c**, orange trace), and three-exponential fitting of the binding trace shows that a majority of the truncated ArfB molecules bind to the ribosome with an apparent rate of 340 ± 20 s^{-1}. In comparison, the same concentration of full-length $ArfB_{GAQ}$(R112C) binds to P+0(Flu) with an apparent rate of 190 ± 10 s^{-1} (**Figure 4.23c**, green trace), but with a 30% fluorescence change. The different amplitudes of fluorescence change suggests that the binding site of the isolated ArfB C-terminal tail is different from that of full-length ArfB. Our biochemical experiments with individual domains do not provide much insight into the role of each domain in binding and engagement. We therefore turned to cryo-electron microscopy with the hopes of capturing structures of ArfB in various stages of the rescue pathway.

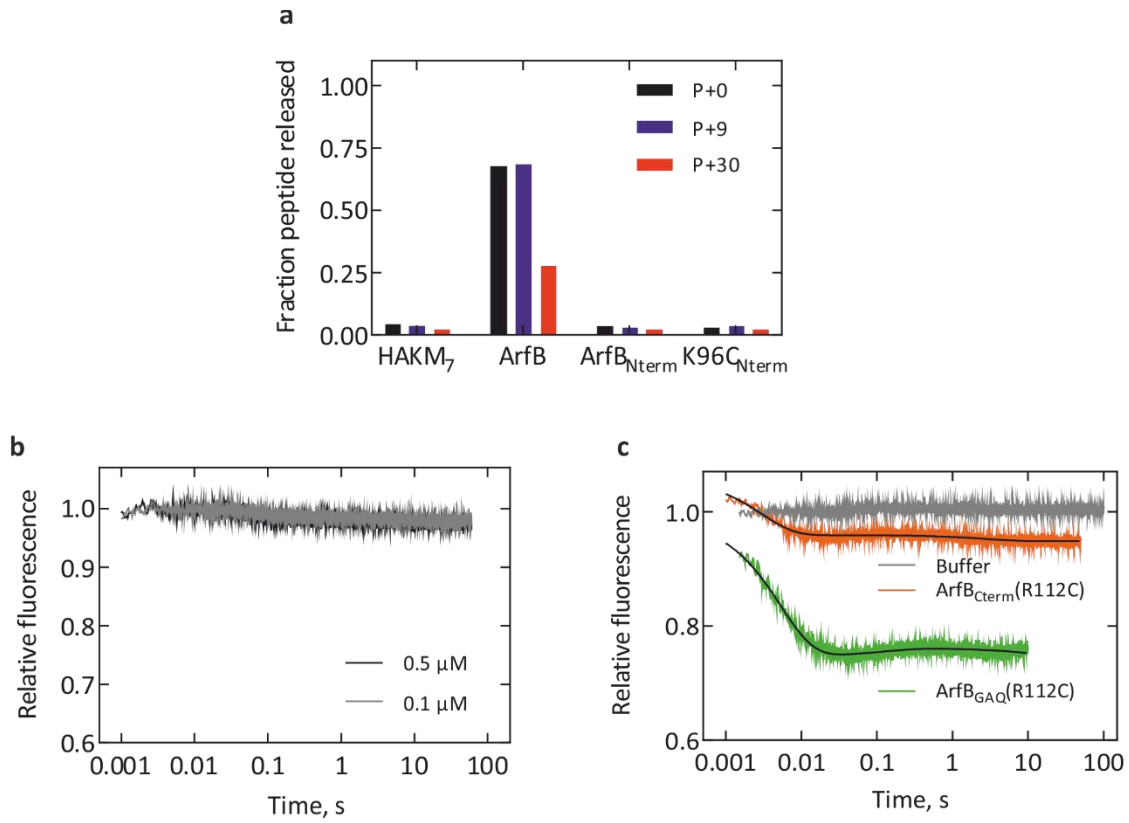

Figure 4.23. Both ArfB domains are essential for binding and hydrolysis. **(a)** The N-terminal domain of ArfB does not show hydrolytic activity. $ArfB_{Nterm}$ (1 µM) was incubated with P+0, P+9, and P+30 (0.1 µM) for 5 min at 37°C. **(b)** $ArfB_{Nterm}$ does not bind to stalled ribosomes. $ArfB_{Nterm}$(K96C) (0.1 µM and 0.5 µM) was rapidly mixed with P+0(Flu) complexes (0.015 µM) in the stopped flow. **(c)** $ArfB_{Cterm}$(540Q) binds to stalled ribosomes in an unspecified position. Truncated $ArfB_{Cterm}$(R112C) (0.1 µM) and full-length $ArfB_{GAQ}$(R112C) was rapidly mixed with P+0(Flu) in the stopped flow. All ArfB variants were labeled with the quencher ATTO-540Q, and all stopped flow experiments were performed at 20°C.

4.5.2 Secondary structure of the ArfB C-terminal tail

Transient secondary structures in intrinsically disordered regions have been shown to affect the rate of protein binding (Arai et al., 2015; Iesmantavicius et al., 2014). To detect the presence of secondary structures in the C-terminal tail of ArfB in solution, we measured the circular dichroism spectra of full-length ArfB and the ArfB N-terminal domain. We find that at 20°C, the negative elipticity at 208 nm is slightly more pronounced for ArfB than for $ArfB_{Nterm}$ (**Figure 4.24a**). The difference is no longer observed at 37°C (**Figure 4.24b**). While these results are still preliminary, they hint at some residual α-helicity of the ArfB C-terminal tail in solution; the observation that the same is not seen at a higher temperature could be due to increased internal dynamics of the peptide.

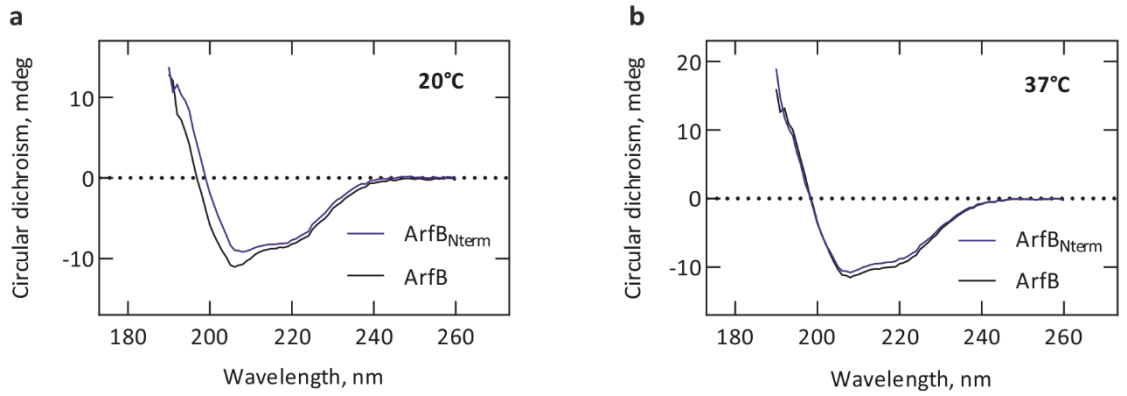

Figure 4.24. Residual helicity of the ArfB C-terminal tail in solution. **(a)** Circular dichroism spectra of ArfB (8 µM) and ArfB$_{Nterm}$ (8 µM) at 20°C. **(b)** Circular dichroism spectra of ArfB (8 µM) and ArfB$_{Nterm}$ (8 µM) at 37°C. Solid lines represent averaged spectra from three independent experiments.

Based on this and the NMR ensemble structures, we hypothesize that ArfB assumes various conformations in solution, including different orientations of the disordered C-terminal tail, as well as conformations where the C-terminal tail is at least partially folded into an α-helix. These different conformations may bind to the ribosome at varying rates, explaining the different binding rates we observe in experiments described in section 4.2.4. However, whether the residual helicity of the ArfB C-terminal tail accelerates or decelerates binding remains unclear.

4.5.3 Biochemical basis for structural analysis of ArfB

Our kinetic data suggests that the interactions between ArfB and the ribosome are highly dynamic, which makes cryo-electron microscopy the most appropriate method for structural analysis, due to its ability to capture dynamic intermediates of protein complexes (reviewed in (Nogales and Scheres, 2015)). To stabilize ArfB on the ribosome, we incubated ArfB with stalled ribosomes in the presence of the apidaecin derivative Api137. Apidaecin is an antimicrobial peptide that binds to the peptide exit tunnel of post-hydrolysis ribosomes, and by forming interactions with the release factors, traps release factors on the ribosome (Florin et al., 2017). In single-round hydrolysis assays, where ArfB and P+0 were incubated with Api137, apidaecin does not impede ArfB-mediated peptidyl-tRNA hydrolysis (**Figure 4.25a**). However, we find that under turnover conditions of ArfB, P+0, and Api137, ArfB does not turnover after performing one round of hydrolysis (**Figure 4.25b**). This suggests that in the

presence of Api137, ArfB remains bound to the post-hydrolysis ribosome and does not dissociate.

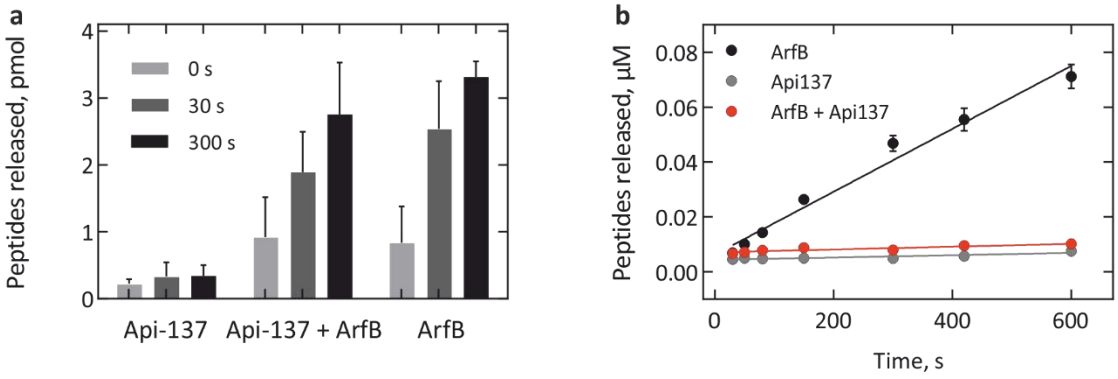

Figure 4.25. Apidaecin traps ArfB on the post-hydrolysis ribosome. **(a)** Apidaecin does not affect single-round ArfB-mediated peptidyl-tRNA hydrolysis. ArfB (1 µM) was incubated with P+0 complexes (0.1 µM) for 5 min at 37°C in the presence of Api137 (1 µM) **(b)** Apidaecin represses ArfB turnover. ArfB (0.02 µM) was incubated with P+0 complexes (0.2 µM) in the presence of Api137 (1 µM). Solid lines represent the linear fit of the time course, and error bars represent the SEM of three independent experiments.

Finally, to ensure that incubation with ArfB does not cause mRNA cleavage, we incubated ArfB with P+36 complexes that are labeled on the 3' end of mRNA with fluorescein (provided by Bee-Zen Peng). We measured the anisotropy of the dye before and after 10 min incubation at 37°C, which showed no significant difference (**Figure 4.26**). This shows that mRNA remains intact following the incubation with ArfB.

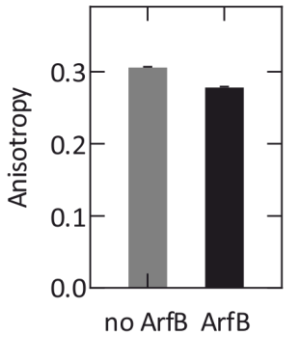

Figure 4.26. ArfB binding does not induce mRNA cleavage. Anisotropy values of the fluorescein dye attached to the 3' end of mRNA, before and after ArfB (0.1 µM) is incubated with P+36 complex (0.01 µM) for 10 min at 37°C. Error bars represent the SEM of three independent experiments.

4.5.4 High resolution structures of ArfB bound to stalled ribosomes

Cryo-EM studies were done in collaboration with Niels Fischer and Valentyn Petrychenko (Department of Structural Dynamics, Max Planck Institute for Biophysical Chemistry), as well as Daniel Wilson and Claudia Müller (Institute for Biochemistry and Molecular Biology, University of Hamburg).

We obtained a 3.2 Å structure of ArfB bound to the P+0 complex (200,000 particles) (**Figure 4.27a**), and a 2.6 Å structure of the P+9 complex (282,252 particles) (**Figure 4.27b**). The P+9 complex sample also yielded structures of the pre-hydrolysis stalled complex with no ArfB bound (3.1 Å, 23,340 particles) (**Figure 4.27c**), as well as the post-hydrolysis ribosome with the tRNA in the hybrid state (3.2 Å, 25,347 particles) (**Figure 4.27d**).

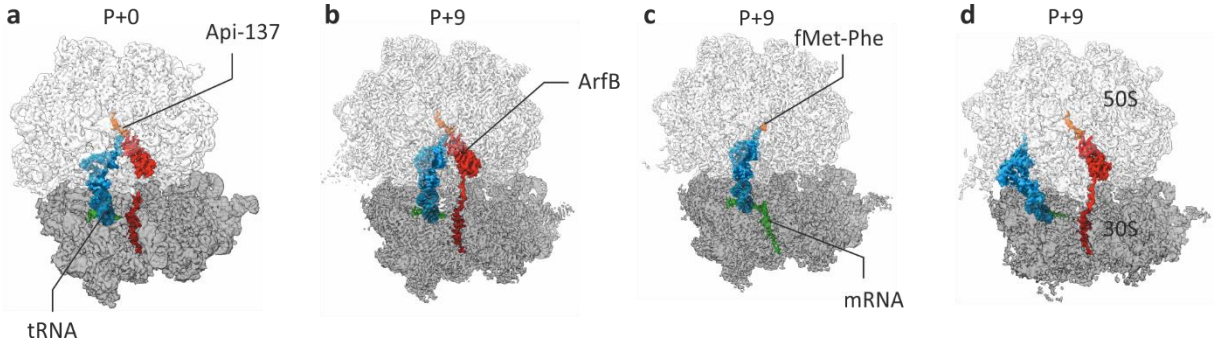

Figure 4.27. Cryo-EM structures of ArfB-bound stalled ribosomes. **(a)** ArfB bound to P+0 complex. Resolution 3.2 Å with 200,000 particles. **(b)** ArfB bound to P+9 complex. Resolution 2.6 Å with 282,252 particles. **(c)** The pre-hydrolysis P+9 complex, 3.1 Å with 23,340 particles. **(d)** The post-hydrolysis P+9 complex, 3.2 Å with 25, 347 particles. The data on ArfB-bound P+0 complex were collected by Claudia Müller, those with P+9 complexes by Niels Fischer. Data analysis and model construction was performed by Niels Fischer, Valentyn Petrychenko, and Claudia Müller. Figure adapted from images provided by Niels Fischer.

The high resolution of the P+9 structure yielded densities for the side chains of highly conserved residues in the linker region and in the C-terminal tail, allowing us to identify specific interactions between ArfB and the ribosome (**Figure 4.28**). These interactions correspond to functionally important residues identified in a previously published mutational analysis (Kogure et al., 2014). In the decoding center, Thr 108 interacts with C1493, while Arg 105 interacts with A1409. Leu 119 stacks with G530. In the C-terminal tail, positively charged residues interact with the negatively charged inner face of the mRNA entry channel. Interestingly, in the ArfB-bound structure of the P+9 complex, the mRNA downstream of the P site was unresolved. Since our biochemical data shows that the mRNA should be intact

(**Figure 4.26**), this suggests that the mRNA is unstructured when the C-terminal tail of ArfB is bound in the mRNA entry channel.

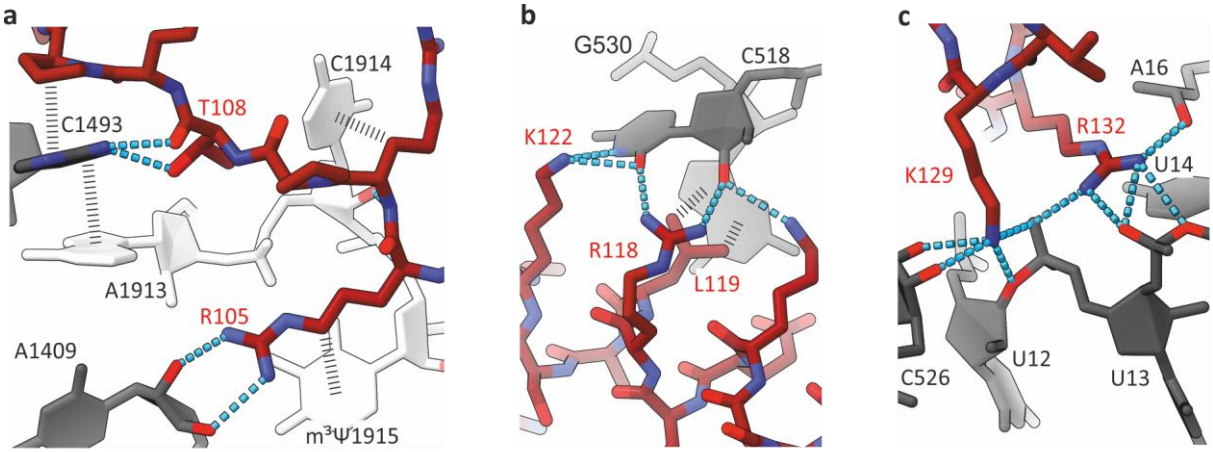

Figure 4.28. Specific interactions between ArfB (red) and the ribosome (grey). Key interactions at **(a)** the C-terminal end of the linker region, **(b)** the N-terminal portion of the C-terminal tail, and **(c)** the C-terminal portion of the C-terminal tail. Figure adapted from images provided by Niels Fischer.

4.5.5 A dynamic model of ArfB binding

Using the ArfB N-terminal domain in our structures as a reference position, we superimposed the NMR ensemble structure of ArfB (Kogure et al., 2014) (PDB 2RTX) on the P+9 complex (**Figure 4.29a**). In this solution structure, the N-terminal domain is folded, whereas the C-terminal tail is unstructured and extends in various directions. We find that certain orientations of the unstructured C-terminal tail can occupy the intersubunit space of the P+9 complex, and appear able to avoid steric clashes with the P site tRNA with minimal adjustments (**Figure 4.29b**). This is a model of the initial encounter complex of ArfB and the ribosome, and it provides a possible structure for our kinetic model of multiple initial binding modes followed by a slow engagement step.

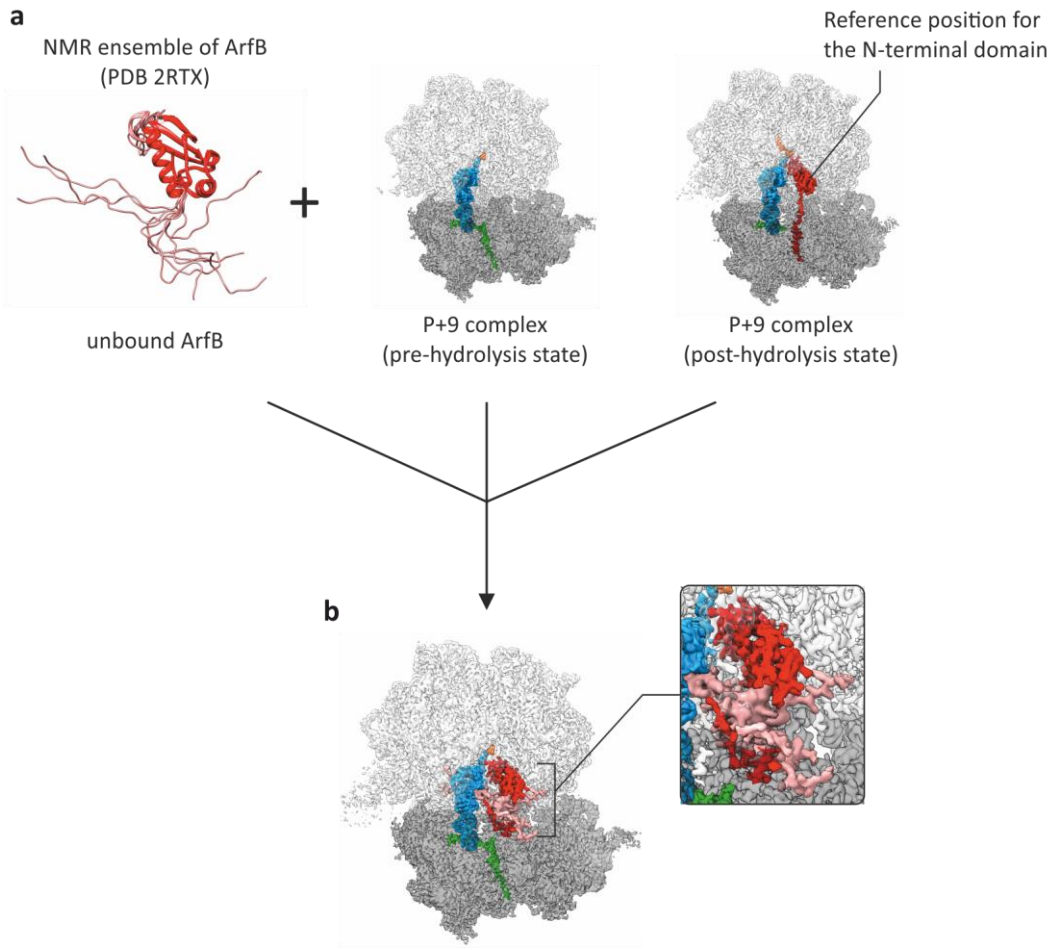

Figure 4.29. Model of the ArfB-ribosome initial encounter complex. **(a)** The solution structure of ArfB (NMR ensemble, PDB 2RTX) was superimposed on the pre-hydrolysis P+9 complex, using the Api137-trapped ArfB N-terminal domain as a reference position. **(b)** Unbound ArfB superimposed on the pre-hydrolysis P+9 complex shows that certain orientations of the ArfB C-terminal tail can occupy the intersubunit space without folding in the mRNA entry channel. Figure adapted from images provided by Niels Fischer.

4.6 Towards studying ArfB in the cellular context

4.6.1 Mass spectrometry analysis of endogenous ArfB

The GGQ motif in the N-terminal domain is responsible for the hydrolytic activity of ArfB. The same motif is responsible for the peptidyl-tRNA hydrolysis activity of RF1 and RF2 (Korostelev, 2011). Methylation of the Gln in the GGQ motif has been shown to increase the rate of hydrolysis (Pierson et al., 2016) in RF1 and RF2. We therefore used mass spectrometry to determine whether the GGQ motif of ArfB is also methylated *in vivo*. Using the pKOV plasmid-based gene replacement system (Link et al., 1997), we generated an *E. coli* strain where chromosomally encoded ArfB has a 3xFLAG tag appended to the N terminus. Using this strain we were able to pull down endogenous ArfB and analyze it by targeted mass spectrometry.

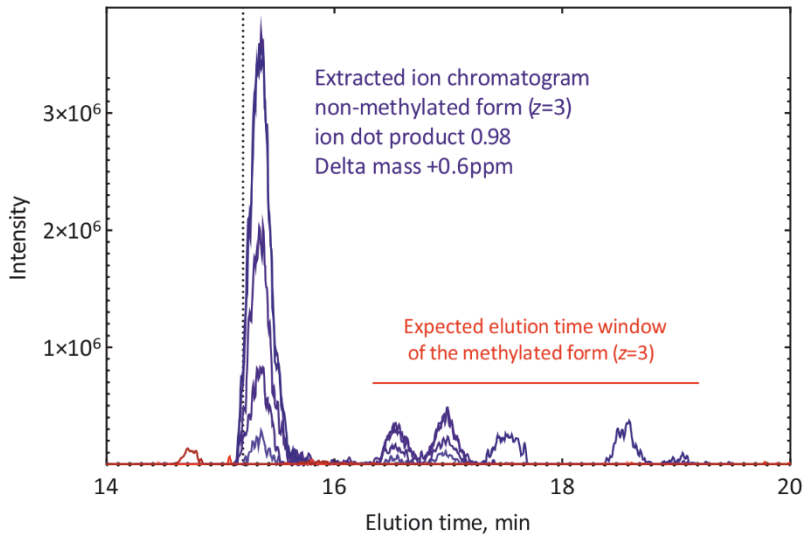

Figure 4.30. Elution profile of the GGQ-containing peptide. The dotted line represents the time point at which MS/MS acquisition of the peptide of interest was triggered; delta mass is the difference between measured and predicted mass of the intact peptide, and the ion dot product is the vector product of the measured and theoretical isotope pattern of the peptide. The expected elution time window of the methylated form of the peptide is indicated in red.

We proteolyzed ArfB with ArgC in order to obtain a peptide containing the GGQ motif, and analyzed the peptides with data-dependent acquisition mass spectrometry. The non-methylated form of the peptide of interest was unambiguously identified by its MS/MS spectrum (data not shown) and its accurate precursor ion masses. The extracted ion chromatogram of the precursor ion pattern has an ion dot product of 0.98, and the delta mass is + 0.6 ppm, indicating that the peptide that triggered MS/MS acquisition is a perfect match

for our peptide of interest. Given that methylation of the GGQ motif should change the hydrophobicity of the peptide while not affecting its charge, we looked for a peak in the expected retention time window within the dynamic range of the mass spectrometer, and did not detect a potential methylated form of the peptide (**Figure 4.30**). This indicates that the GGQ motif of endogenously expressed ArfB is not methylated.

5 DISCUSSION

5.1 ArfB is a specialized rescue factor for non-stop stalled ribosomes

ArfB is one of three rescue systems found in *E. coli*, but it cannot compensate for the loss of the tmRNA-SmpB and ArfA rescue systems; previous studies have shown that ArfB must be overexpressed in order to overcome the synthetic lethality of *ΔssrA ΔarfA* (Chadani et al., 2011b). ArfB is however highly conserved in approximately 30% of the annotated bacterial genomes (Keiler, 2015), which led to the hypothesis that it serves as a rescue factor for more than non-stop stalled ribosomes. In previous studies the PURE system was used to show that ArfB hydrolyzes peptidyl-tRNA on ribosomes stalled on rare codon clusters (Handa et al., 2011); the PURE system is a mixture of transcription and translation factors, so that transcription from a DNA template and translation occur in parallel. These studies used NuPAGE gels to differentiate between released peptides and peptidyl-tRNA and therefore show only the endpoint of the reaction.

Using our system of purified stalled ribosomes, we were able to perform pre-steady state experiments and measure the apparent rate of ArfB-mediated peptidyl-tRNA hydrolysis. As our results in **Figure 4.2** show, the presence of more than 6 nucleotides past the ribosomal P site dramatically decreases the apparent rate of hydrolysis. This is one argument against ribosomes stalled on rare codon clusters as a substrate for ArfB, however it also does not invalidate previous findings. Our experiments show that given enough time, ArfB will fully hydrolyze peptidyl-tRNA on ribosomes stalled in the middle of mRNA; the biological significance of experiments performed in time frames non compatible with the life cycle of bacteria is however questionable.

The slow rate of hydrolysis on P+n (n > 6) complexes raise an interesting question regarding the cellular context of these events. How does these very slow rates measure up to the parallel processes that can take place on a ribosome with a vacant A site? Our competition experiments show that the presence of cognate ternary complex (EF-Tu-GTP-aminoacyl-tRNA) preclude ArfB from rescuing ribosomes. On P+33 complexes, which we use as a model for ribosomes stalled in the middle of an mRNA, even a high concentration of ArfB (2 µM) over a relatively long incubation period (2 min) is insufficient to release the peptide, whereas under all experimental conditions peptide bond formation is favored over peptidyl-tRNA hydrolysis.

We find that this competition is restricted to cognate ternary complex; as shown in **Figure 4.4**, non-cognate ternary complex does not interfere with ArfB function. It is worth noting here that the cellular concentration of ArfB is low: proteomic studies of *E. coli* under many stress conditions have not identified ArfB (Schmidt et al., 2016); in a single-cell proteomics study, only half a copy of ArfB was identified, in comparison with 25,000 copies of RF1 (Taniguchi et al., 2010). This suggests that under physiological conditions ArfB does not rescue ribosomes stalled on rare codon clusters.

We also calculate the specificity constant k_{cat}/K_M for P+0 and P+9 complexes, based on our Michaelis Menten titrations. K_M can be understood as an overall affinity constant for the entire hydrolysis pathway, whereas k_{cat} is the turnover number that represents the number of catalytic events per reaction time. The difference in specificity between the two complexes is approximately 12 fold, showing that ArfB has a clear preference for ribosomes stalled on the 3' end of truncated mRNAs.

Our data conclusively show that ribosomes stalled in the middle of mRNA are not substrates for ArfB-mediated rescue; however ArfB might still be indirectly involved in resolving these complexes. A class of mRNA interferases, endonucleases that target specific mRNA sequences, bind to translating ribosomes and cleave the associated mRNA (Lalaouna and Masse, 2017). These include the toxins RelE, YoeB, YafO, YafQ, and HigB, which are activated under stress conditions such as heat shock and amino acid starvation (reviewed in (Starosta et al., 2014)). In the absence of cognate ternary complex, the toxin binds to the ribosome and cleaves the mRNA in the A site, generating shorter overhangs of mRNA extending past the P site, and creating a more ideal substrate for ArfB. In this way, ArfB may act in concert with mRNA interferases to resolve ribosome stalling during the translational stress response.

5.2 Initial binding

To understand how ArfB discriminates between ribosomes stalled on different lengths of mRNA, we first used FRET-based pre-steady state experiments to observe binding of ArfB to the ribosome. At high T °, we observe a very rapid bimolecular association reaction, with part of the reaction taking place in the dead time of the stopped flow (1-1.5 ms). At lower T°, k_{ON} calculated from the linear dependence of the apparent rate of the first exponent was approximately 500 $\mu M^{-1}\ s^{-1}$, or 5 x $10^8\ M^{-1}\ s^{-1}$. The diffusion-limited association rate of two spherical molecules the size of the ribosome (radius of gyration *r* = 8.7) and ArfB (*r* = 3.3;

computed by Valentyn Petrychenko using the cryo-EM structure and HYDROPRO) is approximately 8.8 x 10^9 according to the encounter frequency equation (Fersht, 1999). This suggests that a portion of ArfB in solution is optimally oriented for binding, and for this portion the rate of association is diffusion-limited. The remaining ArfB molecules require multiple attempts to bind, thus lowering the overall binding rate.

One of the factors that increases the k_{ON} to the diffusion limit is electrostatic steering, where opposite charges of a protein and its binding partner attract and enhance the association rate (Schreiber and Fersht, 1996; Wendt et al., 1997). In our binding experiments performed with added Mg^{2+}, we find that the rate of initial binding is not significantly decreased, and Mg^{2+} concentrations of up to 30 mM do not abolish the binding altogether. In comparison, IF3 binds with a diffusion-limited rate to the large ribosomal subunit, in addition to its canonical binding site on the small subunit during initiation, but this interaction is abolished at 30 mM Mg^{2+} (Goyal et al., 2017). This indicates that unlike IF3, the fast binding of ArfB is not primarily the result of electrostatic interactions, and the structural flexibility of the C-terminal tail giving rise to orientations favorable to binding may be a more important factor.

Upon closer examination of the binding traces, we find that the second and third apparent rate constants also follow a linear dependence on ArfB concentration. Rather than conformational changes that follow initial binding, the exponential fits of our complex binding traces seem to show several binding events that occur in parallel, with k_{ON} values ranging from 500 $\mu M^{-1}\ s^{-1}$ to 1 $\mu M^{-1}\ s^{-1}$. Judging from the amplitude of each exponent, a large proportion of ArfB molecules associate with the ribosome with the fastest k_{ON}. It should be noted here that it is highly probable that there are more than three binding modes in this binding experiment. A three-exponential fit is the simplest model with which we can describe our binding traces; fitting with more exponents will likely result in a better fit, and reveal more bimolecular association reactions occurring in parallel.

An explanation for this phenomenon may lie in the intrinsic disorder of the ArfB C-terminal tail. The NMR ensemble structure of ArfB (PDB 2RTX, (Kogure et al., 2014)) shows that the C-terminal tail assumes multiple orientations in solution (Handa et al., 2010); our circular dichroism measurements indicate that in a population of ArfB in solution, the C-terminal tail is at least partially helical. These different orientations and conformations of the C-terminal tail cause ArfB to bind to the ribosome at different rates. It has been proposed that the

structural flexibility of intrinsically disordered protein regions increases the rate of binding, because there are fewer steric constraints (Shoemaker et al., 2000). However, some intrinsically proteins have also been shown to bind faster when transient secondary structures are stabilized (Arai et al., 2015; Iesmantavicius et al., 2014). Further studies are required to understand the contributions of intrinsic disorder and of transient secondary structures to the initial binding of ArfB to the ribosome.

In addition to the k_{ON} value, the linear dependence of the apparent rate constants on ArfB concentration also gives us a dissociation rate constant k_{OFF}, which is obtained from the y-intercept of the linear fit. For the first binding step, the k_{OFF} is approximately 100 s^{-1}. The rapid association coupled with fast dissociation suggests a scanning mechanism, wherein ArfB forms transient interactions with ribosomes with no tRNA in the A site. The fast rate of scanning would suggest that it occurs independently of mRNA length, which is indeed what we observe in binding experiments with P+9 and P+30 complexes. As shown in **Figure 4.12**, the k_{ON} values for ArfB binding to P+9 and to P+30 complexes are comparable to that of P+0 complexes, indicating that substrate discrimination does not occur in the first, transient binding step, and suggesting the presence of a subsequent step in which ArfB assumes its catalytically active conformation.

Using our high-resolution cryo-EM structures of ArfB on the stalled ribosome, we could superimpose the NMR ensemble structure (Kogure et al., 2014) on the stalled ribosome. As shown in **Figure 4.29**, some orientations of the ArfB C-terminal tail are able to occupy the intersubunit space in the disordered state, while the N-terminal domain of ArfB binds to the large subunit in a near-active state. This provides us with a structural model of the initial capture complex predicted by our kinetic studies of the initial binding step. The various orientations with which ArfB can bind to the ribosome could reflect the multiple bimolecular association reactions we observe in our binding experiments. Furthermore, the C-terminal tail does not bind in the mRNA entry channel at this step, which explains why the rate of initial binding is independent of mRNA length.

This dynamic model of the initial capture complex also points to the existence of a conformational change step following initial binding. The previously published crystal structure (Gagnon et al., 2012) and our own cryo-EM structures show that in its active state, the C-terminal tail of ArfB is folded into an α-helix in the mRNA entry channel. The folding and

binding of the C-terminal tail could be the step in which ArfB becomes “engaged” and catalytically active on the ribosome.

5.3 A slow, rate-limiting engagement step

Our observations of initial binding suggest that ArfB undergoes an engagement step after initial binding to assume its active state on the stalled ribosome. Evidence of this step can be found in chase experiments described in section 4.2.7, where dissociation of ArfB is directly monitored after a period of incubation with stalled ribosomes.

The two exponential traces that describe ArfB dissociation suggest that there is a fast-dissociating population of ArfB for which the k_{OFF} is approximately 0.4 s^{-1}, and a slow-dissociating population for which the k_{OFF} is approximately 0.02 s^{-1}. This could be because we monitor ArfB dissociating from various bound states on the ribosome, or because of heterogeneity in the sample; we therefore report the average dissociation rates in **Table 4.4**. Regardless of mRNA length, and dissociation rates for P+0, P+9, and P+30 are several orders of magnitude slower than the respective k_{OFF} values calculated from the initial binding experiment (**Table 4.3**). This indicates that in this experiment we monitor ArfB dissociation after engagement, and not from the initial encounter complex. Additionally, our FRET-based and anisotropy-based affinity titrations show that ArfB has an affinity for the ribosome in the nanomolar range, while the affinity constant calculated as k_{OFF}/k_{ON} from the initial binding experiments is 20 to 50 fold larger (**Table 4.5**). Together, these data support the existence of an engagement step following initial binding that stabilizes ArfB on the ribosome.

While the initial binding step is not governed by electrostatic interactions, after the engagement step, the interaction between ArfB and the ribosome is mediated by strong electrostatic interactions that can be disrupted by high concentrations of monovalent and divalent salt, as shown by the titrations described in section 4.3.2. This suggests that during the engagement step, strong electrostatic interactions between ArfB and the ribosome are established that are stable at physiological salt concentrations.

Our high resolution structures of ArfB bound to the ribosome show a network of such specific interactions between the ribosome and the linker region and C-terminal tail of ArfB, as shown in **Figure 4.28**. These interactions include Arg residues at positions 105, 118, 132, Lys residues at 122 and 129, and Leu at position 119, which were not resolved in the previously published

crystal structure (Gagnon et al., 2012). The positively charged amino acids interact with negatively charged groups on 16S rRNA, with the exception of Arg 105, which interacts with 23S rRNA. These residues were all previously found to be essential for ArfB activity (Kogure et al., 2014). We propose that these crucial interactions are established during the engagement step and stabilize ArfB binding. However, how these interactions affect the position of the N-terminal domain and activate ArfB-mediated peptidyl-tRNA hydrolysis is still unclear.

5.4 Engagement as the substrate discrimination step

Our single-round hydrolysis experiments show that the apparent rate of ArfB-mediated peptidyl-tRNA hydrolysis is approximately 0.15 s^{-1} on P+0 complexes, which is very slow compared to the rate of canonical release by RF1 and RF2 at approximately 10 s^{-1} (Kuhlenkoetter et al., 2011; Zaher and Green, 2011).

The Gln in the GGQ motif of RF1 and RF2 is methylated, a post-translational modification that increases the rate of hydrolysis and produces uniform rates of peptidyl-tRNA hydrolysis on all amino acids (Pierson et al., 2016). Using an *E. coli* strain with chromosomally tagged ArfB, we were able to immunoprecipitate endogenous ArfB for mass spectrometry analysis. The results summarized in **Figure 4.30** show no evidence of methylation of the GGQ motif. This could be one contributing factor to the slow hydrolysis by ArfB. In the absence of methylation, however, canonical release is approximately 2 s^{-1} (Kuhlenkoetter et al., 2011; Zaher and Green, 2011), which is still faster than the ArfB-mediated reaction.

Peptidyl-tRNA hydrolysis by RF1 and RF2 is highly pH-dependent (Indrisiunaite et al., 2015; Kuhlenkoetter et al., 2011). In the case of ArfB, changing the pH of the solution has no effect on the rate of hydrolysis on both P+0 and P+9 complexes. This leads us to conclude that in our single-round hydrolysis experiments, we do not monitor the catalysis step, but rather the preceding pH-independent engagement step.

We can therefore directly compare the engagement step on P+0 and on P+9 complexes. For the latter, the pH-independent rate is 0.06 s^{-1}; the slower engagement coupled with faster dissociation rate could contribute to effective substrate discrimination by ArfB. Given that the C-terminal tail of ArfB must fold and bind within the mRNA entry channel for ArfB to assume its active state, it is likely that the slow engagement on the P+9 complex involves the dissociation of the mRNA from the mRNA entry channel. This is supported by our observation

that in the cryo-EM structure of ArfB bound to the P+9 complex, the mRNA is displaced by the C-terminal α-helix of ArfB, and is disordered in the intersubunit space.

5.5 Kinetic model of ArfB-mediated ribosome rescue

The elemental rate constants of the ArfB-mediated ribosome rescue pathway can be summarized in the kinetic scheme below (**Figure 5.1**). Initial binding and dissociation from the initial encounter complex is fast, effectively allowing ArfB to rapidly "scan" ribosomes with an empty A site. We show that instead of long-range electrostatic interactions, the fast binding may be a feature of the intrinsic disorder of the C-terminal tail; the structural flexibility allows a portion of ArfB molecules to arrive in the optimal orientation for binding.

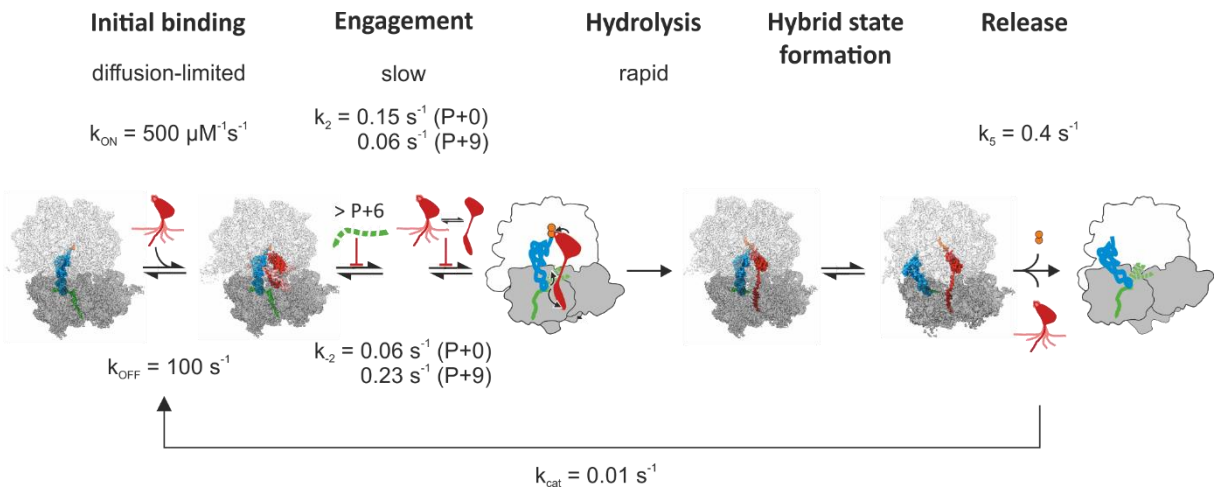

Figure 5.1. Kinetic model of ArfB-mediated ribosome rescue. Cryo-EM models were provided by Niels Fischer and Valentyn Petrychenko.

We observe many parallels between this binding step and published association models of intrinsically disordered proteins (Mollica et al., 2016; Shammas et al., 2016). One such model is conformational selection, in which the protein exists in an equilibrium of conformations, and binding to the more favorable conformation drives the equilibrium towards formation of the favorable conformation. Another model is one of induced fit, where fast binding is followed by folding and accommodation on the binding partner (Shammas et al., 2016). Additionally, it has been proposed that intrinsically disordered proteins have higher association rates due to the "fly-casting" model, wherein intrinsic disorder enables long-range, unspecific, and weak interactions that are strengthened as the protein folds and "reels in" its binding partner (Shoemaker et al., 2000).

While there are still few kinetic studies that provide definitive experimental evidence of either model, our pre-steady state analysis of ArfB binding points to a combination of these proposed binding models. We observe multiple rates of initial binding, which suggests that ArfB is able to associate with the ribosome in various conformations, with some more favorable than others and binding more rapidly; this fits the description of the conformational selection model. However, the engagement step involves the folding of the C-terminal tail that activates ArfB-mediated hydrolysis, which is in accordance with the induced fit model.

Engagement is the step where ArfB discriminates between ribosomes with different lengths of mRNA extending past the P site. On P+0 complexes, this step is where the C-terminal tail folds into an α-helix within the mRNA entry channel, and it occurs at a rate of 0.15 s^{-1}. On P+9 complexes, however, the 9 nucleotides residing in the mRNA entry channel must diffuse into the intersubunit space in order for the ArfB C-terminal tail to bind, resulting in an engagement rate of 0.06 s^{-1}. Once engagement occurs, peptidyl-tRNA hydrolysis is carried out by the GGQ motif.

While it is still unclear how the binding of the C-terminal tail triggers peptidyl-tRNA hydrolysis, the network of interactions revealed by our cryo-EM structures allow us to compare the ArfB-bound ribosome with the RF2-bound ribosome (Korostelev, 2011). In both structures, A1493 is stacked with A1913. This is mediated by the interactions between Thr 108 of ArfB and C1493. While G530 takes part in stop codon recognition in RF2-catalyzed translation termination, it stacks with Leu 119 of ArfB. Furthermore, Arg 105 is situated approximately in the middle of the long flexible linker. The strong interaction of Arg 105 with A1409 observed in our cryo-EM structure could suggest a role in orienting the C-terminal domain after initial binding.

ArfB dissociates from the post-hydrolysis ribosome with an average rate of approximately 0.4 s^{-1}. The k_{cat} of the entire reaction is 0.01 s^{-1}, indicating that turnover of ArfB is limited by dissociation. Interestingly, our structure of ArfB bound to the post-hydrolysis P+9 complex shows that in the post-hydrolysis state, the strong electrostatic interactions between ArfB and the ribosome persist through different rotational states of the subunits. While a single-molecule study of subunit rotation in the presence of ArfB suggested that ArfB stabilizes the ribosome in the rotated state (Casy et al., 2018), it is unclear if there is truly a cause-effect relationship, or if the change in ribosome dynamics is in fact a consequence of peptidyl-tRNA hydrolysis. However, the stability of interactions between the ArfB C-terminal tail and the

ribosome throughout different rotational states could be the reason why dissociation of ArfB from post-hydrolysis complexes is slow.

5.6 ArfB turnover – assisted or not?

While our model is compiled with extensive experimental data on the initial binding and engagement steps, less is known about post-hydrolysis dissociation. With regards to ArfB turnover, our Michaelis-Menten titrations yielded a k_{cat} of 0.01 s^{-1}, which means that an ArfB molecule requires 100 s for each catalytic cycle. This renders ArfB a highly inefficient enzyme compared to canonical release factors (Adio et al., 2018), and leads to the question whether ArfB dissociation is assisted by additional factors. In the case of RF1 and RF2, dissociation is facilitated by RF3 in a GTP-dependent manner and occurs at approximately 1 s^{-1} (Adio et al., 2018; Peske et al., 2014; Zaher and Green, 2011).

In our model system, we measured the effect of translation factors on ArfB dissociation using initial velocity as a readout. Under turnover conditions, the initial velocity of the reaction reflects how quickly each ArfB molecule dissociates and rebinds to a new substrate. We find that adding recycling factors RRF and EF-G caused a moderate increase in initial velocity. Ribosome recycling is a GTP-dependent process: RRF binds to the ribosomal A site and stabilizes the ribosome in the rotated state, and GTP hydrolysis by EF-G promotes subunit splitting (Gao et al., 2005; Peske et al., 2005). The strongest effect is when both EF-G and RRF are present, but there is no clear difference between experiments done with GTP and its slowly-hydrolyzing analog GTP-γS. This could be because GTP-γS was still hydrolyzed during the course of the experiment, or because the effect is independent of GTP hydrolysis. We suggest that EF-G and RRF, by binding to post-hydrolysis ribosomes, effectively titrate away ribosomes that ArfB would otherwise scan upon dissociation. In this way the probability that ArfB binds to a pre-hydrolysis substrate complex is higher, therefore turnover is accelerated.

In addition to recycling factors, HflX is another factor that promotes subunit dissociation (Zhang et al., 2015). Expression of HflX is a part of the bacterial stress response: *hflx* is encoded in a heat stress response operon, and growth of Δ*hflx* strains of *E. coli* is slower at higher temperatures (Noble et al., 1993; Tsui et al., 1996). Given that our data shows ribosome recycling factors have an effect on ArfB turnover, the question arises as to whether HflX might have a similar effect. Hflx binds to the intersubunit side of the 50S subunit and interacts with the peptidyl transferase center, and it is able to dissociate both empty 70S ribosomes and

post-termination complexes (Zhang et al., 2015). Since HflX is expressed in response to heat stress, it is suggested that it targets ribosomes stalled as a result of stress, which in turn are substrates for ArfB-mediated ribosome rescue (Coatham et al., 2016; Zhang et al., 2015).

In unpublished data from our lab, ribosome splitting by recycling factors and by HflX appear to be very similar, also in the presence of ArfB. In fact, on ribosomes rescued by ArfB, the ribosome splitting traces for recycling factors and for HflX have the same delay, which could be due to ArfB dissociation. These results are however preliminary, and further experiments are required to make conclusions regarding whether HflX has a specific role in the ArfB-mediated ribosome rescue pathway. Such experiments could include monitoring the rate of ArfB dissociation, as well as measuring the initial velocity of the hydrolysis reaction, in the presence of HflX.

5.7 On the biological role of ArfB

In investigating the ArfB rescue mechanism, we were able to conclusively show that ArfB preferentially rescues ribosomes when there are fewer than 6 mRNA nucleotides extending past the P site. We also show that ArfB turnover is slow, albeit moderately accelerated by the presence of ribosome recycling machinery. Our results paint a picture of a rescue factor that is somewhat inefficient and present at very low levels in *E. coli*, where more abundant and more efficient rescue systems exist in tmRNA-SmpB and ArfA.

It may be the case that in *E. coli*, ArfB represents the very last line of defense against non-stop stalling, although its conservation in 30% of sequenced bacterial species remains an interesting aspect of its biological role (Keiler, 2015). One common method of examining the function of proteins is to pull-down interacting factors with immunoprecipitation; in this work, we established *E. coli* strains with chromosomally tagged ArfB that can be used to construct an interactome. We have also generated the same chromosomal tags on a background of Δ*ssrA* to potentially compare the interactome with and without tmRNA-SmpB. Another future application of the tagged strains could be to purify ArfB-associated ribosomes and sequence the associated mRNAs, so as to assess whether ArfB targets specific transcripts for rescue.

While the significance of ArfB in bacteria is somewhat unclear, it is known that its eukaryotic homologs play an important role in mitochondrial translation. The human homolog ICT1 in particular is an integral part of the mitochondrial ribosome (Brown et al., 2014), though its

hydrolytic activity has been shown to also be essential for cell viability (Feaga et al., 2016; Haque and Spremulli, 2010; Richter et al., 2010). In our experimental system, purified ICT1 (provided by Dr. Ricarda Richter-Dennerlein) is functional on stalled bacterial ribosomes; it shows hydrolytic activity on our P+0 complexes, while mtRF1a, a known mitochondrial release factor (Soleimanpour-Lichaei et al., 2007), does not (data not shown).

Given the strong structural similarities between ArfB and ICT1 (Handa et al., 2010), it is tempting to speculate on the function of ICT1 based on our understanding of ArfB. The decoding center of mammalian mitochondrial ribosomes is similar to that of bacterial ribosomes, and the mRNA channel in the A site is also conserved (Greber and Ban, 2016). In conjunction with our findings that ICT1 functions on bacterial stalled ribosomes, this seems to suggest that the linker and C-terminal tail regions of ICT1 are capable of forming interactions with the ribosome, much like those we observe in the ArfB-bound ribosome structures.

Furthermore, the mRNA length-dependency of hydrolytic activity should be similar despite the differences between mitochondrial and bacterial ribosomes. The C-terminal tail of ICT1 is also very positively charged, and key residues of the ArfB C-terminal tail, identified in our cryo-EM structure, are conserved (Kogure et al., 2014): namely Arg 118, 119, 132, and Lys 122 and 129. As we show in this study, these residues take part in strong and stable interactions between ArfB and the bacterial mRNA entry channel, and are essential for peptidyl-tRNA hydrolysis. Based on these observations, it is possible that the corresponding residues on ICT1 play a similar role. As such, the competitive inhibition of peptidyl-tRNA hydrolysis by mRNA extending past the P site may also apply in the case of ICT1.

This hypothesis has two implications. The first is regarding translation termination of respiratory chain proteins MT-CO1 and MT-ND6. These two genes do not have in-frame stop codons; rather, the transcript ends with AGA and AGG, respectively (Anderson et al., 1981). Human mitochondria do not have the mitochondrial tRNA isoforms that recognize these arginine codons, and the method of termination for these proteins is unclear. It has been suggested that a -1 frameshift that positions a conventional stop codon UAG in the ribosomal A site (Temperley et al., 2010a; Temperley et al., 2010b). On the other hand, ICT1, given its lack of codon-recognition domains alongside its peptidyl-tRNA hydrolysis activity, represents another proposed termination mechanism. However, both transcripts have 5’UTR regions of more than 6 nucleotides, and according to our findings this would likely render ICT1-mediated

peptide release highly inefficient, lending more credence to the theory of a -1 frameshift facilitating termination.

The other implication of the mRNA length-dependence of ICT1 activity is associated with the regulation of mitochondrial mRNA stability. Mitochondrial mRNAs, with the sole exception of MT-ND6, undergo 3' polyadenylation (Bai et al., 2011; Lapkouski and Hallberg, 2015; Tomecki et al., 2004). While this kind of post-transcriptional modification increases the stability of cellular mRNAs, its effect on mitochondrial mRNAs is transcript-specific (Nagaike et al., 2005; Wydro et al., 2010), and can be removed by the 2'-phosphodiesterase PDE12 (Rorbach et al., 2011). Moreover, in seven of the open reading frames transcribed in mitochondria, polyadenylation completes the stop codon (Temperley et al., 2010b). In light of the findings in this study, we postulate that ICT1 can act when ribosomes translate transcripts that have been deadenylated, and in doing so act in concert with the mRNA degradasome to facilitate mRNA turnover.

In addition to ICT1, C12orf65 is another mitochondrial protein that is similar to ArfB. It has homologous domains to RF2, and its C-terminal tail is also rich in positively-charged amino acids (Kogure et al., 2012). Though it has been classified as a putative release factor, hydrolytic activity has yet to be observed *in vitro* (Ayyub et al., 2020). It has so far proven very difficult to purify active mitochondrial ribosomes, and insights into the ArfB-mediated ribosome rescue pathway is the most reliable analysis of this family of peptidyl-tRNA hydrolases (Burroughs and Aravind, 2019; Duarte et al., 2012).

Though their biological function is still unclear, the importance of ICT1 and C12orf65 is apparent. Apart from being essential for cell viability, ICT1 has also been shown to be differentially expressed in a number of cancers (Lao et al., 2016; Wang et al., 2017; Xie et al., 2017). Patients with mutations in C12orf65 have presented with mitochondrial disease and mitochondrial protein synthesis deficiencies (Antonicka et al., 2010; Wesolowska et al., 2015). A detailed and comprehensive understanding of how ArfB interacts with the ribosome provides a basis for further studies of mitochondrial ribosome rescue.

In this work, we present a detailed mechanistic analysis of ArfB-mediated ribosome rescue. We address the issue of substrate specificity, construct a kinetic model of the rescue pathway, and provide structural insight that supports our model. Our findings may shed light on similar release factors such as the human mitochondrial protein ICT1; they also set the stage for

further biophysical studies of ArfB, not only as a release factor but also as a model for the interactions between a partially disordered protein and its binding partner.

6 REFERENCES

Abe, T., Sakaki, K., Fujihara, A., Ujiie, H., Ushida, C., Himeno, H., Sato, T., and Muto, A. (2008). tmRNA-dependent trans-translation is required for sporulation in Bacillus subtilis. Mol Microbiol *69*, 1491-1498.

Abo, T., Inada, T., Ogawa, K., and Aiba, H. (2000). SsrA-mediated tagging and proteolysis of LacI and its role in the regulation of lac operon. EMBO J *19*, 3762-3769.

Abo, T., Ueda, K., Sunohara, T., Ogawa, K., and Aiba, H. (2002). SsrA-mediated protein tagging in the presence of miscoding drugs and its physiological role in Escherichia coli. Genes Cells *7*, 629-638.

Adio, S., Sharma, H., Senyushkina, T., Karki, P., Maracci, C., Wohlgemuth, I., Holtkamp, W., Peske, F., and Rodnina, M.V. (2018). Dynamics of ribosomes and release factors during translation termination in E. coli. Elife *7*.

Akabane, S., Ueda, T., Nierhaus, K.H., and Takeuchi, N. (2014). Ribosome rescue and translation termination at non-standard stop codons by ICT1 in mammalian mitochondria. PLoS Genet *10*, e1004616.

Amunts, A., Brown, A., Toots, J., Scheres, S.H.W., and Ramakrishnan, V. (2015). Ribosome. The structure of the human mitochondrial ribosome. Science *348*, 95-98.

Anderson, S., Bankier, A.T., Barrell, B.G., de Bruijn, M.H., Coulson, A.R., Drouin, J., Eperon, I.C., Nierlich, D.P., Roe, B.A., Sanger, F.*, et al.* (1981). Sequence and organization of the human mitochondrial genome. Nature *290*, 457-465.

Antonicka, H., Ostergaard, E., Sasarman, F., Weraarpachai, W., Wibrand, F., Pedersen, A.M., Rodenburg, R.J., van der Knaap, M.S., Smeitink, J.A., Chrzanowska-Lightowlers, Z.M.*, et al.* (2010). Mutations in C12orf65 in patients with encephalomyopathy and a mitochondrial translation defect. Am J Hum Genet *87*, 115-122.

Arai, M., Sugase, K., Dyson, H.J., and Wright, P.E. (2015). Conformational propensities of intrinsically disordered proteins influence the mechanism of binding and folding. Proc Natl Acad Sci U S A *112*, 9614-9619.

Armalyte, J., Jurenaite, M., Beinoraviciute, G., Teiserskas, J., and Suziedeliene, E. (2012). Characterization of Escherichia coli dinJ-yafQ toxin-antitoxin system using insights from mutagenesis data. J Bacteriol *194*, 1523-1532.

Ayyub, S.A., Gao, F., Lightowlers, R.N., and Chrzanowska-Lightowlers, Z.M. (2020). Rescuing stalled mammalian mitoribosomes - what can we learn from bacteria? J Cell Sci *133*.

Bai, Y., Srivastava, S.K., Chang, J.H., Manley, J.L., and Tong, L. (2011). Structural basis for dimerization and activity of human PAPD1, a noncanonical poly(A) polymerase. Mol Cell *41*, 311-320.

Ban, N., Nissen, P., Hansen, J., Moore, P.B., and Steitz, T.A. (2000). The complete atomic structure of the large ribosomal subunit at 2.4 A resolution. Science *289*, 905-920.

Barends, S., Karzai, A.W., Sauer, R.T., Wower, J., and Kraal, B. (2001). Simultaneous and functional binding of SmpB and EF-Tu-TP to the alanyl acceptor arm of tmRNA. J Mol Biol *314*, 9-21.

Barends, S., Zehl, M., Bialek, S., de Waal, E., Traag, B.A., Willemse, J., Jensen, O.N., Vijgenboom, E., and van Wezel, G.P. (2010). Transfer-messenger RNA controls the translation of cell-cycle and stress proteins in Streptomyces. EMBO Rep *11*, 119-125.

Belardinelli, R., Sharma, H., Caliskan, N., Cunha, C.E., Peske, F., Wintermeyer, W., and Rodnina, M.V. (2016). Choreography of molecular movements during ribosome progression along mRNA. Nat Struct Mol Biol *23*, 342-348.

Bessho, Y., Shibata, R., Sekine, S., Murayama, K., Higashijima, K., Hori-Takemoto, C., Shirouzu, M., Kuramitsu, S., and Yokoyama, S. (2007). Structural basis for functional mimicry of long-variable-arm tRNA by transfer-messenger RNA. Proc Natl Acad Sci U S A *104*, 8293-8298.

Bhushan, S., Hoffmann, T., Seidelt, B., Frauenfeld, J., Mielke, T., Berninghausen, O., Wilson, D.N., and Beckmann, R. (2011). SecM-stalled ribosomes adopt an altered geometry at the peptidyl transferase center. PLoS Biol *9*, e1000581.

Boggild, A., Sofos, N., Andersen, K.R., Feddersen, A., Easter, A.D., Passmore, L.A., and Brodersen, D.E. (2012). The crystal structure of the intact E. coli RelBE toxin-antitoxin complex provides the structural basis for conditional cooperativity. Structure *20*, 1641-1648.

Borg, A., Pavlov, M., and Ehrenberg, M. (2016). Complete kinetic mechanism for recycling of the bacterial ribosome. RNA *22*, 10-21.

Brown, A., Amunts, A., Bai, X.C., Sugimoto, Y., Edwards, P.C., Murshudov, G., Scheres, S.H.W., and Ramakrishnan, V. (2014). Structure of the large ribosomal subunit from human mitochondria. Science *346*, 718-722.

Brzezniak, L.K., Bijata, M., Szczesny, R.J., and Stepien, P.P. (2011). Involvement of human ELAC2 gene product in 3' end processing of mitochondrial tRNAs. RNA Biol *8*, 616-626.

Buhr, F., Jha, S., Thommen, M., Mittelstaet, J., Kutz, F., Schwalbe, H., Rodnina, M.V., and Komar, A.A. (2016). Synonymous Codons Direct Cotranslational Folding toward Different Protein Conformations. Mol Cell *61*, 341-351.

Burroughs, A.M., and Aravind, L. (2019). The Origin and Evolution of Release Factors: Implications for Translation Termination, Ribosome Rescue, and Quality Control Pathways. Int J Mol Sci *20*.

Buskirk, A.R., and Green, R. (2017). Ribosome pausing, arrest and rescue in bacteria and eukaryotes. Philos Trans R Soc Lond B Biol Sci *372*.

Calloni, G., Chen, T., Schermann, S.M., Chang, H.C., Genevaux, P., Agostini, F., Tartaglia, G.G., Hayer-Hartl, M., and Hartl, F.U. (2012). DnaK functions as a central hub in the E. coli chaperone network. Cell reports *1*, 251-264.

Casy, W., Prater, A.R., and Cornish, P.V. (2018). Operative Binding of Class I Release Factors and YaeJ Stabilizes the Ribosome in the Nonrotated State. Biochemistry *57*, 1954-1966.

Cayley, S., Lewis, B.A., Guttman, H.J., and Record, M.T., Jr. (1991). Characterization of the cytoplasm of Escherichia coli K-12 as a function of external osmolarity. Implications for protein-DNA interactions in vivo. J Mol Biol *222*, 281-300.

Chadani, Y., Ito, K., Kutsukake, K., and Abo, T. (2012). ArfA recruits release factor 2 to rescue stalled ribosomes by peptidyl-tRNA hydrolysis in Escherichia coli. Mol Microbiol *86*, 37-50.

Chadani, Y., Matsumoto, E., Aso, H., Wada, T., Kutsukake, K., Sutou, S., and Abo, T. (2011a). trans-translation-mediated tight regulation of the expression of the alternative ribosome-rescue factor ArfA in Escherichia coli. Genes Genet Syst *86*, 151-163.

Chadani, Y., Ono, K., Kutsukake, K., and Abo, T. (2011b). Escherichia coli YaeJ protein mediates a novel ribosome-rescue pathway distinct from SsrA- and ArfA-mediated pathways. Mol Microbiol *80*, 772-785.

Chadani, Y., Ono, K., Ozawa, S., Takahashi, Y., Takai, K., Nanamiya, H., Tozawa, Y., Kutsukake, K., and Abo, T. (2010). Ribosome rescue by Escherichia coli ArfA (YhdL) in the absence of trans-translation system. Mol Microbiol *78*, 796-808.

Chen, Y., Kaji, A., Kaji, H., and Cooperman, B.S. (2017). The kinetic mechanism of bacterial ribosome recycling. Nucleic Acids Res *45*, 10168-10177.

Choy, J.S., Aung, L.L., and Karzai, A.W. (2007). Lon protease degrades transfer-messenger RNA-tagged proteins. J Bacteriol *189*, 6564-6571.

Christensen, S.K., Mikkelsen, M., Pedersen, K., and Gerdes, K. (2001). RelE, a global inhibitor of translation, is activated during nutritional stress. Proc Natl Acad Sci U S A *98*, 14328-14333.

Coatham, M.L., Brandon, H.E., Fischer, J.J., Schummer, T., and Wieden, H.J. (2016). The conserved GTPase HflX is a ribosome splitting factor that binds to the E-site of the bacterial ribosome. Nucleic Acids Res *44*, 1952-1961.

Cook, G.M., Robson, J.R., Frampton, R.A., McKenzie, J., Przybilski, R., Fineran, P.C., and Arcus, V.L. (2013). Ribonucleases in bacterial toxin-antitoxin systems. Biochim Biophys Acta *1829*, 523-531.

Cruz-Vera, L.R., Rajagopal, S., Squires, C., and Yanofsky, C. (2005). Features of ribosome-peptidyl-tRNA interactions essential for tryptophan induction of tna operon expression. Mol Cell *19*, 333-343.

Culviner, P.H., and Laub, M.T. (2018). Global Analysis of the E. coli Toxin MazF Reveals Widespread Cleavage of mRNA and the Inhibition of rRNA Maturation and Ribosome Biogenesis. Mol Cell *70*, 868-880 e810.

D'Souza, A.R., and Minczuk, M. (2018). Mitochondrial transcription and translation: overview. Essays Biochem *62*, 309-320.

Davis, J.H., and Williamson, J.R. (2017). Structure and dynamics of bacterial ribosome biogenesis. Philos Trans R Soc Lond B Biol Sci *372*.

Demo, G., Svidritskiy, E., Madireddy, R., Diaz-Avalos, R., Grant, T., Grigorieff, N., Sousa, D., and Korostelev, A.A. (2017). Mechanism of ribosome rescue by ArfA and RF2. Elife *6*.

Deutscher, M.P., and Reuven, N.B. (1991). Enzymatic basis for hydrolytic versus phosphorolytic mRNA degradation in Escherichia coli and Bacillus subtilis. Proc Natl Acad Sci U S A *88*, 3277-3280.

Dever, T.E., Dinman, J.D., and Green, R. (2018). Translation Elongation and Recoding in Eukaryotes. Cold Spring Harb Perspect Biol *10*.

Doerfel, L.K., Wohlgemuth, I., Kothe, C., Peske, F., Urlaub, H., and Rodnina, M.V. (2013). EF-P is essential for rapid synthesis of proteins containing consecutive proline residues. Science *339*, 85-88.

Doerfel, L.K., Wohlgemuth, I., Kubyshkin, V., Starosta, A.L., Wilson, D.N., Budisa, N., and Rodnina, M.V. (2015). Entropic Contribution of Elongation Factor P to Proline Positioning at the Catalytic Center of the Ribosome. J Am Chem Soc *137*, 12997-13006.

Dong, G., Nowakowski, J., and Hoffman, D.W. (2002). Structure of small protein B: the protein component of the tmRNA-SmpB system for ribosome rescue. EMBO J *21*, 1845-1854.

Duarte, I., Nabuurs, S.B., Magno, R., and Huynen, M. (2012). Evolution and diversification of the organellar release factor family. Mol Biol Evol *29*, 3497-3512.

Dunkle, J.A., and Cate, J.H. (2010). Ribosome structure and dynamics during translocation and termination. Annu Rev Biophys *39*, 227-244.

Dyson, H.J., and Wright, P.E. (2002). Coupling of folding and binding for unstructured proteins. Curr Opin Struct Biol *12*, 54-60.

Dyson, H.J., and Wright, P.E. (2005). Intrinsically unstructured proteins and their functions. Nat Rev Mol Cell Biol *6*, 197-208.

Feaga, H.A., Quickel, M.D., Hankey-Giblin, P.A., and Keiler, K.C. (2016). Human Cells Require Non-stop Ribosome Rescue Activity in Mitochondria. PLoS Genet *12*, e1005964.

Feaga, H.A., Viollier, P.H., and Keiler, K.C. (2014). Release of nonstop ribosomes is essential. MBio *5*, e01916.

Feng, S., Chen, Y., Kamada, K., Wang, H., Tang, K., Wang, M., and Gao, Y.G. (2013). YoeB-ribosome structure: a canonical RNase that requires the ribosome for its specific activity. Nucleic Acids Res *41*, 9549-9556.

Fersht, A. (1999). Structure and mechanism in protein science: a guide to enzyme catalysis and protein folding (Macmillan).

Fischer, N., Neumann, P., Bock, L.V., Maracci, C., Wang, Z., Paleskava, A., Konevega, A.L., Schroder, G.F., Grubmuller, H., Ficner, R.*, et al.* (2016). The pathway to GTPase activation of elongation factor SelB on the ribosome. Nature *540*, 80-85.

Florin, T., Maracci, C., Graf, M., Karki, P., Klepacki, D., Berninghausen, O., Beckmann, R., Vazquez-Laslop, N., Wilson, D.N., Rodnina, M.V.*, et al.* (2017). An antimicrobial peptide that inhibits translation by trapping release factors on the ribosome. Nat Struct Mol Biol *24*, 752-757.

Fu, Z., Kaledhonkar, S., Borg, A., Sun, M., Chen, B., Grassucci, R.A., Ehrenberg, M., and Frank, J. (2016). Key Intermediates in Ribosome Recycling Visualized by Time-Resolved Cryoelectron Microscopy. Structure *24*, 2092-2101.

Gagnon, M.G., Seetharaman, S.V., Bulkley, D., and Steitz, T.A. (2012). Structural basis for the rescue of stalled ribosomes: structure of YaeJ bound to the ribosome. Science *335*, 1370-1372.

Ganguly, D., Otieno, S., Waddell, B., Iconaru, L., Kriwacki, R.W., and Chen, J. (2012). Electrostatically accelerated coupled binding and folding of intrinsically disordered proteins. J Mol Biol *422*, 674-684.

Gao, N., Zavialov, A.V., Li, W., Sengupta, J., Valle, M., Gursky, R.P., Ehrenberg, M., and Frank, J. (2005). Mechanism for the disassembly of the posttermination complex inferred from cryo-EM studies. Mol Cell *18*, 663-674.

Garza-Sanchez, F., Schaub, R.E., Janssen, B.D., and Hayes, C.S. (2011). tmRNA regulates synthesis of the ArfA ribosome rescue factor. Mol Microbiol *80*, 1204-1219.

Garza-Sanchez, F., Shoji, S., Fredrick, K., and Hayes, C.S. (2009). RNase II is important for A-site mRNA cleavage during ribosome pausing. Mol Microbiol *73*, 882-897.

Gerdes, K. (2000). Toxin-antitoxin modules may regulate synthesis of macromolecules during nutritional stress. J Bacteriol *182*, 561-572.

Gerdes, K., Gultyaev, A.P., Franch, T., Pedersen, K., and Mikkelsen, N.D. (1997). Antisense RNA-regulated programmed cell death. Annu Rev Genet *31*, 1-31.

Gong, F., and Yanofsky, C. (2002). Instruction of translating ribosome by nascent peptide. Science *297*, 1864-1867.

Goralski, T.D.P., Kirimanjeswara, G.S., and Keiler, K.C. (2018). A New Mechanism for Ribosome Rescue Can Recruit RF1 or RF2 to Nonstop Ribosomes. MBio *9*.

Gorochowski, T.E., Ignatova, Z., Bovenberg, R.A., and Roubos, J.A. (2015). Trade-offs between tRNA abundance and mRNA secondary structure support smoothing of translation elongation rate. Nucleic Acids Res *43*, 3022-3032.

Goyal, A., Belardinelli, R., Maracci, C., Milon, P., and Rodnina, M.V. (2015). Directional transition from initiation to elongation in bacterial translation. Nucleic Acids Res *43*, 10700-10712.

Goyal, A., Belardinelli, R., and Rodnina, M.V. (2017). Non-canonical Binding Site for Bacterial Initiation Factor 3 on the Large Ribosomal Subunit. Cell reports *20*, 3113-3122.

Greber, B.J., and Ban, N. (2016). Structure and Function of the Mitochondrial Ribosome. Annu Rev Biochem *85*, 103-132.

Greber, B.J., Bieri, P., Leibundgut, M., Leitner, A., Aebersold, R., Boehringer, D., and Ban, N. (2015). Ribosome. The complete structure of the 55S mammalian mitochondrial ribosome. Science *348*, 303-308.

Greber, B.J., Boehringer, D., Leitner, A., Bieri, P., Voigts-Hoffmann, F., Erzberger, J.P., Leibundgut, M., Aebersold, R., and Ban, N. (2014). Architecture of the large subunit of the mammalian mitochondrial ribosome. Nature *505*, 515-519.

Gumbart, J., Schreiner, E., Wilson, D.N., Beckmann, R., and Schulten, K. (2012). Mechanisms of SecM-mediated stalling in the ribosome. Biophys J *103*, 331-341.

Hanawa-Suetsugu, K., Takagi, M., Inokuchi, H., Himeno, H., and Muto, A. (2002). SmpB functions in various steps of trans-translation. Nucleic Acids Res *30*, 1620-1629.

Handa, Y., Hikawa, Y., Tochio, N., Kogure, H., Inoue, M., Koshiba, S., Guntert, P., Inoue, Y., Kigawa, T., Yokoyama, S*., et al.* (2010). Solution structure of the catalytic domain of the mitochondrial protein ICT1 that is essential for cell vitality. J Mol Biol *404*, 260-273.

Handa, Y., Inaho, N., and Nameki, N. (2011). YaeJ is a novel ribosome-associated protein in Escherichia coli that can hydrolyze peptidyl-tRNA on stalled ribosomes. Nucleic Acids Res *39*, 1739-1748.

Haque, M.E., and Spremulli, L.L. (2010). ICT1 comes to the rescue of mitochondrial ribosomes. EMBO J *29*, 1019-1020.

Hayes, C.S., Bose, B., and Sauer, R.T. (2002a). Proline residues at the C terminus of nascent chains induce SsrA tagging during translation termination. J Biol Chem *277*, 33825-33832.

Hayes, C.S., Bose, B., and Sauer, R.T. (2002b). Stop codons preceded by rare arginine codons are efficient determinants of SsrA tagging in Escherichia coli. Proc Natl Acad Sci U S A *99*, 3440-3445.

Hayes, C.S., and Keiler, K.C. (2010). Beyond ribosome rescue: tmRNA and co-translational processes. FEBS Lett *584*, 413-419.

Hayes, C.S., and Sauer, R.T. (2003). Cleavage of the A site mRNA codon during ribosome pausing provides a mechanism for translational quality control. Mol Cell *12*, 903-911.

Hazan, R., Sat, B., and Engelberg-Kulka, H. (2004). Escherichia coli mazEF-mediated cell death is triggered by various stressful conditions. J Bacteriol *186*, 3663-3669.

Hellen, C.U.T. (2018). Translation Termination and Ribosome Recycling in Eukaryotes. Cold Spring Harb Perspect Biol *10*.

Herman, C., Thevenet, D., Bouloc, P., Walker, G.C., and D'Ari, R. (1998). Degradation of carboxy-terminal-tagged cytoplasmic proteins by the Escherichia coli protease HflB (FtsH). Genes Dev *12*, 1348-1355.

Himeno, H., Kurita, D., and Muto, A. (2014). tmRNA-mediated trans-translation as the major ribosome rescue system in a bacterial cell. Front Genet *5*, 66.

Holberger, L.E., and Hayes, C.S. (2009). Ribosomal protein S12 and aminoglycoside antibiotics modulate A-site mRNA cleavage and transfer-messenger RNA activity in Escherichia coli. J Biol Chem *284*, 32188-32200.

Holzmann, J., Frank, P., Loffler, E., Bennett, K.L., Gerner, C., and Rossmanith, W. (2008). RNase P without RNA: identification and functional reconstitution of the human mitochondrial tRNA processing enzyme. Cell *135*, 462-474.

Hui, M.P., Foley, P.L., and Belasco, J.G. (2014). Messenger RNA degradation in bacterial cells. Annu Rev Genet *48*, 537-559.

Huter, P., Arenz, S., Bock, L.V., Graf, M., Frister, J.O., Heuer, A., Peil, L., Starosta, A.L., Wohlgemuth, I., Peske, F.*, et al.* (2017a). Structural Basis for Polyproline-Mediated Ribosome Stalling and Rescue by the Translation Elongation Factor EF-P. Mol Cell *68*, 515-527 e516.

Huter, P., Muller, C., Beckert, B., Arenz, S., Berninghausen, O., Beckmann, R., and Wilson, D.N. (2017b). Structural basis for ArfA-RF2-mediated translation termination on mRNAs lacking stop codons. Nature *541*, 546-549.

Iesmantavicius, V., Dogan, J., Jemth, P., Teilum, K., and Kjaergaard, M. (2014). Helical propensity in an intrinsically disordered protein accelerates ligand binding. Angew Chem Int Ed Engl *53*, 1548-1551.

Indrisiunaite, G., Pavlov, M.Y., Heurgue-Hamard, V., and Ehrenberg, M. (2015). On the pH dependence of class-1 RF-dependent termination of mRNA translation. J Mol Biol *427*, 1848-1860.

Ito, K., Chadani, Y., Nakamori, K., Chiba, S., Akiyama, Y., and Abo, T. (2011). Nascentome analysis uncovers futile protein synthesis in Escherichia coli. PLoS One *6*, e28413.

Ivanova, N., Pavlov, M.Y., and Ehrenberg, M. (2005). tmRNA-induced release of messenger RNA from stalled ribosomes. J Mol Biol *350*, 897-905.

Ivanova, N., Pavlov, M.Y., Felden, B., and Ehrenberg, M. (2004). Ribosome rescue by tmRNA requires truncated mRNAs. J Mol Biol *338*, 33-41.

Jackson, R.J., Hellen, C.U., and Pestova, T.V. (2010). The mechanism of eukaryotic translation initiation and principles of its regulation. Nat Rev Mol Cell Biol *11*, 113-127.

Jacobson, G.R., and Rosenbusch, J.P. (1976). Abundance and membrane association of elongation factor Tu in E. coli. Nature *261*, 23-26.

James, N.R., Brown, A., Gordiyenko, Y., and Ramakrishnan, V. (2016). Translational termination without a stop codon. Science *354*, 1437-1440.

Janssen, B.D., Garza-Sanchez, F., and Hayes, C.S. (2015). YoeB toxin is activated during thermal stress. Microbiologyopen *4*, 682-697.

Janssen, B.D., and Hayes, C.S. (2012). The tmRNA ribosome-rescue system. Adv Protein Chem Struct Biol *86*, 151-191.

Jiang, L., Schaffitzel, C., Bingel-Erlenmeyer, R., Ban, N., Korber, P., Koning, R.I., de Geus, D.C., Plaisier, J.R., and Abrahams, J.P. (2009). Recycling of aborted ribosomal 50S subunit-nascent chain-tRNA complexes by the heat shock protein Hsp15. J Mol Biol *386*, 1357-1367.

Jin, H., Kelley, A.C., Loakes, D., and Ramakrishnan, V. (2010). Structure of the 70S ribosome bound to release factor 2 and a substrate analog provides insights into catalysis of peptide release. Proc Natl Acad Sci U S A *107*, 8593-8598.

Julio, S.M., Heithoff, D.M., and Mahan, M.J. (2000). ssrA (tmRNA) plays a role in Salmonella enterica serovar Typhimurium pathogenesis. J Bacteriol *182*, 1558-1563.

Keiler, K.C. (2015). Mechanisms of ribosome rescue in bacteria. Nat Rev Microbiol *13*, 285-297.

Keiler, K.C., and Ramadoss, N.S. (2011). Bifunctional transfer-messenger RNA. Biochimie *93*, 1993-1997.

Keiler, K.C., Waller, P.R., and Sauer, R.T. (1996). Role of a peptide tagging system in degradation of proteins synthesized from damaged messenger RNA. Science *271*, 990-993.

Kogure, H., Handa, Y., Nagata, M., Kanai, N., Guntert, P., Kubota, K., and Nameki, N. (2014). Identification of residues required for stalled-ribosome rescue in the codon-independent release factor YaeJ. Nucleic Acids Res *42*, 3152-3163.

Kogure, H., Hikawa, Y., Hagihara, M., Tochio, N., Koshiba, S., Inoue, Y., Guntert, P., Kigawa, T., Yokoyama, S., and Nameki, N. (2012). Solution structure and siRNA-mediated knockdown analysis of the mitochondrial disease-related protein C12orf65. Proteins *80*, 2629-2642.

Kolter, R., and Yanofsky, C. (1982). Attenuation in amino acid biosynthetic operons. Annu Rev Genet *16*, 113-134.

Komine, Y., Kitabatake, M., Yokogawa, T., Nishikawa, K., and Inokuchi, H. (1994). A tRNA-like structure is present in 10Sa RNA, a small stable RNA from Escherichia coli. Proc Natl Acad Sci U S A *91*, 9223-9227.

Konno, T., Kurita, D., Takada, K., Muto, A., and Himeno, H. (2007). A functional interaction of SmpB with tmRNA for determination of the resuming point of trans-translation. RNA *13*, 1723-1731.

Korber, P., Stahl, J.M., Nierhaus, K.H., and Bardwell, J.C. (2000). Hsp15: a ribosome-associated heat shock protein. EMBO J *19*, 741-748.

Korostelev, A., Asahara, H., Lancaster, L., Laurberg, M., Hirschi, A., Zhu, J., Trakhanov, S., Scott, W.G., and Noller, H.F. (2008). Crystal structure of a translation termination complex formed with release factor RF2. Proc Natl Acad Sci U S A *105*, 19684-19689.

Korostelev, A., Zhu, J., Asahara, H., and Noller, H.F. (2010). Recognition of the amber UAG stop codon by release factor RF1. EMBO J *29*, 2577-2585.

Korostelev, A.A. (2011). Structural aspects of translation termination on the ribosome. RNA *17*, 1409-1421.

Kuhlenkoetter, S., Wintermeyer, W., and Rodnina, M.V. (2011). Different substrate-dependent transition states in the active site of the ribosome. Nature *476*, 351-354.

Kurita, D., Chadani, Y., Muto, A., Abo, T., and Himeno, H. (2014). ArfA recognizes the lack of mRNA in the mRNA channel after RF2 binding for ribosome rescue. Nucleic Acids Res *42*, 13339-13352.

Kurita, D., Sasaki, R., Muto, A., and Himeno, H. (2007). Interaction of SmpB with ribosome from directed hydroxyl radical probing. Nucleic Acids Res *35*, 7248-7255.

Lakowicz, J.R. (1988). Principles of frequency-domain fluorescence spectroscopy and applications to cell membranes. Subcell Biochem *13*, 89-126.

Lalaouna, D., and Masse, E. (2017). Cut in translation: ribosome-dependent mRNA decay. EMBO J *36*, 1120-1122.

Lao, X., Feng, Q., He, G., Ji, M., Zhu, D., Xu, P., Tang, W., Xu, J., and Qin, X. (2016). Immature Colon Carcinoma Transcript-1 (ICT1) Expression Correlates with Unfavorable Prognosis and Survival in Patients with Colorectal Cancer. Ann Surg Oncol *23*, 3924-3933.

Lapkouski, M., and Hallberg, B.M. (2015). Structure of mitochondrial poly(A) RNA polymerase reveals the structural basis for dimerization, ATP selectivity and the SPAX4 disease phenotype. Nucleic Acids Res *43*, 9065-9075.

Laurberg, M., Asahara, H., Korostelev, A., Zhu, J., Trakhanov, S., and Noller, H.F. (2008). Structural basis for translation termination on the 70S ribosome. Nature *454*, 852-857.

Lee, S., Ishii, M., Tadaki, T., Muto, A., and Himeno, H. (2001). Determinants on tmRNA for initiating efficient and precise trans-translation: some mutations upstream of the tag-encoding sequence of Escherichia coli tmRNA shift the initiation point of trans-translation in vitro. RNA *7*, 999-1012.

Lind, C., Sund, J., and Aqvist, J. (2013). Codon-reading specificities of mitochondrial release factors and translation termination at non-standard stop codons. Nat Commun *4*, 2940.

Link, A.J., Phillips, D., and Church, G.M. (1997). Methods for generating precise deletions and insertions in the genome of wild-type Escherichia coli: application to open reading frame characterization. J Bacteriol *179*, 6228-6237.

Loveland, A.B., Demo, G., Grigorieff, N., and Korostelev, A.A. (2017). Ensemble cryo-EM elucidates the mechanism of translation fidelity. Nature *546*, 113-117.

Ma, C., Kurita, D., Li, N., Chen, Y., Himeno, H., and Gao, N. (2017). Mechanistic insights into the alternative translation termination by ArfA and RF2. Nature *541*, 550-553.

Martin, W.F., Garg, S., and Zimorski, V. (2015). Endosymbiotic theories for eukaryote origin. Philos Trans R Soc Lond B Biol Sci *370*, 20140330.

Martinez, A.K., Gordon, E., Sengupta, A., Shirole, N., Klepacki, D., Martinez-Garriga, B., Brown, L.M., Benedik, M.J., Yanofsky, C., Mankin, A.S*., et al.* (2014). Interactions of the TnaC nascent peptide with rRNA in the exit tunnel enable the ribosome to respond to free tryptophan. Nucleic Acids Res *42*, 1245-1256.

McCoy, L.S., Xie, Y., and Tor, Y. (2011). Antibiotics that target protein synthesis. Wiley Interdiscip Rev RNA *2*, 209-232.

Melnikov, S., Ben-Shem, A., Garreau de Loubresse, N., Jenner, L., Yusupova, G., and Yusupov, M. (2012). One core, two shells: bacterial and eukaryotic ribosomes. Nat Struct Mol Biol *19*, 560-567.

Merrick, W.C., and Pavitt, G.D. (2018). Protein Synthesis Initiation in Eukaryotic Cells. Cold Spring Harb Perspect Biol *10*.

Miller, M.R., and Buskirk, A.R. (2014). The SmpB C-terminal tail helps tmRNA to recognize and enter stalled ribosomes. Front Microbiol *5*, 462.

Milon, P., Carotti, M., Konevega, A.L., Wintermeyer, W., Rodnina, M.V., and Gualerzi, C.O. (2010). The ribosome-bound initiation factor 2 recruits initiator tRNA to the 30S initiation complex. EMBO Rep *11*, 312-316.

Milon, P., Konevega, A.L., Gualerzi, C.O., and Rodnina, M.V. (2008). Kinetic checkpoint at a late step in translation initiation. Mol Cell *30*, 712-720.

Milon, P., Konevega, A.L., Peske, F., Fabbretti, A., Gualerzi, C.O., and Rodnina, M.V. (2007). Transient kinetics, fluorescence, and FRET in studies of initiation of translation in bacteria. Methods Enzymol *430*, 1-30.

Milon, P., Maracci, C., Filonava, L., Gualerzi, C.O., and Rodnina, M.V. (2012). Real-time assembly landscape of bacterial 30S translation initiation complex. Nat Struct Mol Biol *19*, 609-615.

Milon, P., and Rodnina, M.V. (2012). Kinetic control of translation initiation in bacteria. Crit Rev Biochem Mol Biol *47*, 334-348.

Moll, I., and Engelberg-Kulka, H. (2012). Selective translation during stress in Escherichia coli. Trends Biochem Sci *37*, 493-498.

Mollica, L., Bessa, L.M., Hanoulle, X., Jensen, M.R., Blackledge, M., and Schneider, R. (2016). Binding Mechanisms of Intrinsically Disordered Proteins: Theory, Simulation, and Experiment. Front Mol Biosci *3*, 52.

Moore, S.D., and Sauer, R.T. (2005). Ribosome rescue: tmRNA tagging activity and capacity in Escherichia coli. Mol Microbiol *58*, 456-466.

Mora, L., Heurgue-Hamard, V., de Zamaroczy, M., Kervestin, S., and Buckingham, R.H. (2007). Methylation of bacterial release factors RF1 and RF2 is required for normal translation termination in vivo. J Biol Chem *282*, 35638-35645.

Nagaike, T., Suzuki, T., Katoh, T., and Ueda, T. (2005). Human mitochondrial mRNAs are stabilized with polyadenylation regulated by mitochondria-specific poly(A) polymerase and polynucleotide phosphorylase. J Biol Chem *280*, 19721-19727.

Nakahigashi, K., Kubo, N., Narita, S., Shimaoka, T., Goto, S., Oshima, T., Mori, H., Maeda, M., Wada, C., and Inokuchi, H. (2002). HemK, a class of protein methyl transferase with similarity to DNA methyl transferases, methylates polypeptide chain release factors, and hemK knockout induces defects in translational termination. Proc Natl Acad Sci U S A *99*, 1473-1478.

Nakatogawa, H., Murakami, A., and Ito, K. (2004). Control of SecA and SecM translation by protein secretion. Curr Opin Microbiol *7*, 145-150.

Nameki, N., Tadaki, T., Himeno, H., and Muto, A. (2000). Three of four pseudoknots in tmRNA are interchangeable and are substitutable with single-stranded RNAs. FEBS Lett *470*, 345-349.

Neubauer, C., Gao, Y.G., Andersen, K.R., Dunham, C.M., Kelley, A.C., Hentschel, J., Gerdes, K., Ramakrishnan, V., and Brodersen, D.E. (2009). The structural basis for mRNA recognition and cleavage by the ribosome-dependent endonuclease RelE. Cell *139*, 1084-1095.

Neubauer, C., Gillet, R., Kelley, A.C., and Ramakrishnan, V. (2012). Decoding in the absence of a codon by tmRNA and SmpB in the ribosome. Science *335*, 1366-1369.

Noble, J.A., Innis, M.A., Koonin, E.V., Rudd, K.E., Banuett, F., and Herskowitz, I. (1993). The Escherichia coli hflA locus encodes a putative GTP-binding protein and two membrane proteins, one of which contains a protease-like domain. Proc Natl Acad Sci U S A *90*, 10866-10870.

Nogales, E., and Scheres, S.H. (2015). Cryo-EM: A Unique Tool for the Visualization of Macromolecular Complexity. Mol Cell *58*, 677-689.

Okan, N.A., Mena, P., Benach, J.L., Bliska, J.B., and Karzai, A.W. (2010). The smpB-ssrA mutant of Yersinia pestis functions as a live attenuated vaccine to protect mice against pulmonary plague infection. Infect Immun *78*, 1284-1293.

Ott, M., Amunts, A., and Brown, A. (2016). Organization and Regulation of Mitochondrial Protein Synthesis. Annu Rev Biochem *85*, 77-101.

Pedersen, K., Christensen, S.K., and Gerdes, K. (2002). Rapid induction and reversal of a bacteriostatic condition by controlled expression of toxins and antitoxins. Mol Microbiol *45*, 501-510.

Pedersen, K., Zavialov, A.V., Pavlov, M.Y., Elf, J., Gerdes, K., and Ehrenberg, M. (2003). The bacterial toxin RelE displays codon-specific cleavage of mRNAs in the ribosomal A site. Cell *112*, 131-140.

Peng, B.Z., Bock, L.V., Belardinelli, R., Peske, F., Grubmuller, H., and Rodnina, M.V. (2019). Active role of elongation factor G in maintaining the mRNA reading frame during translation. Sci Adv *5*, eaax8030.

Peske, F., Kuhlenkoetter, S., Rodnina, M.V., and Wintermeyer, W. (2014). Timing of GTP binding and hydrolysis by translation termination factor RF3. Nucleic Acids Res *42*, 1812-1820.

Peske, F., Rodnina, M.V., and Wintermeyer, W. (2005). Sequence of steps in ribosome recycling as defined by kinetic analysis. Mol Cell *18*, 403-412.

Pierson, W.E., Hoffer, E.D., Keedy, H.E., Simms, C.L., Dunham, C.M., and Zaher, H.S. (2016). Uniformity of Peptide Release Is Maintained by Methylation of Release Factors. Cell reports *17*, 11-18.

Prysak, M.H., Mozdzierz, C.J., Cook, A.M., Zhu, L., Zhang, Y., Inouye, M., and Woychik, N.A. (2009). Bacterial toxin YafQ is an endoribonuclease that associates with the ribosome and blocks translation elongation through sequence-specific and frame-dependent mRNA cleavage. Mol Microbiol *71*, 1071-1087.

Rae, C.D., Gordiyenko, Y., and Ramakrishnan, V. (2019). How a circularized tmRNA moves through the ribosome. Science *363*, 740-744.

Ramrath, D.J., Yamamoto, H., Rother, K., Wittek, D., Pech, M., Mielke, T., Loerke, J., Scheerer, P., Ivanov, P., Teraoka, Y.*, et al.* (2012). The complex of tmRNA-SmpB and EF-G on translocating ribosomes. Nature *485*, 526-529.

Reeve, B., Hargest, T., Gilbert, C., and Ellis, T. (2014). Predicting translation initiation rates for designing synthetic biology. Front Bioeng Biotechnol *2*, 1.

Richter, R., Rorbach, J., Pajak, A., Smith, P.M., Wessels, H.J., Huynen, M.A., Smeitink, J.A., Lightowlers, R.N., and Chrzanowska-Lightowlers, Z.M. (2010). A functional peptidyl-tRNA hydrolase, ICT1, has been recruited into the human mitochondrial ribosome. EMBO J *29*, 1116-1125.

Roche, E.D., and Sauer, R.T. (1999). SsrA-mediated peptide tagging caused by rare codons and tRNA scarcity. EMBO J *18*, 4579-4589.

Roche, E.D., and Sauer, R.T. (2001). Identification of endogenous SsrA-tagged proteins reveals tagging at positions corresponding to stop codons. J Biol Chem *276*, 28509-28515.

Rodnina, M.V. (2013). The ribosome as a versatile catalyst: reactions at the peptidyl transferase center. Curr Opin Struct Biol *23*, 595-602.

Rodnina, M.V. (2016). The ribosome in action: Tuning of translational efficiency and protein folding. Protein Sci *25*, 1390-1406.

Rodnina, M.V. (2018). Translation in Prokaryotes. Cold Spring Harb Perspect Biol *10*.

Rodnina, M.V., Fischer, N., Maracci, C., and Stark, H. (2017). Ribosome dynamics during decoding. Philos Trans R Soc Lond B Biol Sci *372*.

Rodnina, M.V., Gromadski, K.B., Kothe, U., and Wieden, H.J. (2005). Recognition and selection of tRNA in translation. FEBS Lett *579*, 938-942.

Rodnina, M.V., Pape, T., Fricke, R., and Wintermeyer, W. (1995). Elongation factor Tu, a GTPase triggered by codon recognition on the ribosome: mechanism and GTP consumption. Biochem Cell Biol *73*, 1221-1227.

Rodnina, M.V., Savelsbergh, A., Katunin, V.I., and Wintermeyer, W. (1997). Hydrolysis of GTP by elongation factor G drives tRNA movement on the ribosome. Nature *385*, 37-41.

Rodnina, M.V., and Wintermeyer, W. (1995). GTP consumption of elongation factor Tu during translation of heteropolymeric mRNAs. Proc Natl Acad Sci U S A *92*, 1945-1949.

Rodnina, M.V., and Wintermeyer, W. (2011). The ribosome as a molecular machine: the mechanism of tRNA-mRNA movement in translocation. Biochem Soc Trans *39*, 658-662.

Rodnina, M.V., Wintermeyer, W., and Green, R. (2011). Ribosomes structure, function, and dynamics (Springer Science & Business Media).

Romero, P., Obradovic, Z., Li, X., Garner, E.C., Brown, C.J., and Dunker, A.K. (2001). Sequence complexity of disordered protein. Proteins *42*, 38-48.

Rorbach, J., Nicholls, T.J., and Minczuk, M. (2011). PDE12 removes mitochondrial RNA poly(A) tails and controls translation in human mitochondria. Nucleic Acids Res *39*, 7750-7763.

Schaub, R.E., Poole, S.J., Garza-Sanchez, F., Benbow, S., and Hayes, C.S. (2012). Proteobacterial ArfA peptides are synthesized from non-stop messenger RNAs. J Biol Chem *287*, 29765-29775.

Schmeing, T.M., and Ramakrishnan, V. (2009). What recent ribosome structures have revealed about the mechanism of translation. Nature *461*, 1234-1242.

Schmidt, A., Kochanowski, K., Vedelaar, S., Ahrne, E., Volkmer, B., Callipo, L., Knoops, K., Bauer, M., Aebersold, R., and Heinemann, M. (2016). The quantitative and condition-dependent Escherichia coli proteome. Nature biotechnology *34*, 104-110.

Schreiber, G., and Fersht, A.R. (1996). Rapid, electrostatically assisted association of proteins. Nat Struct Biol *3*, 427-431.

Seo, H.S., Kiel, M., Pan, D., Raj, V.S., Kaji, A., and Cooperman, B.S. (2004). Kinetics and thermodynamics of RRF, EF-G, and thiostrepton interaction on the Escherichia coli ribosome. Biochemistry *43*, 12728-12740.

Shammas, S.L., Crabtree, M.D., Dahal, L., Wicky, B.I., and Clarke, J. (2016). Insights into Coupled Folding and Binding Mechanisms from Kinetic Studies. J Biol Chem *291*, 6689-6695.

Shammas, S.L., Rogers, J.M., Hill, S.A., and Clarke, J. (2012). Slow, reversible, coupled folding and binding of the spectrin tetramerization domain. Biophys J *103*, 2203-2214.

Shammas, S.L., Travis, A.J., and Clarke, J. (2013). Remarkably fast coupled folding and binding of the intrinsically disordered transactivation domain of cMyb to CBP KIX. J Phys Chem B *117*, 13346-13356.

Sharma, P.K., Xiang, Y., Kato, M., and Warshel, A. (2005). What are the roles of substrate-assisted catalysis and proximity effects in peptide bond formation by the ribosome? Biochemistry *44*, 11307-11314.

Shimizu, Y. (2012). ArfA recruits RF2 into stalled ribosomes. J Mol Biol *423*, 624-631.

Shimizu, Y., and Ueda, T. (2002). The role of SmpB protein in trans-translation. FEBS Lett *514*, 74-77.

Shoemaker, B.A., Portman, J.J., and Wolynes, P.G. (2000). Speeding molecular recognition by using the folding funnel: the fly-casting mechanism. Proc Natl Acad Sci U S A *97*, 8868-8873.

Simanshu, D.K., Yamaguchi, Y., Park, J.H., Inouye, M., and Patel, D.J. (2013). Structural basis of mRNA recognition and cleavage by toxin MazF and its regulation by antitoxin MazE in Bacillus subtilis. Mol Cell *52*, 447-458.

Soleimanpour-Lichaei, H.R., Kuhl, I., Gaisne, M., Passos, J.F., Wydro, M., Rorbach, J., Temperley, R., Bonnefoy, N., Tate, W., Lightowlers, R.*, et al.* (2007). mtRF1a is a human mitochondrial translation release factor decoding the major termination codons UAA and UAG. Mol Cell *27*, 745-757.

Someya, T., Nameki, N., Hosoi, H., Suzuki, S., Hatanaka, H., Fujii, M., Terada, T., Shirouzu, M., Inoue, Y., Shibata, T.*, et al.* (2003). Solution structure of a tmRNA-binding protein, SmpB, from Thermus thermophilus. FEBS Lett *535*, 94-100.

Starosta, A.L., Lassak, J., Jung, K., and Wilson, D.N. (2014). The bacterial translation stress response. FEMS Microbiol Rev *38*, 1172-1201.

Sunohara, T., Jojima, K., Tagami, H., Inada, T., and Aiba, H. (2004). Ribosome stalling during translation elongation induces cleavage of mRNA being translated in Escherichia coli. J Biol Chem *279*, 15368-15375.

Taniguchi, Y., Choi, P.J., Li, G.W., Chen, H., Babu, M., Hearn, J., Emili, A., and Xie, X.S. (2010). Quantifying E. coli proteome and transcriptome with single-molecule sensitivity in single cells. Science *329*, 533-538.

Temperley, R., Richter, R., Dennerlein, S., Lightowlers, R.N., and Chrzanowska-Lightowlers, Z.M. (2010a). Hungry codons promote frameshifting in human mitochondrial ribosomes. Science *327*, 301.

Temperley, R.J., Wydro, M., Lightowlers, R.N., and Chrzanowska-Lightowlers, Z.M. (2010b). Human mitochondrial mRNAs--like members of all families, similar but different. Biochim Biophys Acta *1797*, 1081-1085.

Theillet, F.X., Binolfi, A., Bekei, B., Martorana, A., Rose, H.M., Stuiver, M., Verzini, S., Lorenz, D., van Rossum, M., Goldfarb, D*., et al.* (2016). Structural disorder of monomeric alpha-synuclein persists in mammalian cells. Nature *530*, 45-50.

Tomecki, R., Dmochowska, A., Gewartowski, K., Dziembowski, A., and Stepien, P.P. (2004). Identification of a novel human nuclear-encoded mitochondrial poly(A) polymerase. Nucleic Acids Res *32*, 6001-6014.

Tsui, H.C., Feng, G., and Winkler, M.E. (1996). Transcription of the mutL repair, miaA tRNA modification, hfq pleiotropic regulator, and hflA region protease genes of Escherichia coli K-12 from clustered Esigma32-specific promoters during heat shock. J Bacteriol *178*, 5719-5731.

Tuller, T., Waldman, Y.Y., Kupiec, M., and Ruppin, E. (2010). Translation efficiency is determined by both codon bias and folding energy. Proc Natl Acad Sci U S A *107*, 3645-3650.

Ueda, K., Yamamoto, Y., Ogawa, K., Abo, T., Inokuchi, H., and Aiba, H. (2002). Bacterial SsrA system plays a role in coping with unwanted translational readthrough caused by suppressor tRNAs. Genes Cells *7*, 509-519.

Ujiie, H., Matsutani, T., Tomatsu, H., Fujihara, A., Ushida, C., Miwa, Y., Fujita, Y., Himeno, H., and Muto, A. (2009). Trans-translation is involved in the CcpA-dependent tagging and degradation of TreP in Bacillus subtilis. J Biochem *145*, 59-66.

Vesper, O., Amitai, S., Belitsky, M., Byrgazov, K., Kaberdina, A.C., Engelberg-Kulka, H., and Moll, I. (2011). Selective translation of leaderless mRNAs by specialized ribosomes generated by MazF in Escherichia coli. Cell *147*, 147-157.

Wallin, G., and Aqvist, J. (2010). The transition state for peptide bond formation reveals the ribosome as a water trap. Proc Natl Acad Sci U S A *107*, 1888-1893.

Wang, C., Liang, C., Feng, W., Xia, X., Chen, F., Qiao, E., Zhang, X., Chen, D., Ling, Z., and Yang, H. (2017). ICT1 knockdown inhibits breast cancer cell growth via induction of cell cycle arrest and apoptosis. Int J Mol Med *39*, 1037-1045.

Weixlbaumer, A., Jin, H., Neubauer, C., Voorhees, R.M., Petry, S., Kelley, A.C., and Ramakrishnan, V. (2008). Insights into translational termination from the structure of RF2 bound to the ribosome. Science *322*, 953-956.

Wells, S.E., Hillner, P.E., Vale, R.D., and Sachs, A.B. (1998). Circularization of mRNA by eukaryotic translation initiation factors. Mol Cell *2*, 135-140.

Wendt, H., Leder, L., Harma, H., Jelesarov, I., Baici, A., and Bosshard, H.R. (1997). Very rapid, ionic strength-dependent association and folding of a heterodimeric leucine zipper. Biochemistry *36*, 204-213.

Wesolowska, M., Gorman, G.S., Alston, C.L., Pajak, A., Pyle, A., He, L., Griffin, H., Chinnery, P.F., Miller, J.A., Schaefer, A.M.*, et al.* (2015). Adult Onset Leigh Syndrome in the Intensive Care Setting: A Novel Presentation of a C12orf65 Related Mitochondrial Disease. J Neuromuscul Dis *2*, 409-419.

Wydro, M., Bobrowicz, A., Temperley, R.J., Lightowlers, R.N., and Chrzanowska-Lightowlers, Z.M. (2010). Targeting of the cytosolic poly(A) binding protein PABPC1 to mitochondria causes mitochondrial translation inhibition. Nucleic Acids Res *38*, 3732-3742.

Xie, W., Wu, M., Fu, T., Li, X., Wang, Z., Hu, Y., Zhu, L., and Zhang, G. (2017). ICT1 predicts a poor survival and correlated with cell proliferation in diffuse large B-cell lymphoma. Gene *627*, 255-262.

Yamaguchi, Y., Park, J.H., and Inouye, M. (2011). Toxin-antitoxin systems in bacteria and archaea. Annu Rev Genet *45*, 61-79.

Yanofsky, C. (1981). Attenuation in the control of expression of bacterial operons. Nature *289*, 751-758.

Yu, C.H., Dang, Y., Zhou, Z., Wu, C., Zhao, F., Sachs, M.S., and Liu, Y. (2015). Codon Usage Influences the Local Rate of Translation Elongation to Regulate Co-translational Protein Folding. Mol Cell *59*, 744-754.

Zaher, H.S., and Green, R. (2011). A primary role for release factor 3 in quality control during translation elongation in Escherichia coli. Cell *147*, 396-408.

Zavialov, A.V., Buckingham, R.H., and Ehrenberg, M. (2001). A posttermination ribosomal complex is the guanine nucleotide exchange factor for peptide release factor RF3. Cell *107*, 115-124.

Zeng, F., Chen, Y., Remis, J., Shekhar, M., Phillips, J.C., Tajkhorshid, E., and Jin, H. (2017). Structural basis of co-translational quality control by ArfA and RF2 bound to ribosome. Nature *541*, 554-557.

Zhang, Y., Mandava, C.S., Cao, W., Li, X., Zhang, D., Li, N., Zhang, Y., Zhang, X., Qin, Y., Mi, K.*, et al.* (2015). HflX is a ribosome-splitting factor rescuing stalled ribosomes under stress conditions. Nat Struct Mol Biol *22*, 906-913.

7 APPENDIX

7.1 Supplementary data

Table 7.1. Summary of rate constants

	P+0	P+9	P+30
Hydrolysis rate, s^{-1}	0.15 ± 0.01	0.06 ± 0.01	0.004 ± 0.001
Fast k_{ON}, $\mu M^{-1}s^{-1}$	500 ± 60	300 ± 30	300 ± 40
Fast k_{OFF}, s^{-1}	100 ± 20	140 ± 10	120 ± 10
Medium k_{ON}, $\mu M^{-1}s^{-1}$	101.2 ± 10.2	84.1 ± 20.4	80.2 ± 12.9
Medium k_{OFF}, s^{-1}	3.9 ± 2.5	0.78 ± 5.6	2.5 ± 3.2
Slow k_{ON}, $\mu M^{-1}s^{-1}$	0.73 ± 0.04	0.06 ± 0.01	1.8 ± 0.5
Slow k_{OFF}, s^{-1}	0.39 ± 0.01	0.33 ± 0.01	0.11 ± 0.14
$k_{diss\ avg}$, s^{-1}	0.06 ± 0.01	0.23 ± 0.01	0.33 ± 0.01
K_M, µM	0.25 ± 0.09	2.5 ± 1.3	
k_{cat}, s^{-1}	0.010 ± 0.001	0.019 ± 0.006	

Table 7.2. Apparent rates of initial binding

		ArfB, µM					
		0.05	0.1	0.2	0.3	0.4	0.5
P+0	**k_{app1}, s^{-1}**	130 ± 3	140 ± 1	220 ± 1	290 ± 2	320 ± 2	390 ± 2
	k_{app2}, s^{-1}	11 ± 1	10 ± 1	30 ± 1	30 ± 1	40 ± 1	70 ± 1
	k_{app3}, s^{-1}	0.4 ± 0.2	0.5 ± 0.1	0.5 ± 0.1	0.6 ± 0.1	0.7 ± 0.1	1.0 ± 0.1
P+9	**k_{app1}, s^{-1}**	160 ± 3	161 ± 2	170 ± 1	220 ± 1	280 ± 1	280 ± 1
	k_{app2}, s^{-1}	15 ± 1	13 ± 1	14 ± 1	23 ± 1	37 ± 1	37 ± 1
	k_{app3}, s^{-1}	0.7 ± 0.1	0.5 ± 0.1	0.3 ± 0.1	0.3 ± 0.1	0.4 ± 0.1	0.4 ± 0.1
P+30	**k_{app1}, s^{-1}**	160 ± 3	160 ± 2	180 ± 1	200 ± 1	245 ± 1	261 ± 1
	k_{app2}, s^{-1}	0.1 ± 0.2	7.0 ± 0.2	8.0 ± 0.1	13 ± 1	19 ± 1	24 ± 1
	k_{app3}, s^{-1}	1.4 ± 0.2	0.4 ± 0.1	0.4 ± 0.1	0.6 ± 0.1	0.9 ± 0.1	1.2 ± 0.1

7.2 List of figures

7.3 List of tables

7.4 List of abbreviations

µM	micromolar
A site	aminoacyl site
Ala	alanine
Arg	arginine
CD	circular dichroism
cryo-EM	cryo-electron microscopy
E site	exit site
EF-G	elongation factor G
EF-Tu	elongation factor Tu
fMet	N-formylmethionine
FRET	Förster resonance energy transfer
g	gram
GDP	guanosine diphosphate
GTP	guanosine triphosphate
Glu	glutamate
Gln	glutamine
Gly	glycine
IDP	intrinsically disordered protein
IF	initiation factor
Leu	leucine
Lys	lysine
M	molar, mole/L
min	minute
mL	milliliter
mM	millimolar
mRNA	messenger RNA
MS	mass spectrometry
nm	nanometer
nM	nanomolar
OD	absorbance

P site	peptidyl site
PDB	protein data bank
Phe	phenylalanine
Pi	inorganic phosphate
pmol	picomole
Pro	proline
RF	release factor
RNA	ribonucleic acid
rpm	rotation per minute
RRF	ribosome recycling factor
rRNA	ribosomal RNA
S	svedberg unit
s	second
TC	ternary complex
tRNA	transfer RNA
Thr	threonine
Val	valine

8 ACKNOWLEDGEMENTS

阮若拍開心內的門
gún nā phah-khui sim-lāi ê mn̂g
就會看見故鄉的田園
tsiū ē khuànn-kìnn kòo-hiong ê tshân-hn̂g
雖然路頭千里遠
sui-jiân lōo-thâu tshian-lí hn̄g
總會暫時予阮思念想欲轉
tsóng ē tsiām-sî hōo gún su-liām siūnn-beh tn̂g

故鄉故鄉今何在
kòo-hiong, kòo-hiong kim hô-tsāi
望你永遠在阮心內
bāng lí íng-uán tsāi gún sim-lāi
阮若拍開心內的門
gún nā phah-khui sim-lāi ê mn̂g
就會看見故鄉的田園
tsiū ē khuànn-kìnn kòo-hiong ê tshân-hn̂g

- Excerpt from *阮若打開心內的門窗* (1958)
  Song by 呂泉生, Lyrics by 王昶雄

First and foremost I thank Prof. Dr. Marina Rodnina for giving me the chance to work in her lab. It is a rare privilege to observe and take part in scientific research at this level, and I deeply appreciate all the opportunities and resources that have been made available to me these past five years. I thank Dr. Cristina Maracci, who took over the role of my supervisor at a very important juncture of my PhD. The guidance and structure she provided from that time forward were vital to the success of this project. I also thank Dr. Wolf Holtkamp, who came up with this project and introduced an intrepid young rotation student to the world of ribosome rescue. In his easy-going way he taught me not to fear mistakes, which in turn gave me the confidence to tackle a project very far removed from what I had previously studied.

I am also very grateful to Dr. Niels Fischer for our cryo-EM collaboration. A PhD project is a marathon and his participation towards the very end provided me with much-needed motivation to cross the finish line, not to mention some wonderful high-resolution structures. Dr. Ingo Wohlgemuth helped me with mass spectrometry analysis, has been incredibly generous in sharing his time and expertise with me in our collaboration, and I look forward

to further developing our ideas. I thank also Dr. Bee-Zen Peng, who always has a word of encouragement and some sweets from home for me when I need it most. Even more invaluable has been her willingness to share her experience and advice. Finally I must also mention the members of the Rodnina Department, from post-docs to technical staff, who have always been very kind and helpful, and without whom my work would have been much more difficult.

The song *阮若打開心內的門窗* is quoted at the beginning of this chapter. The lyrics, written in my mother tongue of Taiwanese Hokkien, can be roughly translated to: “if we open the doors to our hearts, we can then see the fields of our homeland. Even though the road is very long, this will at least ease the pain for a while.” The road has indeed been very long, and the homesickness hard to bear. But my friends here in Goettingen have done so much to support me through good times and bad; though I mention only a few by name, I am indebted to many that I met here.

Marija has been my companion in the lab, at concerts, and on the treacherous trails of Berchtesgaden in the early summer. Among the graduate school achievements I am most proud of are the extracurricular initiatives we worked on together. Franzi, the wise one, is always there with level-headed advice and open-minded sympathy, especially when life in Germany proved to be overwhelming. Last but not least, I owe much of my sanity to Madhobi. From long walks into the woods surrounding Goettingen to weekly discussions in the swimming pool, and now long phone calls, she is endlessly insightful and ensures that I do not feel alone in my anxieties. These friendships alone have been worth the trying times I experienced in my PhD many times over.

In the same vein, I do not know what I would have done without the constant support of my friends from home. Karen, Eloise, and Yuri have been incredibly patient despite my very sporadic communications, and are always there to distract me or simply listen. I only hope that I can be as good a friend moving forward as they have been to me these past few years.

Of course, I have to thank my family. They are my driving force and my safety net. Dad instilled in me since childhood a healthy respect for science and a curiosity in nature. Mom taught me how to take care of myself, so that even when I am stressed in a foreign land, I do not neglect my own health and quality of life. My sister and my best friend Connie: even

though she teases me too much sometimes, I know that there is nothing I can't share with her, and that she'll always have my back. They say it takes a village to raise a child – I say it takes a village for a PhD to be completed. And at the center of my village is my family.

Finally, I write this in a very strange time. Because of the COVID-19 pandemic, so many things that we counted on just a couple of months ago - international travel, the economy, access to healthcare, just to name a few – face huge disruptions. In the midst of all this, I would like to express my gratitude to the public health scientists, medical community, public servants, and private sector of Taiwan, for enabling a pandemic response that has thus far been successful. Because of them I have the great luxury of focusing on finishing my PhD, without having to worry too much about my friends and family back home.

I could ramble on forever about the kindnesses I have been shown over the course of my PhD and about the people who have made it so memorable; or I could speculate about the future. But I won't. Instead I will just close with this sentence from one of my favorite authors:

"It is good to have an end to journey toward; but it is the journey that matters, in the end."

- Ursula K. Le Guin, *The Left Hand of Darkness*

Written on 23rd April, 2020 in Goettingen, Germany